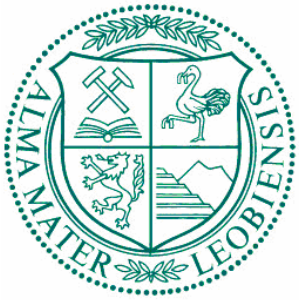

Investigation of Fluid Flow in Hydrocarbon Reservoirs during Supercritical CO2-Injection

Dissertation

Submitted to the Department of Mineral Resources and Petroleum Engineering and the Committee on Graduate Studies of the Montanuniversität Leoben, Austria in Partial Fulfillment of the Requirements for the Degree of

Doktor der Montanistischen Wissenschaften

Written by

Adel A Saleh Elzwi, M.Sc.

Leoben –Dec. 2009

Investigation of Fluid Flow in Hydrocarbon Reservoirs during Supercritical CO2-Injection

Doctoral Thesis

By:

Adel A Saleh Elzwi, M. Sc.

بِسْمِ ٱللَّهِ ٱلرَّحْمَٰنِ ٱلرَّحِيمِ

يَرْفَعِ ٱللَّهُ ٱلَّذِينَ ءَامَنُواْ مِنكُمْ
وَٱلَّذِينَ أُوتُواْ ٱلْعِلْمَ دَرَجَٰتٍ ۚ وَٱللَّهُ بِمَا تَعْمَلُونَ خَبِيرٌ

صدق الله العظيـــــــــــــــم

﴿ سُورَةُ ٱلْمُجَادَلَةِ ﴾

آية (11)

Dedication

*"Praise be to Allah, the Cherisher and Sustainer of the worlds * Most Gracious, Most Merciful * Master of the Day of Judgment". And I wish to dedicate my work on this doctoral dissertation to my parents, and my family without whose support and encouragement and the healthy environment they provided, this work would not have been possible.*

Affidavit

I declare in lieu of oath, that I wrote this thesis and performed the associated research myself, using only literature cited in this volume.

Adel Elzwi, M.Sc.

Leoben, December 2009

Publications of the Author

This research and its coupled investigations were published in the following scientific journals:

- A. ELZWI: "***Example Comparison of Minimum Miscibility Pressure Correlations***", Oil and Gas European Magazine (International Edition of Erdöl Erdgas Kohle), Pages 14-19, Volume 35, March 1/2009

- A. ELZWI and L. GANZER: "***A new Correlation for Predicting CO2 Minimum Miscibility Pressure***", Oil and Gas European Magazine (International Edition of Erdöl Erdgas Kohle), Pages , Volume 35, Dec. 4/2009

Acknowledgements

I would like to express my sincere gratitude to Prof. Leonhard Ganzer for accepting me in his research group and assisting and supporting me. I am really thankful to him for his guidance during the development of this research. His knowledge, support, and friendship have made my work possible.

My appreciation also goes to Dr. Diethard Kratzer, who was always willing to help me in different matters, during and after my work with HOT Eng.

I am also thankful to the Arabian Gulf Oil Company, AGOCO, for providing the field data for this research.

I cannot fully express my gratitude to my Family (my wife and children), for their understanding and wholehearted support they have given to me.

Table of Contents

List of Figures:

List of Tables

Kurzfassung

„CO2 miscible displacement“-Prozesse haben sich als sehr erfolgreiche Methoden zur verbessereten Ölgewinnung in vielen Kohlenwasserstoff-Lagerstätten erwiesen. Das Durchführen von Gasinjektionsprozessen bei optimalen Betriebszuständen und die genaue Implementierung des Designs sind Schlüsselfaktoren für eine erfolgreiche „Enhanced Oil Recovery“.

CO2 wird in vielen sekundären und tertiären Verdrängungsprozessen im superkritischen Zustand injiziert. Aufbauend auf der Definition des superkritischen Zustandes, auf dem Weg zwischen Injektor und Produktionssonde, wird sich das CO2 entweder im Dampf oder im flüssigen Aggregatszustand befinden. Es ist allgemein bekannt, dass das CO2 nicht beim ersten Kontakt mit dem Erdöl mischbar ist, und Mischbarkeit entsteht nach einigen Kontakten als ein „Vaporizing miscibility“-Prozess; das bedeutet, dass sogar bei hohen Drücken das CO2 das Erdöl für einige Distanz unmischbar verdrängen wird bevor Mischbarkeit erreicht werden kann; das verdrängte Erdöl vor der Verdrängungsfront wird „Ölbank“ genannt und hat die originale Erdölzusammensetzung. Hinter der Front ist eine Zweiphasenströmung dominant. Nachdem Mischbarkeit entsteht, wird die Erdölzusammensetzung verändert und Eigenschaften werden grundlegend verändert; vor allem nimmt die Viskosität ab, und der Sättigungsdruck nimmt zu basierend auf den Sättigungsdruck-Kurven eines „Pressure-Composition (P-X)“-Plots eines „Swelling“-Tests. Daraus resultiert ein sich verändernder Sättigungsdruck-Zustand. Im Gegensatz zur „Ölbank“ wird das neue Erdöl im untersättigten Zustand bis zu einer Entfernung verbleiben, bis der Sättigungsdruck größer wird als der durchschnittliche Lagerstättendruck. In diesem Fall wird Gas freigesetzt und es entsteht eine Zweiphasenströmung, Öl und Gas; dieser Strömungszustand kann stattfinden bevor die mischbare Bank die Produktionssonde erreicht, wo der Druckabfall sehr hoch ist und die Wahrscheinlichkeit der Unterschreitung des Sättigungsdruckes sehr hoch ist.

Die Ziele dieser Forschungsarbeit sind folgende: (1) ein gutes Verständnis von solchen „CO2 miscible“-Prozessen sowohl auf der Mikroskala als auch auf der Makroskala zu bekommen, (2) den Effekt der Betriebszustände vor allem des Druckes auf die Flüssigkeitsströmung (Öl, Gas CO2, kohlenwasserstoffreiches CO2, flüssigkeitsähnliches CO2) in der Lagerstätte während CO2- Injektionsprozessen zu untersuchen, weil die Durchführung des Prozesses im superkritischen Zustand das injizierte CO2 in eine flüssige Phase verwandeln kann und deswegen eine vierte Phase (flüssigkeitsähnliches CO2) vorhanden ist. Die Wahrscheinlichkeit, dass Feststoffe sich nach der Extraktion von leichten und mittleren Kohlenwasserstoffen aus Restöl ablagern, fügt eine fünfte Phase hinzu welche die Effizienz des Verdrägungsprozesses beeinflussen.

CHAPTER 1 Abstract

CO2 miscible displacement process proved itself as a successful method for enhanced oil recovery in many oil reservoirs. Performing any gas injection process at optimum operating conditions and accurate implementation of the design are key elements to successful enhanced oil recovery.

CO2 is injected in many secondary and tertiary displacement processes at supercritical conditions (T > 87 °F, P > 1070.6 psia). On the way from an injector to a producer, Figure 1-1, CO2 experiences at least three different pressure regions; high pressure region around the injector, the average reservoir pressure region, and low pressure region around the production well and reaches minimum at the well flowing pressure.

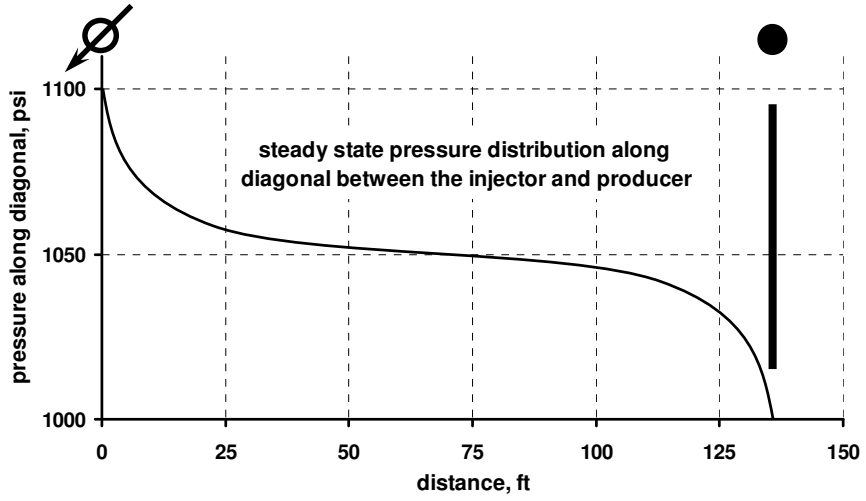

Figure 1-1: Pressure profile between injector and producer, (After [4])

Based on the definition of the supercritical conditions, and along the path from the injector to the producer, CO2 will behave vapor like or liquid like depending on the thermodynamic conditions, Figure 1-2. It is established that CO2 is not first contact miscible with crude oils, and miscibility develops after few contacts as a vaporizing miscibility process, this means that, even at the high pressure region, CO2 will immiscibly displace the oil for some distance before miscibility can be achieved,

this displaced oil ahead of the displacement front is called “oil bank” with the original oil composition. The oil bank is followed by a transition zone with increased gas concentrations. After miscibility is developed, the oil composition is altered and basic properties are significantly changed. Particularly viscosity decreases, and the saturation pressure increases according to the saturation pressure behavior on a Pressure-Composition plot (P-X) in a swelling test shown in Figure 3-8. This results in a variable bubble point case. Thus in contrast to the “oil bank” the new oil will remain undersaturated until at some distance from the injector where the saturation pressure is greater than the average reservoir pressure, in which case gas evolves forming two phases, oil and gas. This flow behavior may occur before the miscible bank reaches the production well where pressure drop is skyrocketing and the chance of going below the new saturation pressure is high.

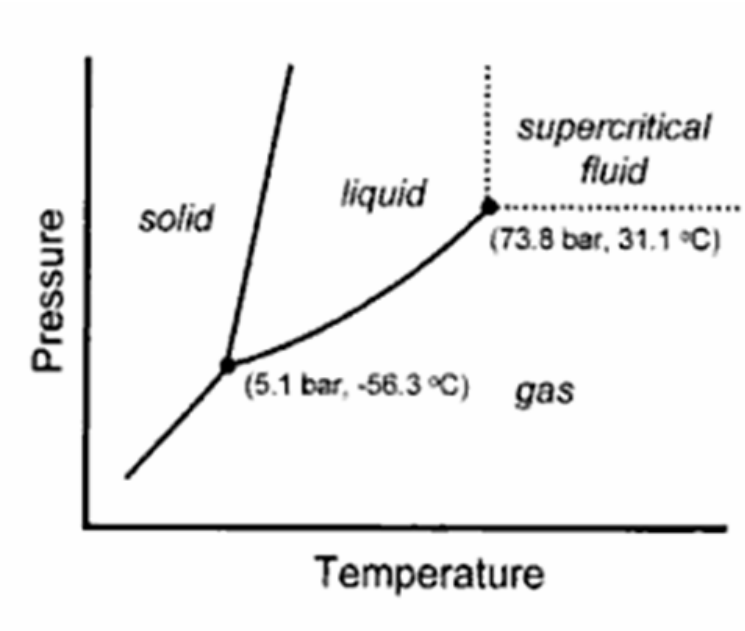

Figure 1-2: CO2 phase diagram showing critical point and the supercritical state, (After Joseph and William, 2003)

CHAPTER 2 Objectives of the Thesis

The goal of this research is; firstly to gain a good understanding of the CO2 miscible process on the micro- and macro-scale, secondly to investigate the effect of the operating conditions especially pressure on the flow of fluids (oil, gas CO2, hydrocarbon-rich CO2, and liquid-like CO2) in a reservoir during a CO2 injection process. Because performing the process at supercritical conditions can change the injected CO2 into a liquid phase and thus a fourth phase is present (liquid-like CO2). The possibility that solids deposit after extraction of light and intermediate hydrocarbons from residual oil adds a fifth phase which has an effect on the efficiency of the displacement process. This phenomenon introduces difficulty in handling three hydrocarbon phases by normal equation of states (EOS), and therefore the behavior of the system will be difficult to predict.

From the previous introduction and objectives, the following questions arise:

1. To what extent remains slim-tube determined minimum miscibility pressure reliable?
2. How does the saturation pressure changes along the path from an injector to a producer?
3. In case the saturation pressure exceeds the reservoir pressure, what is the composition of the evolved gas?
4. What about oil viscosity and density?
5. How do commercial simulators handle supercritical CO2?
6. What about supercritical CO2 relative permeability curves?
7. Do the high CO2 concentrations, at surface, represent a breakthrough?

An attempt to answer these questions is presented in the results and conclusions chapters.

Tools:

Eclipse PVTi is used for fluid characterization. Eclipse E100 and Eclipse E300 compositional are used for fluid flow simulation.

Methodology

Simulation of multiple-contact miscible displacement can only be done by means of one dimensional, 1-D, models, and with difficulty [4]. In order to answer the above questions, a 1-D, homogeneous, linear model is considered to serve the purpose of the thesis, the distance between the injector and the producer is sufficient to track saturation pressure changes along the injection path. The oil and vapor content of CO2, methane, intermediate hydrocarbons C2-C6, and C7+, as well as oil properties such as density and viscosity will be tracked along the displacement path. Recovery is compared for different injection schemes.

Case study: Sarir C-North filed

A relatively mature undersaturated oil reservoir is considered as a case study to investigate the effects of operating conditions on recovery process. The formation is consolidated sandstones with different shale contents. Lateral and vertical heterogeneity is high, and the area is faulted.

The reservoir is currently being operated below its MMP, but still way above its bubble point pressure, Pb. A water flood program is being designed for pressure maintenance as well as recovery improvement.

Structure of the thesis:

1. Phase behavior and miscibility
2. CO2 interaction with fluids and rock
3. Water alternating gas process, WAG
4. Fluid characterization using Peng-Robinson Equation of State, PR-EOS, by means of PVTi for use in the dynamic flow simulation using the compositional simulator Eclipse 300

5. Use of available slim-tube experiments, and appropriate correlations to predict reliable minimum miscibility pressure, MMP
6. Simulation of linear 1-D model
7. Simulation of real 3-D model: Performing several simulation runs at various operating conditions (primarily pressure) below, at and above MMP.
8. Results, and conclusions

CHAPTER 3 Phase Behavior and Miscibility

3.1 Equation of State, EOS

An Equation of State (EOS) is an analytical expression relating pressure to temperature and volume. The modifications to the EOS as from Van der Waal through the recently widely used EOS by Peng-Robinson [41] or Soave-Redlich-Kwong [49] are attempts to describe phase transition from a single phase through a two phase region. The behavior of the two phase envelop is of a specific importance, because in a single phase state, whether a liquid or gas, the problem is less complicated. The EOS was essentially developed as an empirical equation for real gas, as a result it has problems in predicting liquid properties e.g. density. The two parameter Van der Waal's EOS in terms of the deviation factor Z is expressed as:

$$Z^3 - (1+B)Z^2 + AZ - AB = 0$$

Where:

$$A = \frac{ap}{R^2T^2}$$

$$B = \frac{bp}{RT}$$

Z= deviation factor

P= system pressure, psia

T= system temperature, R°

a= temperature dependent parameter

b= co-volume

The EOS in its cubic form yields three real roots A, B and D (volumes) for a given pressure as seen in Figure 3-1. The largest root (volume) corresponds to the volume

of the saturated vapor, while the smallest positive volume corresponds to the saturated liquid. The third root has no physical meaning [54].

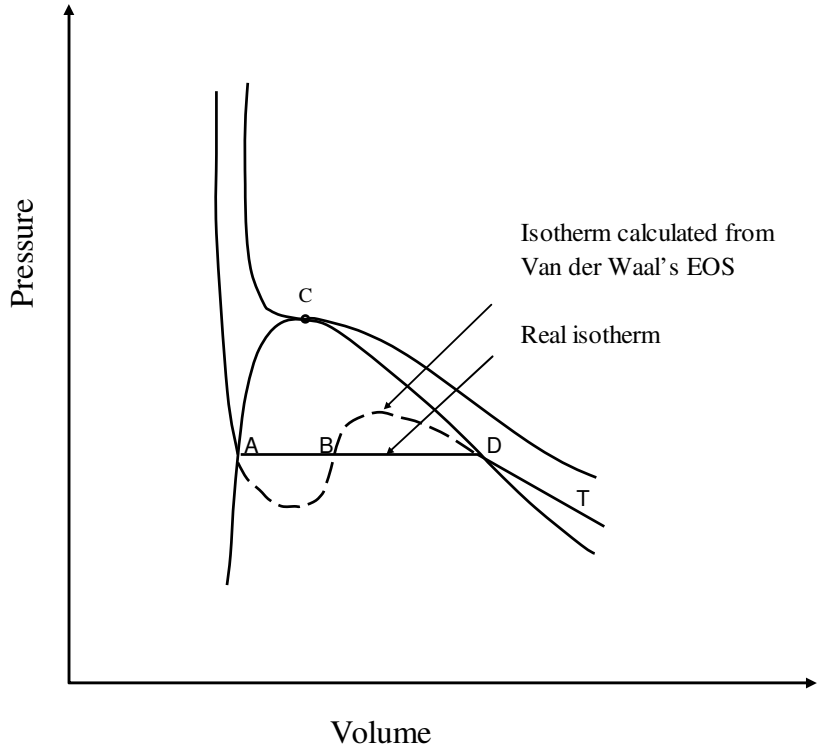

Figure 3-1: Pressure-volume diagram for a pure component as predicted by Van der Waal's EOS

In one phase region the EOS yields one real root, but in some supercritical regions, EOS can yield three real roots. From these three roots, the largest root is the value of a physical meaning [54].

3.2 Supercritical CO2

CO2 is injected in many secondary and tertiary displacement processes at supercritical conditions: T>Tc= 87.6 F ° [304 K] and P>Pc= 1070.6 psia [73.8 bar]. The definition of a supercritical fluid is best described using a typical P-T phase diagram as shown in Figure 3-2. Above the critical pressure of a substance, a phase transition to gaseous state is no longer observed as the liquid form of the substance is heated. Similarly, above the critical temperature of a substance, a phase transition

to liquid state is no longer observed as the gaseous form of the substance is pressurized. In the region above the critical temperature and pressure, a substance can no longer be classified either a gas or a liquid since it has properties of both [44]. In this region above the critical pressure and temperature the substance is said to be supercritical fluid. From a practical point of view, supercritical fluids can be thought of as gases that have been compressed to densities at which they can exhibit liquid-like interactions.

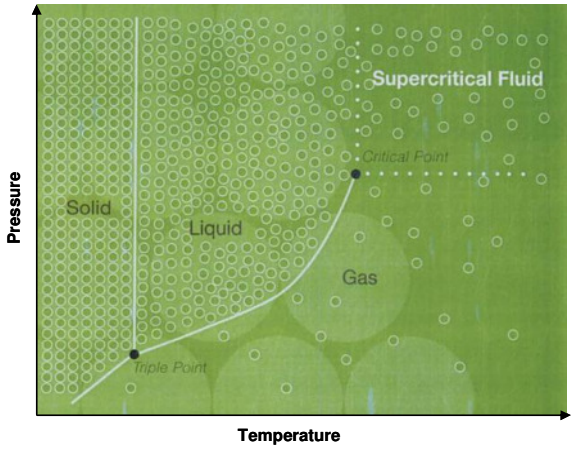

Figure 3-2 : Phase diagram for a pure component, (After Ram and Shim)

The supercritical phenomenon was discovered in 1822 by Cagniard, before Hannay and Hogarth observed its solvent power in 1879 [43]. *Supercritical fluids exhibit liquid-like solvent properties and gas-like transport properties,* Table 3-1.

Table 3-1: Physical properties of carbon dioxide [44]

Parameter	Gas	Liquid	Supercritical phase
Density [g/cm^3]	10^{-3}	0.6 to 1.6	0.4 to 1.0
Diffusion coefficient [cm^2/s]	10^{-1}	2×10^{-6}	7×10^{-4}
Viscosity [g/cm/s]	10^{-4}	3×10^{-2}	3×10^{-4}

Supercritical fluids can not be liquefied even with extreme compression, however with increased pressure the density changes from vapor-like to liquid-like. Diffusivity of supercritical CO2 is much higher than that of a liquid, and can be easily varied with variations of pressure and temperature, and it is typically an order

of magnitude higher than liquids. Viscosity of supercritical CO2 is nearly 100-fold lower than that of liquids.

3.3 Phase Behavior

Pressure, Volume, Temperature (PVT) is a fundamental subject to reservoir engineering, especially in the calculation of oil and gas reserves as well as in the calculation of the efficiency of enhanced oil recovery processes. In this chapter, a general review and summaries about the basic principles of phase behavior and miscible processes are discussed.

3.3.1 Single-Component System

The simplest system, only one component exists. The pressure- temperature (P-T) behavior of single component systems is characterized by a curved-line called "the vapor-pressure line". The end point of the line is called critical point, Figure 3-3. Above and to left of the critical point the component is a single phase (liquid), below and to right of the critical point the component is a single-phase (gas). Two phase (vapor plus liquid) exists along the vapor pressure curve. The pressure-volume (P-V) describes the isothermal behavior of the two-phase systems.

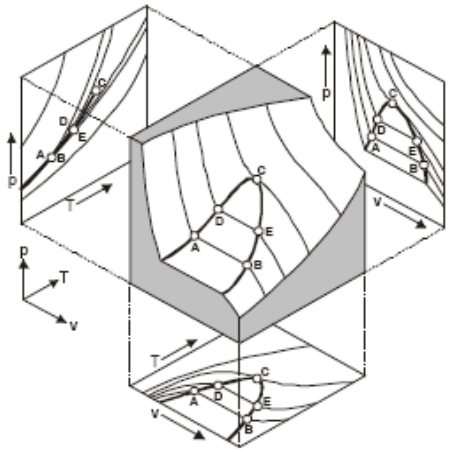

Figure 3-3: Phase equilibrium surface of a pure substance (From Gyulay, 1967)

3.3.2 Binary Systems

Two-component systems are slightly more complex than single-component systems. The composition is defined by mole fractions, which is the ratio between the number of mole of one component to the total of moles making that system. Binary systems are characterized, on a P-T relation, by a phase envelop rather than a curve, Figure 3-4. The critical point is defined as the point where the dew- and bubble point curves intersect.

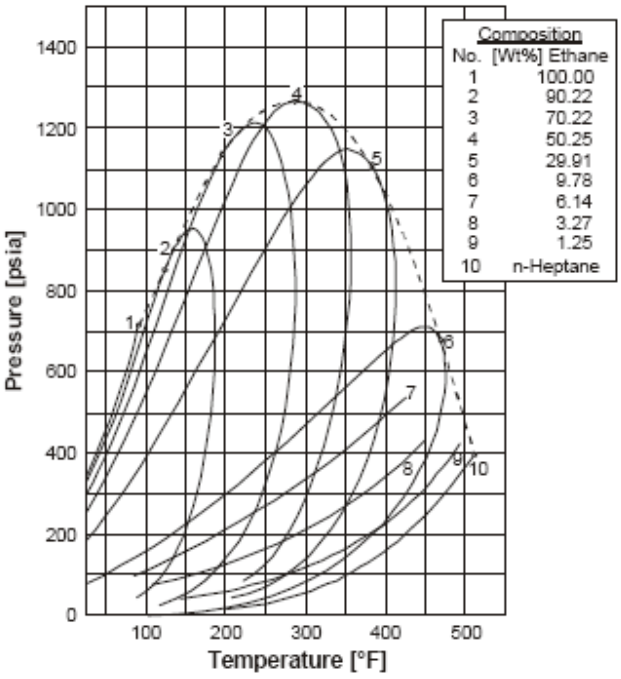

Figure 3-4: Pressure - temperature phase diagram of binary system, (After KAY, 1938)

In comparison to the single-phase system, two additional characteristic points, these are: the cricondenbare which is the point of highest pressure on the curve, and the cricondentherm which is the point of highest temperature on the curve. The quality lines describe the states where a certain mole percent of liquid and vapor are in equilibrium.

3.3.3 Ternary Systems

Phase behavior of three component systems are described on a triangular representation called ternary diagrams, Figure 3-5. Natural accumulations of oil reserves are composed of many hydrocarbon components plus some non-hydrocarbons such as nitrogen, carbon dioxide and hydrogen sulfide. It is useful to represent multi-component hydrocarbon mixtures using a pseudo-ternary diagram.

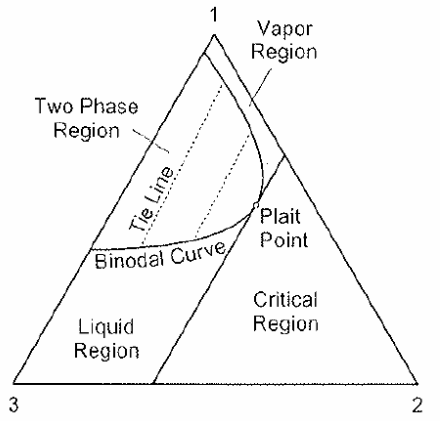

Figure 3-5: Typical features of a ternary phase diagram

Three groups of pseudo-components are formed, each component is assigned to a corner of the ternary plot, the components are classified into three groups: a volatile pseudo-component composed of methane and nitrogen located on the upper corner of the triangle, an intermediate pseudo-component composed of intermediate hydrocarbon components like ethane through hexane located on the lower right corner of the plot, and a third pseudo-component composed of the heavy fraction located on the lower left corner of the plot. Each corner of the plot represents 100% of its pseudo-component. Binary mixtures are located on the sides of the ternary diagram, whereas mixtures are located inside the triangle. Any mixture with an overall composition lying inside the two phase region will split into liquid and vapor phases. Liquid and vapor compositions in equilibrium are connected by a tie-line. Liquid and vapor curves meet at the plate point which represents the critical composition.

3.3.4 Pressure/Composition Diagrams

For multi-component systems, in addition to the ternary diagrams, pressure/composition (P-X) diagram is a useful method for displaying phase behavior data, Figure 3-6. Injection gas is added to the reservoir fluid in different concentrations. The saturation pressure for each mixture will be observed. At sufficiently high concentrations of the injection gas, the dew points of the mixtures are observed. Plotting the observed bubble point and dew point pressures versus concentrations of the injection gas is called P-X diagram. The highest pressure at which two phases can coexist is called the cricondenbar. Mixtures exist as single phases at pressures above the cricondenbar. Below the bubble point and the dew point curves liquid and vapor coexist in equilibrium. Pressure/composition diagrams for mixtures of miscible displacement injection fluids and reservoir oils can predict more complex phase behavior, because in addition to the single phase and two phase regions, a region of liquid/liquid equilibrium and a region of liquid/liquid/vapor equilibrium, also a solid phase may be seen on a P-X diagram. These regions can also be seen on a ternary diagram

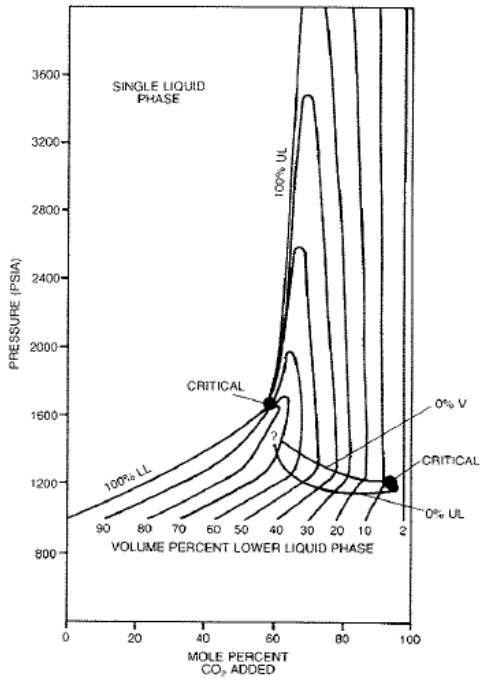

Figure 3-6: Pressure versus CO2 concentration phase diagram (After Gardner and Patel)

3.4 Classification of Miscible Displacement

Miscibility between two fluids is achieved when the interfacial tension IFT, and thus the capillary forces are eliminated. As a result, the capillary number, which is the product of Darcy velocity and displacing fluid viscosity divided by the IFT, goes to infinity and the residual oil saturation can be reduced to its lowest possible value, Figure 3-7. Generally miscible displacement processes are divided into to main categories first- and multi-contact processes.

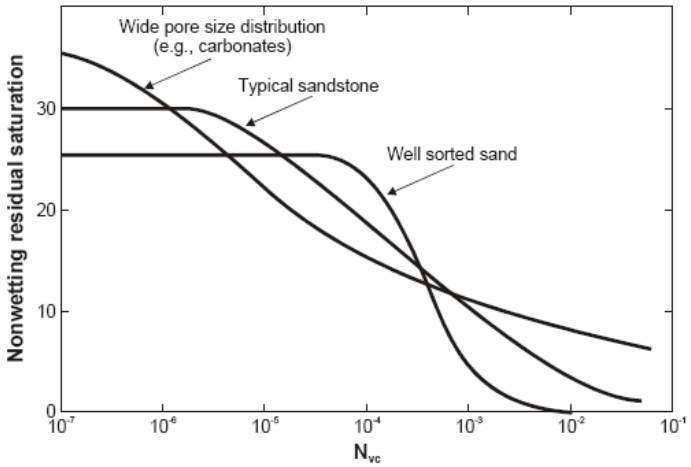

Figure 3-7: Capillary number correlation (After Lake, 1989)

3.4.1 First-Contact Miscibility Process, (FCM)

In first-contact miscible processes, the solvent mixes with the oil completely, in all proportions, so that all mixtures are single phase. Examples of first-contact solvents are propane, butane, mixture of liquefiable petroleum gases (LPG), or low-molecular-weight alcohols such as isopropyl. Unfortunately, large slugs of the alcohols are required to prevent dilution of the solvent, and that makes it an uneconomic solvent.

For first-contact miscibility to be achieved between solvent and oil, the displacement pressure must be equal to or higher than the P-X cricondenbar, which

is obtained from the swelling test results, Figure 3-8, because then all mixtures will be single phase. The cricondenbar for LPG and oil mixtures are typically low, which make first-contact miscibility achievable at practically attainable pressures. The cricondenbar in this case is called the first-contact miscibility pressure (FCMP), whereas in the case of CO2-oil mixtures, the cricondenbar usually is high. That is why first contact miscibility can not be achieved at practically achievable pressures, and in this case only multiple contact process can provide miscibility.

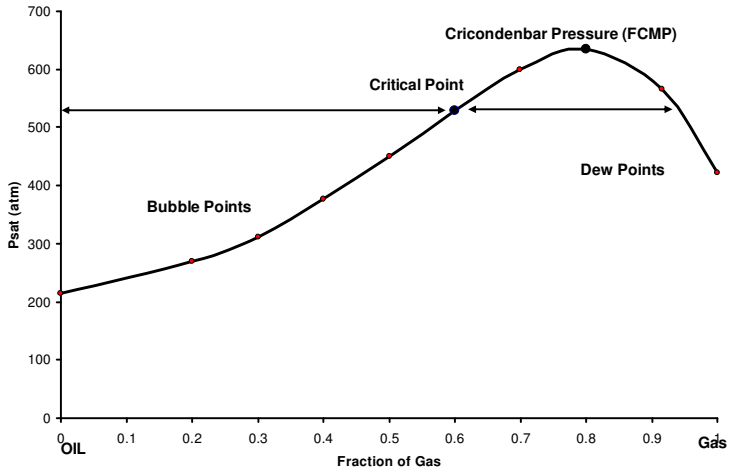

Figure 3-8: A typical P-X diagram for a reservoir oil and injection gas

In FCM, the straight line (dilution path) between the solvent and the oil does not pass through the two phase region on the pseudo-ternary diagram, Figure 3-9. This is an important characteristic of the first-contact miscible process in addition to the fact that the solvent and the crude oil must lie on opposite sides of the critical tie-line. This is a necessary condition for both first- and multi-contact miscibility to be achieved.

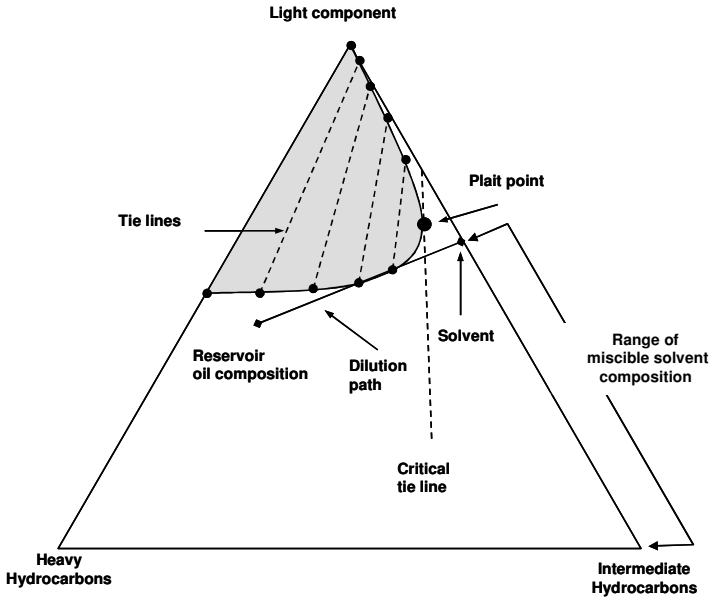

Figure 3-9: Schematic of the first-contact miscibility process (After Lake, 1989)

3.4.2 Multi-contact Miscibility Process, (MCM)

In case FCMP can not be practically achieved, miscibility can be achieved after multiple contacts between solvent and crude oil, and is called dynamic miscibility. Multi-contact miscibility can be classified further into three categories based upon the mechanism that provides miscibility: vaporizing-gas process, condensing-gas process, and combined condensing/vaporizing process.

3.4.2.1 Vaporizing-Gas Drive Mechanism, (VGD)

The process is basically that the solvent (e.g., natural gas, lean gases, flue gases) vaporizes the intermediate-molecular-weight hydrocarbons (i.e., C5 to C12 which is also called the gasoline cut) from the reservoir oil into the injection gas, depending on the pressure, temperature and injection gas composition. Nitrogen also tends to exchange place with solution gas in the oil and thus improve natural gas recovery. The mixture of injection gas and the vaporized hydrocarbons form a transition zone between pure injectant and the crude oil. This zone creates miscibility with the

crude oil. CO2 provides dynamic miscibility, however it extracts heavier-molecular-weight hydrocarbons (i.e., C5 to C30) than do natural gas, flue gas and nitrogen.

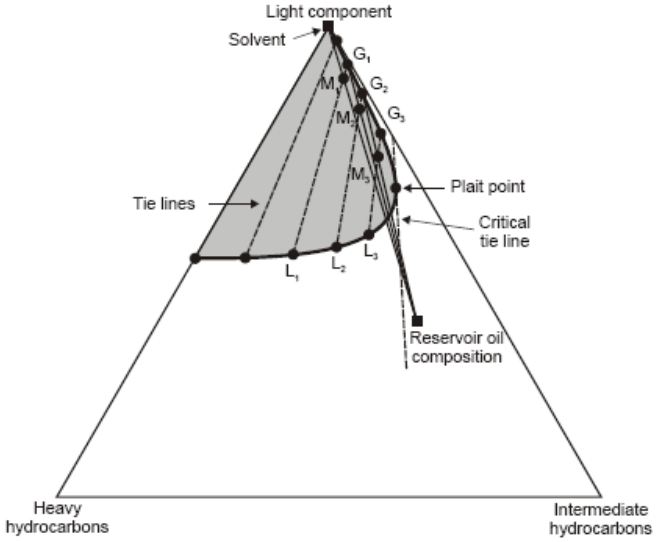

Figure 3-10: Schematic of the vaporizing-gas drive process (After Lake, 1989)

As mentioned in the first-contact miscibility process, the solvent and the reservoir oil must be in opposite sides of the critical tie-line. Figure 3-10 depicts a typical vaporizing-gas drive process at constant pressure and temperature. Initially the system is a single phase (crude oil). The injection gas (solvent) initially immiscibly displaces the oil and leaves some oil behind the gas front. This oil with the injection gas forms the mixture (M1) that splits into two phases. The injection gas extracts intermediate-molecular-weight hydrocarbons and forms an equilibrium vapor phase (G1). Consequently, composition of the oil (liquid) changes to equilibrium liquid phase (L1) and is left behind as a residual oil. The equilibrium vapor phase (G1) contacts the original oil again and two equilibrium phases are formed. This process initiates a transition zone. Further contacts of injection gas with the original oil, the injection gas becomes richer in natural gases and its composition moves along the dew point curve to the critical composition. At the critical composition the gas is directly miscible with the reservoir fluid. Note that, when using a slim-tube experiment in simulating vaporizing-gas drive mechanism, ahead of the transition

zone only oil exists, while behind the transition zone residual oil and injection gas are present, whereas for the first-contact miscibility no residual oil is left behind. Note also that high API gravity and subsequently lower-viscosity oils are generally displaced by vaporizing-gas drive mechanism.

3.4.2.2 Condensing-Gas Drive Mechanism, (CGD)

In this process only natural gases are used as solvents, other gases (i.e., lean gas, flue gas, nitrogen, CO2) can not provide the condensing-gas drive mechanism. The reason as implied by the name, is that the injection gas consists mainly of low-molecular-weight hydrocarbons (C2 to C6) that condense in the oil and generate a miscible transition zone between the solvent and the fresh oil.

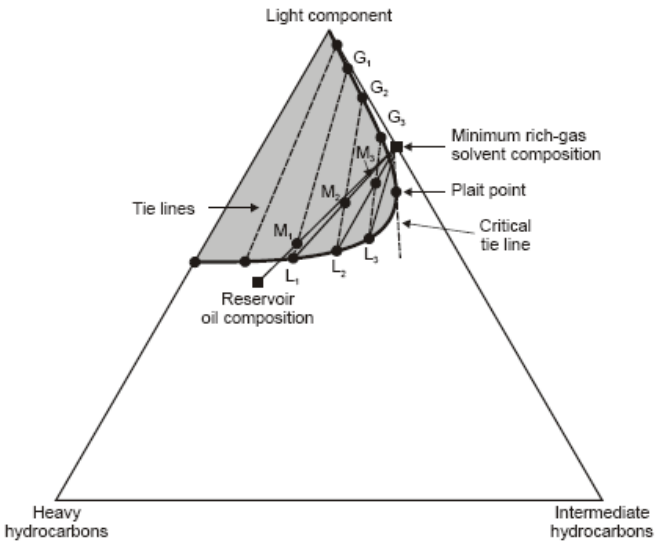

Figure 3-11: Schematic of the condensing-gas drive process (After Lake, 1989)

Figure 3-11 illustrates the condensing-gas drive mechanism. Initially the gas displaces the oil immiscibly. Suppose that after the first contact of the fresh oil and the injection gas the mixture (M1) is formed and splits into two equilibrium phases (G1) and (L1). Further injection of the gas pushes the equilibrium gas (G1) ahead into the reservoir. This gas is no longer contributing to the miscibility. The

equilibrium liquid (L1) mixes with the injection gas extracting (condensing) more intermediate hydrocarbons and splits into two equilibrium phases (G2) and (L2). By continuous injection, the equilibrium gases are moved ahead leaving the equilibrium liquids to extract (be enriched by) intermediate hydrocarbons. The composition of the oil is altered progressively along the bubble point curve until it reaches the plait point. At the plait point the injection gas and the reservoir oil are directly miscible. This explanation of the condensing-gas drive mechanism assumes that the injection gas is moving and contacting non-flowing oil. This is just a simplification, but it qualitatively describes the compositional part of the mechanism.

3.4.2.3 Combined Condensing-Vaporizing Drive Mechanism

It was demonstrated that ternary diagrams can explain the miscibility process for a condensing-gas drive mechanism with three component systems. On the other hand, the pseudo-ternary diagram for multi-component systems can be generated by mixing the reservoir fluid with light and intermediate hydrocarbons, flashing the mixture, and measuring the equilibrium compositions. When these equilibrium compositions are projected onto pseudo-ternary diagrams, they result in very similar phase envelopes to the ternary-diagram systems, therefore it was assumed that the displacement mechanism of the reservoir oil by enriched gas is also condensing-gas drive. This assumption presupposes no change in the distribution of components, while in reality, distribution of components do change, and thus the shape of the phase envelope changes. Displacement experiments and equation of state analysis indicate that neither vaporizing- nor condensing-gas drive mechanism can separately explain the multi-contact phase behavior of reservoir oil by enriched-gas [63].

To understand the combined condensing/vaporizing mechanism, consider a system with four groups of components:

1. lean components: such as methane, nitrogen, carbon dioxide

2. Light intermediate components: such as ethane, propane and butane, these are the enriching components, this group is present in both the oil and the injection gas
3. Middle intermediate components: this group ranges from between butane and decane to about C30, this group contains components that can vaporize from the oil into the injection gas, and is present in the displaced oil but insignificantly found in the injection gas
4. Heavy components: consists of about C30+, these components are the most difficult to vaporize

From the definition of the groups, one can see that when gas comes into contact with the oil the following actions take place:

1. Condensation: light intermediates condense from the injection gas into the oil
2. Vaporization: simultaneously, the middle intermediates are stripped from the oil into the injection gas
3. After a few contacts, the oil gets richer in light intermediates, but leaner in middle intermediates, and thus the oil gets lighter by net condensation
4. The fraction of the middle intermediates in the oil can not be entirely replaced with the light intermediates , therefore after a few contacts the oil gets saturated in light intermediates and thus gets heavier by net vaporization
5. After all the intermediates are vaporized, the residual oil is very heavy (i.e., C30+) [63].

3.4.2.4 CO2-Miscibility Process

Miscibility between CO2 and crude oils can be dynamically achieved at pressure greater than a certain pressure called MMP, which will be explained in detail in the next section. This type of miscibility is due to vaporizing-gas drive mechanism if the fluid at the displacement front is a CO2-rich gas, and due to extraction of hydrocarbons if the fluid at the displacement front is a CO2-rich liquid. However, it

has the advantage that the dynamic miscibility can be attained at substantially lower MMP than with natural gas, lean gas or nitrogen. CO2 can extract gasoline fraction, as well as intermediate molecular weight C5 through C30.

Dominant displacement characteristics for carbon dioxide displacement process, based on pressure and temperature are summarized in Table 3-2 [21]:

Table 3-2: CO2 displacement characteristics

Carbon dioxide injection process	Reservoir criteria	Oil recovery mechanisms
Low pressure applications	Pressure less than 1000 psia Shallow and viscous oil fields where water or thermal methods are inefficient	Oil swelling and viscosity reduction
Intermediate pressure, high temperature applications	1000<p<2000 to 3000 psia up to reservoir pressure	Oil swelling, viscosity reduction and crude vaporization
Intermediate pressure, low temperature applications (<122 °F)	1000<p<2000 to 3000 psia temperature <122°F	Oil swelling, viscosity reduction and blow down recovery
High pressure miscible applications	Pressure greater than 2000 to 3000 psia	Miscible displacement

Metcalfe and Yarborough [36], however suggest that both VGD and CGD mechanisms are relevant to CO2 displacements depending on the displacement pressure and temperature. When pressures and temperatures are high, VGD is dominant (CO2 extracts intermediate hydrocarbons, range not specified), while at corresponding pressure levels but relatively lower temperatures CGD (absorption of CO2 into the oil phase) more correctly describes the process.

The complicated CO2/crude oil phase behavior can rarely be represented in simplified ternary diagrams, especially in the presence of large amounts of C1, instead quaternary diagrams are more useful, Figure 3-12 [36].

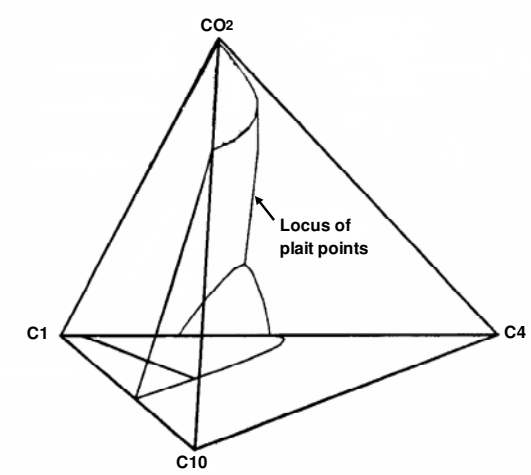

Figure 3-12: Quaternary diagram, (After [37])

Compared to water-flooding, on the other hand, CO2 flooding has the disadvantage of an unfavorable mobility ratio (lower CO2 viscosity relative to that of oil) which adversely affects sweep efficiency. This shortcoming can be offset by water alternating gas (WAG), which will be discussed later in CHAPTER 5 .

3.5 Minimum Miscibility Pressure, (MMP)

MMP is an important parameter for screening and selecting reservoirs for miscible-gas injection, Figure 3-13. In order to achieve a multi-contact miscibility between any injection gas and the reservoir oil, the system pressure must exceed a certain pressure specific to that system. This pressure is called minimum miscibility pressure, MMP. There are different definitions with regard to MMP at a constant temperature:

1. Generally: the lowest-pressure level at which miscible displacement occurs [11], [62]
2. From slim-tube test the most common and well accepted definition: the pressure corresponding to 90% oil recovery at 1.2 PV
3. In a ternary diagram: the lowest pressure at which the critical tie-line passes though the oil composition

There are different definitions with regard to MMP at a constant temperature, as will be explained in detail in CHAPTER 7 .

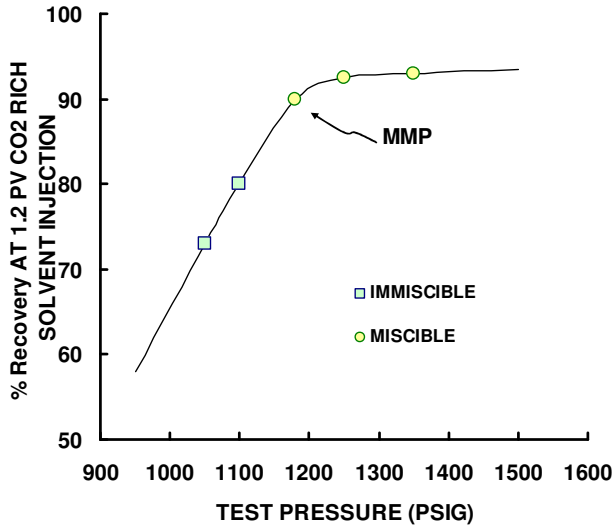

Figure 3-13: Typical slim-tube determined MMP of fixed oil composition and fixed temperature

If the reservoir is saturated (P<Pb), then MMP is assumed to be equal to Pb. A little effort was made to define MMP below bubble point pressure due to various reasons: firstly, it is not known how to interpret the results of experimental slim-tube tests below Pb, secondly, the injection gas will displace the free gas preferentially rather than to be mixed with the oil to develop miscibility, thirdly, the free gas will contain a significant amount of light hydrocarbons and light intermediates that will mix with the injection gas and hinder the development of miscibility [62].

MMP can be experimentally obtained using slim-tube tests or a raising-bubble apparatus. It can also be correlated to various conditions, taking into account composition characteristics.

3.5.1 Experimental Methods for Determining MMP

3.5.1.1 Slim-tube Experiments

Figure 3-14 schematically illustrates a slim-tube apparatus which usually consists of a 40-ft (13.3 m) long, ¼-inch OD coiled stainless steel tube packed with 160-200 mesh Ottawa sand, and the injection velocity is in the range of 4 to 8 cm^3/hr. The coiled tube is long enough to minimize the effect of transition zone length and retard or suppress viscous fingering. The small diameter avoids gravity segregation. The grain size provides permeability as high as 3 Darcies or even higher [31], [61], [62], [60]. This high permeability maintains uniform pressure distribution throughout the test.

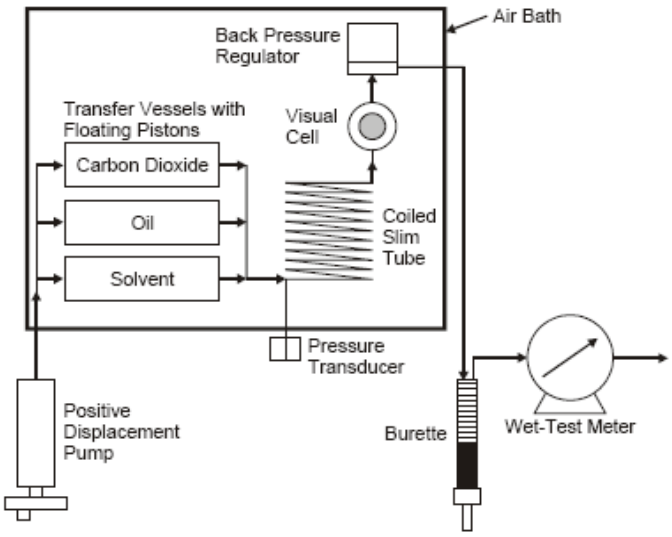

Figure 3-14: Schematic of a slim-tube apparatus (After [16])

The pore volume is determined by evacuating the coiled and measuring the amount of a solvent to completely saturate the pore volume. Initially the packed sand is filled with oil, the supply cylinder is then filled with the injection gas, and the temperature allowed reach to equilibrium. The injection gas is then injected at a constant rate about 4 cm^3/hr, using a positive displacement pump. The effluents are continuously flashed to atmospheric conditions, and separator gas and liquid volumes are recorded over time. The apparatus is cleaned after each test using

solvents. The test is repeated at different pressures. Plotting pressure versus recovery yields two straight lines, which intersect at the MMP, see Figure 3-13.

Yellig and Metcalfe [62] observed that the sharpness of the break in the recovery curve depends on the temperature, oil and injection gas composition, slim-tube dimensions and operating conditions.

Visual observations are also useful in judging miscibility using the slim-tube apparatus, flow characteristics before, at and after break through, and the transition zone characteristics: color and size can provide qualitative assessment to the miscibility development [19].

It should be noted that slim-tube test is not intended to simulate gas injection process at reservoir flow conditions, where viscous fingering, gravity overriding, dispersion, heterogeneity, etc., can affect the real displacement process. In slim-tube test all these flow effects are minimized. The Slim-tube test is used to study the overall multiple-contact mass transfer [62] resulting from continuous contact between reservoir fluid and injection gas. The slim-tube apparatus which results typically in high recoveries approaching 100% is quite different from the real displacement process in a consolidated reservoir rock and the recoveries may not necessarily correlate [29].

3.5.1.2 Rising-Bubble Apparatus

The Rising Bubble Apparatus (RBA) is an alternative, quicker and less costly means of determining MMP[16]. Figure 3-15 schematically illustrates a typical RBA. The apparatus has a rectangular cross-sectional glass tube with dimensions 1×5 mm cross section and 20 cm visual portion. The tube is mounted vertically in a high pressure sight gauge in a temperature controlled bath. The tube is back lighted for visualization. A hollow needle is mounted at the bottom of the sight gauge and the needle diameter can be varied to control the bubble size. A video camera is

mounted on a holder parallel to the bath of the rising bubble in the sight gauge to obtain a permanent record of the shape evolution of the rising bubble.

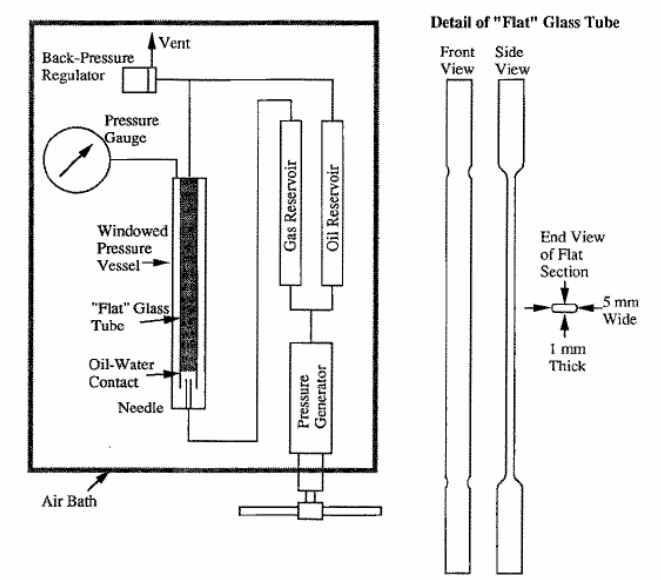

Figure 3-15: Schematic of a rising bubble apparatus, (After [16])

Initially the sight gauge is filled with water, then oil is injected displacing the water downwards, so that the glass contains oil down to the oil-water interface, this contact can be adjusted to the desired level. Then a bubble of gas is formed at the tip of the hollow needle in the water region (below the oil-water interface), when the buoyant force lifting the bubble exceeds the adhesive forces holding the bubble, the bubble rises through the water to assure the bubble formation and size, then through the water-oil contact, and up through the oil column. The video camera records the evolution of the shape of the rising bubble.

The development of the shape of the rising bubble through the oil column indicates miscibility, or MMP. The evolution of the rising bubble for a vaporizing-gas drive process, and for a condensing-gas drive process has special characteristics, see Figure 3-16.

MMP is defined as the pressure at which the interfacial tension at the interface between a gas bubble and a liquid approaches zero, causing the gas bubble to dissipate in a characteristic manner [8].

At pressures above MMP the bubble may readily disperse upon contact with the oil.

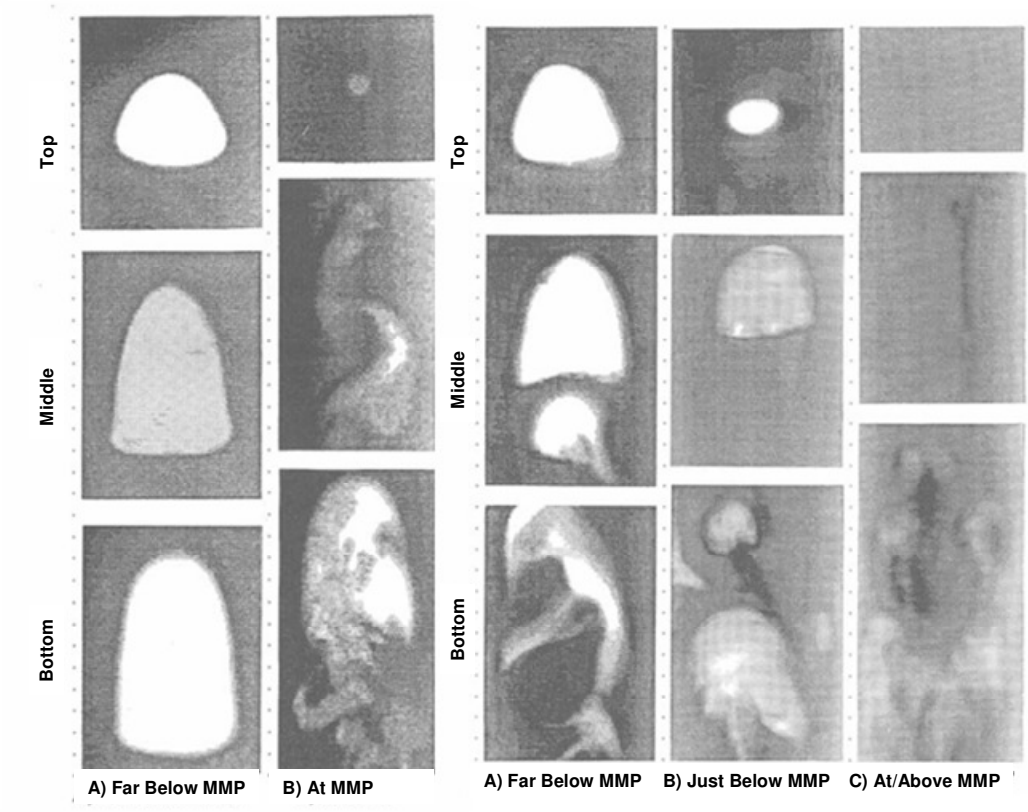

Figure 3-16: Bubble behavior, Left: VGD, Right: CGD, (After [16])

The RBA has the following advantages over the slim-tube test:

- MMP determined with slim-tube tests depends on the criterion used to interpret recovery performance, so in contrast to the slim-tube, pressure dependence of oil recovery is not used to indicate MMP with the RBA [9]
- The pressure drop across the coiled tube, although this drop is usually about 50 psig [22] nevertheless, it adds uncertainty to the pressure at which oil recovery is measured
- The RBA is a quicker means for measuring MMP. It takes no more than 2 hours for MMP determination, whereas slim-tube takes one to two weeks per MMP determination

- The RBA is much cheaper than slim-tube test
- The statement of Yellig and Metcalfe for using the slim-tube test as the industry standard was before the invention of the RBA

On the other hand the RBA has the following disadvantages:

- The RBA determined MMP is generally conservative (i.e., lower) compared to slim-tube determined MMP [55]
- For systems that exhibit solid precipitation, the slim-tube would be superior than RBA, although the solids may plug the slim-tube in extreme cases [55]

3.5.2 Literature Review of MMP Correlations

Experimental methods are the most reliable sources for MMP determination, however they are both expensive and time consuming. Therefore results of these experiments are used to develop reliable correlations. These correlations are used primarily for screening purposes to study miscibility development at various conditions.

In 1960, the earliest attempt for the estimation of MMP was based on Benham [3] investigations. He observed that pseudo-ternary diagrams could be used to describe the mechanism for obtaining miscibility conditions [17]. He correlated miscibility conditions using: temperature, pressure, reservoir-fluid C5+ molecular weight, injection-fluid C2-C4 molecular weight and the methane concentration in the injection fluid. Benham suggests use of his correlation for predicting miscibility conditions by rich gas for wide range of temperature, pressure and molecular weights.

In 1973, Metcalfe et al. [35] presented a mathematical model that simulates the flow of fluid into the reservoir as a series of constant pressure and temperature cells. His computer program is an extension of the model of Cook et al. that was used to study gas cycling rather than miscibility prediction. It was assumed that vapor and liquid

of each cell are in equilibrium. In the first cell gas is mixed with the liquid and flashed. The excess volume of liquid and vapor is transferred to the next cell. In his work MMP was defined as the pressure at which (1) the over-all composition shows that a single phase has been formed, and (2) a composition that exhibits first contact miscibility with the injected fluid is formed along the bubble point curve.

In 1974, Holm and Josendal [22] developed a correlation based on Benham et al.[3] the correlation is used for predicting the pressure required for miscible displacement in CO2 flooding. The correlation parameters are: reservoir temperature and C5+ molecular weight of the reservoir fluid. Holm and Josendal stated that the development of miscibility by CO2 does not depend upon the presence of light hydrocarbons, C2-C4, in the reservoir oil. Also they stated that the presence of methane in the reservoir oil does not significantly affect MMP, but inversely affects the over-all efficiency of the process. Theses two statements were also noticed by later investigators [37], [62].

In 1978, Cronquist [19] used 58 experimental MMP data from different sources to develop a general correlation, which covers a wide range of API gravities and temperatures. The correlation parameters are: Temperature (˚F), C5+ mole weight, and mole percent of methane and nitrogen.

In 1980, Yellig and Metcalfe[62] based on their experimental work proposed a correlation using only temperature for predicting CO2 MMP for an oil. They fully explained the large effect of temperature on the development of miscibility, and stated that there is little or no effect of oil composition on MMP, this observation contradicts with Holm and Josendal statement about the effect of the oil composition, especially regarding C5+. Yellig and Metcalfe suggested the use of bubble point pressure as the MMP for saturated oil reservoirs (P<Pb). They also suggested use of slim-tube test to be the standard technique in MMP determination.

In 1981, Johnson and Pollin [29] presented a correlation that can predict MMP for a wide range of gravities and for pure and diluted CO2. The correlation parameters are oil gravity, molecular weight, reservoir temperature and injection gas composition.

In 1982, Holm and Josendal [23] supported their original correlation [22] which emphasizes the effect of oil composition on MMP. Furthermore they correlated MMP with the content of C5-C30 in the oil, and with the density of CO2 which is a function of temperature and pressure.

In 1985, Kue [32] developed a correlation for condensing drive mechanisms using the Peng-Robinson equation of state, which was applicable for wider range of temperature, pressure and fluid compositions. The key feature of this correlation is finding the plait point at which the vapor and liquid compositions are the same. In his approach, at a specified pressure and temperature injection gas is mixed with the reservoir fluid so that the mixture is in the two-phase region, and flash calculation is performed for each phase. The flashed liquid is mixed with the injection gas and flash calculation is repeated till the liquid fraction composition and the vapor composition are the same. When liquid and vapor compositions are the same, then this (by definition) is the plait point and the pressure of the performed flash calculations is the MMP.

In 1985, Glasø [20] proposed a generalized correlation which was derived from the graphical correlations given by Benham et al. [3]. His correlation predicts MMP for any multi-contact miscible displacements (i.e.,VGD, CGD and CO2) using LPG, CO2 or N2 gas. The input parameters for this correlation are: temperature, mole percent of the methane in the injection gas, molecular weight of C2-C6 intermediates in the injection gas and the molecular weight of C7+ fraction of the oil. In addition, a paraffinicity characterization factor as reported by Watson [59], was defined as a correction to the C7+ molecular weight to account for oil composition effect on solubility of hydrocarbon gas in oil and thus on MMP. Glasø

uses 58 mol % methane and 42 mol% propane as a mixture that has equivalent solvency to CO2, and methane/ethane mixture as an equivalent mixture to N2.

In 1985, Alston et al. [2] developed a correlation for predicting MMP, which accounts for impurities within CO2 stream. The correlation parameters are: temperature, oil C5+ molecular weight, volatile oil fraction (C1 and N2), intermediate oil fraction (C2, C3, C4, H2S and CO2), and the composition of CO2. Due to impurities that may dilute CO2, Alston et al. suggested a correction factor to the MMP in terms of weighted average pseudo-critical temperature.

In 1985, Sebastain et at. [47] studied the effect of up to 55 mole % impurities in CO2-rich injection gas on MMP. And similar to Alston et al. [2] a correlation was developed, but using the mole average pseudo-critical temperature of the gas and the MMP of pure CO2 with the same oil at the same conditions.

In 1986, Firoozabadi and Aziz [18] modeled the vaporizing-gas drive process with the Peng-Robinson equation of state and a compositional simulator. Based on a comparison of numerical and experimental results, they proposed a simple correlation for the estimation of MMP of Nitrogen and lean-gas (C1) systems. They noticed that exclusion of C6 from the intermediate fraction improves MMP prediction. This observation fits well with previous definition of intermediate fraction by Benham [3] Holm and Josendal [23] and others. The MMP was correlated as a function of molecular weights of heavy fractions of the oil, temperature and the molar concentration of intermediates in the oil.

In 1987, Luks et al. [33], similar to Kue's [32] method, presented a new algorithm for calculating MMP of condensing and vaporizing mechanisms.

In 1987, Orr and Silva [40] proposed a correlation for CO2 MMP as an extension to that of Holm and Josendal [23]. The correlation differs from that of Holm and Josendal by replacing the weight fraction of C5-through C30 in the C5+ fraction by

a C2+ weight fraction with partition coefficients. They demonstrated that the size of molecules is inversely proportional to the extraction efficiency.

In 1988, Eakin and Mitch [13] based on 102 rising bubble apparatus experiment observations, produced a general equation for MMP estimation using CO2, N2 and LNG solvents. The input parameters are solvent composition, oil C7+ fraction molecular weight and the pseudo-reduced temperature.

In 1988, Nouar and Flock [39] proposed a method for MMP estimation primarily for a VGD, and it can be used for CGD as well, using a very lean hydrocarbon gas (C1). The correlation is based on the ternary diagram concept. In their approach, MMP was correlated to temperature, and molecular weights of the intermediate and heavy components in a ternary diagram, and defined MMP as the pressure at which the limiting tie-line passes through the point representing the oil composition.

In 1990, Monroe et al. [37] studied four component mixture containing CO2, methane, butane, and decane using quaternary diagram, and explained the insensitivity of one-dimensional, 1-D, displacement to the presence of methane. They indicated that methane strongly preferentially partitions into the more mobile vapor phase and concentrates in the leading edge of the transition zone so that the injection CO2 when it comes in contact with the hydrocarbon mixtures does not see methane. This explains why efficiency and MMP of 1-D CO2 injection processes is insensitive to the presence of methane in the oil composition as indicated by Yellig and Metcalfe, Hole and Josendal and others. Monroe et al. disagreed with the idea of using Pb as MMP for systems below Pb revealed by Yellig and Metcalfe, and stated that it is possible to have near miscible displacement for such systems. Also they established the existence of a third critical tie-line, named as cross-over tie-line [24], which influences the miscibility process.

In 1996, John and Orr [28] extended the four-component displacement theory to displacement by a single gas component of multi-component reservoir fluid on a

ternary diagram. In their work they concluded that multi-contact miscibility can be achieved even below the bubble point pressure (in the two phase region). They demonstrated that three-component displacement systems can only show VGD or CGD, whereas quaternary diagrams (i.e., four component representations) can display features of both VGD and CGD. They also demonstrated that displacement of oil contains methane (C1), ethane (C2) and heavier components by CO2 have features of both VGD/CGD, and proposed a mathematical procedure that can be used to find the key tie-line that controls miscibility.

In 1998, Wang and Orr [58] extended the work of John and Orr [28] for displacement involving any number of components in either the gas or the oil. They presented a numerical approach for solving the tie-line intersection equations for calculating MMPs.

3.5.3 Miscibility below Slim-tube Determined MMP

Most researchers use slim-tube determined MMP to generate and/or calibrate correlations, and/or tune EOS models. However, a slim-tube test is a simplified one dimensional experiment, and most of the factors affecting a real gas injection process whether miscible or immiscible are minimized. A slim-tube test is usually conducted at pressures greater than the bubble point pressure, Pb, and if the real reservoir pressure is lower than the Pb, Yellig and Metcalfe [62] suggested using the Pb as MMP. This suggestion was denied later by Monroe et al. [37].

It is well established that MMP is an important screening factor for the selection of solvent type, and thus operating conditions, nevertheless one can notice the following:

1. No industry agreement upon definition of the slim-tube determined MMP except the general definition, that it is the lowest pressure at which miscibility can be achieved. Even the criteria used in slim-tube tests vary. Some

researchers use 94 % oil recovery at 1.2 PV, others use 90% recovery at 1 PV, and others suggest 80% oil recovery at breakthrough and 40,000 scf/stb GOR.

2. No standard apparatus is used for MMP determination, although Yellig and Metcalfe [62] suggest slim-tube apparatus to be the industry standard, however characteristics of the apparatus (permeability, ID) vary from one lab to another, and injection rates are different, although every lab tries to use characteristics that can minimize flow effects.
3. No standard method or correlation for MMP below Pb, some authors suggest MMP is greater than or equal to Pb, others noticed that miscibility can be achieved even below bubble point pressure, others argue that even below Pb, near miscibility can be achieved.
4. Finally, the overall recovery in a gas injection process below slim-tube MMP in a real reservoir is not significantly lower than performing the process below experimental MMP.

3.6 Evaluation of Laboratory 1-D Experiments

The development of miscibility during 1-D miscible displacement using CO2 or natural gas has been discussed in literature. The methodology by which different researchers explain their observations differ depends upon the purpose of their research. 1-D models such as slim-tubes, long cores, and numerical simulations are usually represented by a source and a sink located at the two ends of the model. Generally, the methodologies in judging miscibility conditions can be divided into two main categories:

1. Experimental:
    a. Monitoring the produced fluid compositions: in this type of observation, the produced fluids are some times treated as groups of hydrocarbons such as light, intermediate, and heavier fractions, however the borders of the groups are not fixed. In other instances the effluents are treated as individual components. The maximum number of hydrocarbons studied is four.

b. Estimating components distribution along the displacement path: here the estimations are based upon the change in the color of the produced zones. An indication of a new zone arrival is when the color of the oil gets lighter.

2. Numerical: simulation of 1-D models backed by tuned EOS is a good means which can predict phase behavior along the displacement path.

Holm and Josendal [22] during their explanation of mechanisms of oil displacement by carbon dioxide, used a slim-tube apparatus to measure MMP during CO2 injection. The produced fluids were collected in a trap, then oil and the separated gas production composition was measured. Residual oil and possible asphaltic deposits were removed using solvents. Holm and Josendal noticed the increase in oil density which is a surprise at first to the observer as they said, and decrease in the oil viscosity as CO2 dissolves into it. They divided the composition of the produced fluids into light hydrocarbons (C3-C6), gasoline fraction (C7-C30), and heavier components, and based on the oil recovery and produced fluids compositions they explained CO2 floods at various pressures by the following diagrams, Figure 3-17 a and b for a stock-tank oil (i.e., C1 removed), and Figure 3-17 c for oil in place (i.e., with C1, C2, etc.). CO2 is injected at supercritical conditions.

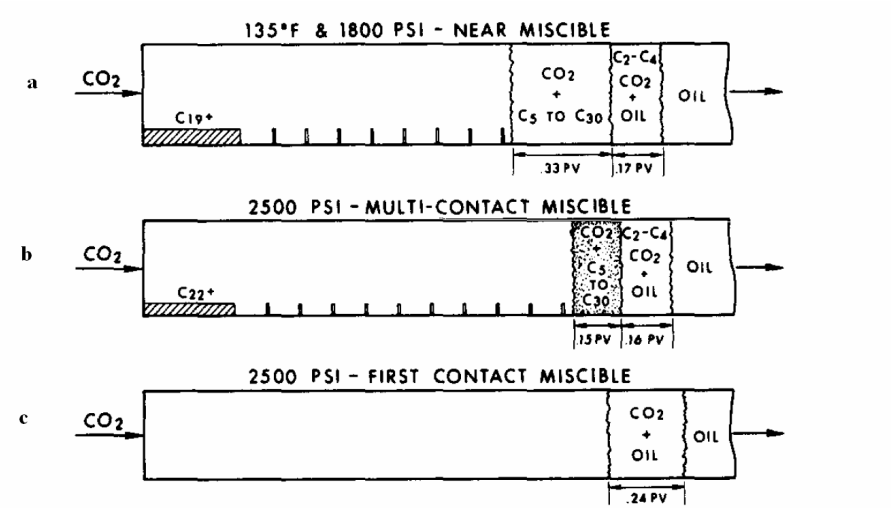

Figure 3-17: Schematic of slim-tube CO2 displacement at miscible and near miscible conditions at 135 °F (After [22])

Holm and Josendal explained the diagrams a, and b (near-miscible, and multiple-contact miscible) as follows; at first, CO2 is absorbed into the oil, then light hydrocarbons (C2 to C4) are vaporized from the oil. An equilibrium gas is developed. The extra injection of CO2 extracts heavier hydrocarbons approximately C5 through C30, this forms a transition zone separating original oil from pure CO2. For diagram c (first-contact miscible) no extraction occurred, and the transition zone was a single phase (oil + CO2) and the composition of the oil in the transition zone was the same as that of the original oil in place. They confirmed the presence of a miscible bank which forms, disperses, and re-forms again. Holm and Josendal also concluded that the presence of methane in the injection gas adversely affect CO2 flood performance, whereas the presence of methane in the oil in place has little effect on MMP.

Shelton and Schneider [48] during their study of the effect of water injection on miscible flooding using CO2, they calculated the recovery performance by analyzing produced fluids, and described the miscible displacement process in a uniform linear system as shown in Figure 3-18 .

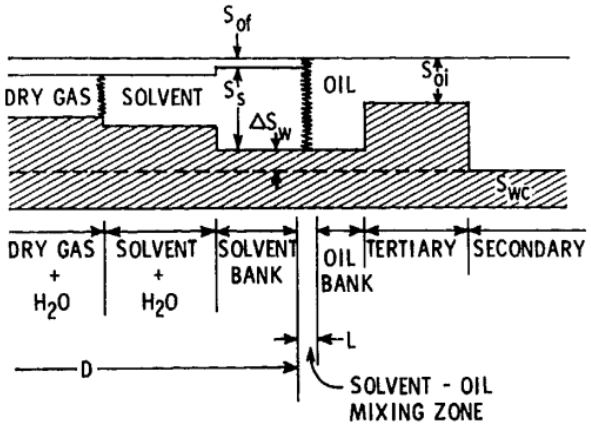

Figure 3-18: Banks formed in Tertiary system by solvent or solvent -and water injection at 120 °F and 1665 psia (After [48])

Tiffin and Yellig [56] evaluated the effect of mobile water on multiple-contact miscible gas injection (CO2), they evaluated the overall oil recovery and the

displacement mechanism indicated by produced fluid compositions. They monitored fluid compositions at the outlet, and subdivided the effluent molar composition into four fractions (CO2, C1, C2 through C6, and C7+), then normalized these fractions by dividing them by the amount of each fraction in the original reservoir oil, and then plotted the normalized compositions as functions of HCPV of CO2 injected for oil and water-wet cores and different WAG ratios, Figure 3-19, they highlighted the presence of C1 and intermediate components bank (with respect to the C7+ fraction) in the produced fluids.

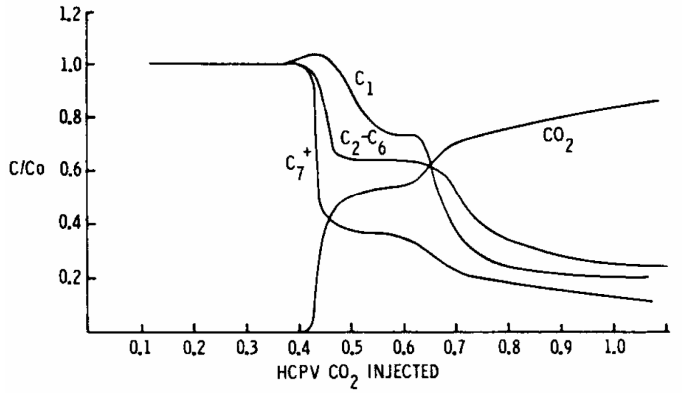

Figure 3-19: Normalized produced-fluid compositions, during CO2 tertiary displacement, at 130 °F and 1900 psia, (After[56])

Nghiem and Li [38] used compositional model to simulate CO2 slim-tube displacement and produced results consistent with experimental observations. They neglected the effects of gravity and capillary pressure. They discretized the slim-tube into 40 equal grid cells, CO2 is injected in cell 1, and fluids are produced from cell 40, they preserved the pressure at the outlet cell at the initial pressure of the slim-tube.

Nghiem and Li put emphasis on the behavior of density, saturation change for the oil, CO2-rich liquid, and gas phases with respect to distance between the injection and the producing cells at three pressures representing immiscible, near-miscible, and miscible displacements respectively. Figure 3-20 depicts saturation and density profile along the 1-D model (simulating slim-tube) at 0.81 PV CO2 injected during near miscible displacement.

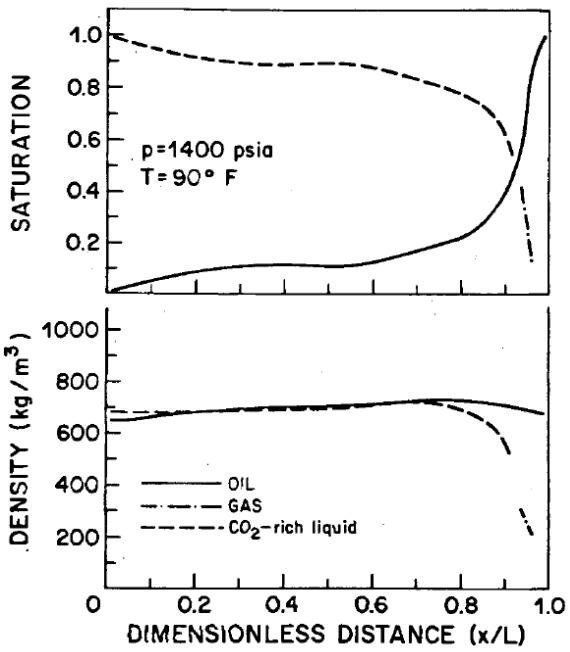

Figure 3-20: Computed saturation and density profiles at 90 °F and 1400 psia and at 0.81 PV CO2 injected, (After[38])

Zick [63] performed slim-tube experiments using a depleted reservoir fluid sample. The effluent was separated at room conditions into liquid and vapor phases. The vapor volume and composition were measured. Zick investigated the effect of increasing methane concentration in the solvent on MMP. Zick simulated using PR-EOS condensing- and vaporizing-gas drive processes for three component mixtures of methane-butane-decane, and compared component saturation, density, and K-value profiles along the slim-tube during the condensing and vaporizing gas drive processes, Figure 3-21.

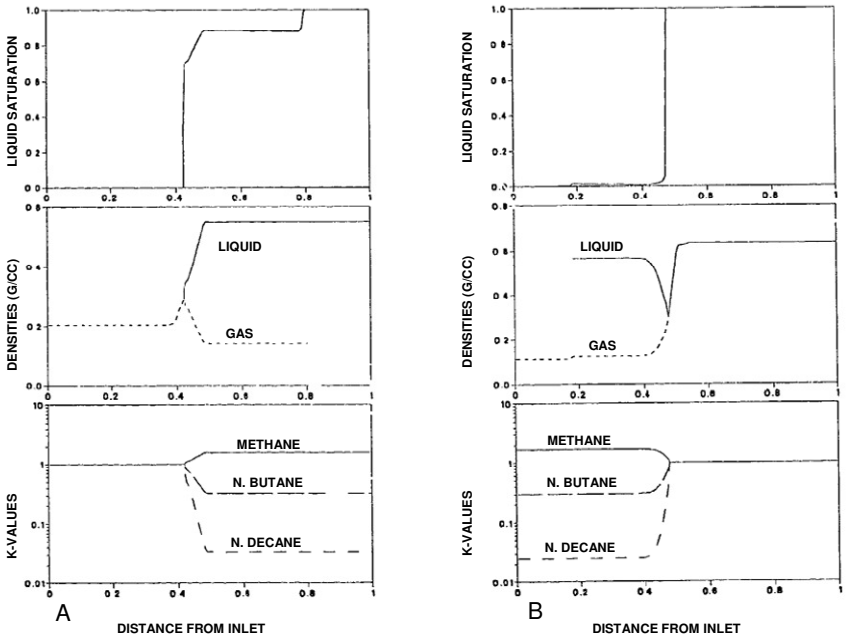

Figure 3-21: Simulated slim-tube profile for (A) condensing-gas (B) vaporizing-gas drive, (After[63])

Monroe et al. [37] investigated continuous CO2 displacement for four component systems using pure CO2 to displace C1/C4/C10 mixtures. They reproduced measured phase compositions and densities with PR-EOS, and used their tuned EOS to predict saturation profiles using 1-D CO2 displacement and constructed composition paths for each component, Figure 3-22.

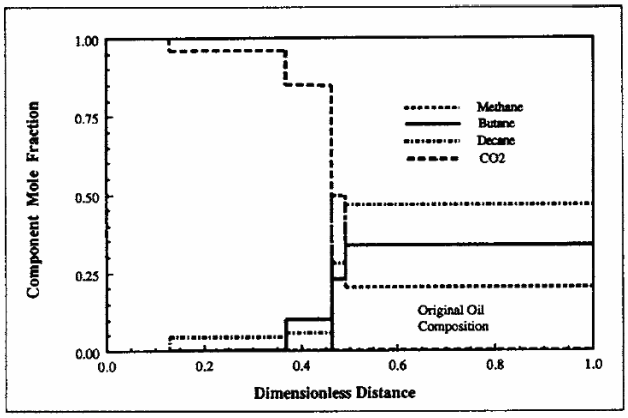

Figure 3-22: Composition profile for displacement of a CO2/C1/C4/C10 mixture by CO2 at 160 F and 1600 psia (After [37])

They also reported recovery of each component versus pore volume injected, Figure 3-23. The primary goal was to examine the effect of dissolved C1 on the over all displacement and they concluded that the displacement efficiency in 1-D CO2 floods is insensitive to the amount of dissolved C1, this conclusion agrees with Holm, Josendal [23], and actually explains why MMP is insensitive to the amount of dissolved C1.

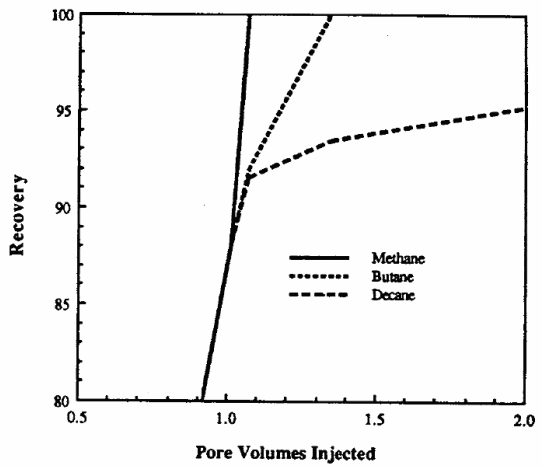

Figure 3-23: Component recovery in CO2 displacement of C1/C4/C10 mixture, (After [37])

CHAPTER 4 CO2-Rock and Mobile Water Interaction

4.1 CO2/Mobile Water

Water saturation in a reservoir ranges from its initial value, Swc, to maximum of 1-Sor, and formation water can be stagnant or mobile depending on the height above an oil/water contact. However, after a secondary recovery (water flood) mobile water can occur over the entire reservoir volume contacted by the flood front. In tertiary recovery process like CO2 miscible displacement, the effect of mobile water i.e., Sw>Swc is an important factor affecting the displacement efficiency, because water will be displaced along with the oil and two-phase flow occurs ahead of the displacement front [12]. Also solvent may breakthrough resulting in simultaneous solvent/water flow in some regions.

The low viscosity of CO2 results in an unfavorable gas/oil mobility ratio in most CO2 floods, and subsequently adversely affects sweep-out [19]. For example, at a reservoir temperature of 110 °F, CO2 has a viscosity of 0.04 cp at 1,500 psi, whereas at 2500 psi, the viscosity is about 0.06 cp, Figure 4-1. In WAG operations, water is injected in slugs alternating CO2 slugs, thus CO2 mobility is reduced by reducing its relative permeability.

It is recommended [19] that in the presence of mobile water, the mobility ratio between an oil bank and the solvent displacing the oil bank be calculated in the following form:

$$M = \frac{\left(\frac{k_s}{\mu s} + \frac{k_w}{\mu_w}\right)_{sw\,avg}}{\left(\frac{k_o}{\mu_o} + \frac{k_w}{\mu_w}\right)_{ow\,avg}}$$

Where:

k_s and μ_s are solvent relative permeability and viscosity respectively measured in the lab

sw avg and *ow avg*: are the average solvent/water and the average oil/water saturation

It has been experimentally proven that the presence of water as a connate saturation or mobile saturation, whether from water flood or aquifer encroachment, has no significant effect on the fluid-fluid phase behavior and thus no impact on miscibility i.e., the development of the multiple contact miscibility between a solvent (CO2) and residual oil will be as if all water is stagnant, despite the fact that mobile water has a significant impact on relative permeability characteristics[56].

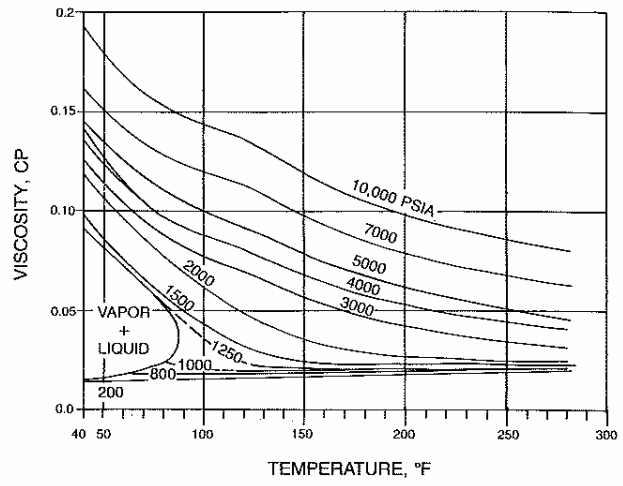

Figure 4-1: Viscosity of CO2 as a function of pressure and temperature, (After [19])

Also water blocks part of the oil away from the solvent (CO2) and thus reduces the ability of the solvent to contact the oil. This also affects miscibility. In such a case, CO2 is somewhat more efficient than other solvents that it can diffuse in water and contact blocked oil. Campbell and Orr[5] demonstrated that CO2 contacts trapped oil in dead-end pores by diffusing through water to reach, to swell, and to reconnect isolated droplets. Figure 4-2 schematically illustrates the mechanism by which CO2 recovers trapped oil in dead-ends or from water shielded oil droplets. At first, CO2

diffuses through the water, when CO2 contacts the oil, the oil swells and forces the water to leave the pore. The oil is then recovered as if no mobile water was present. *Generally the mobile water has a detrimental effect on the miscible displacement of the non-wetting phase, whereas the effect on the miscibility of the wetting phase is less significant.*

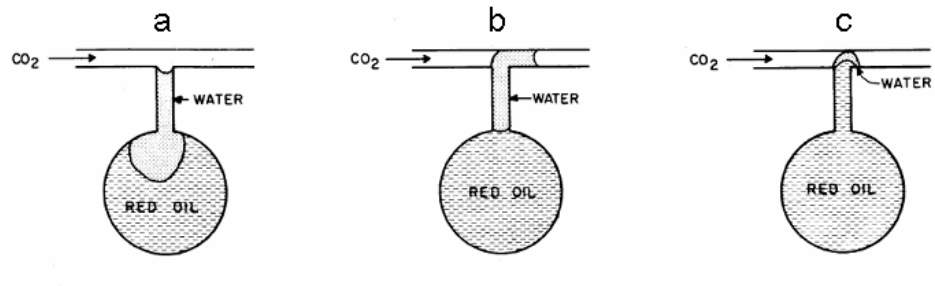

Figure 4-2: Oil recovery from dead-end pore by CO2 at 77 °F and 1200 psia (After [5])

Another side of CO2 injection in the presence of mobile water is the solubility of CO2 in brine. This means that a portion of the volume of CO2 injected in a miscible flood will be dissolved either by the formation water or the injected water in a secondary water flood or WAG process [19] this results in less volume of CO2 available for miscible displacement for the oil, as seen in Figure 4-3, Figure 4-4.
Solubility of CO2 in fresh water increases with increasing pressure but decreases with increasing temperature and salinity.

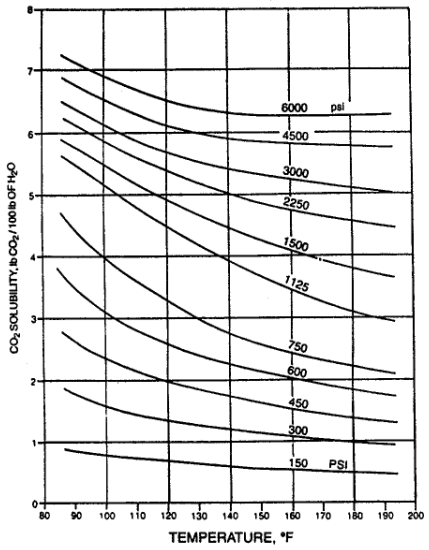

Figure 4-3: Effect of temperature and pressure on solubility of CO2 in fresh water (After [19])

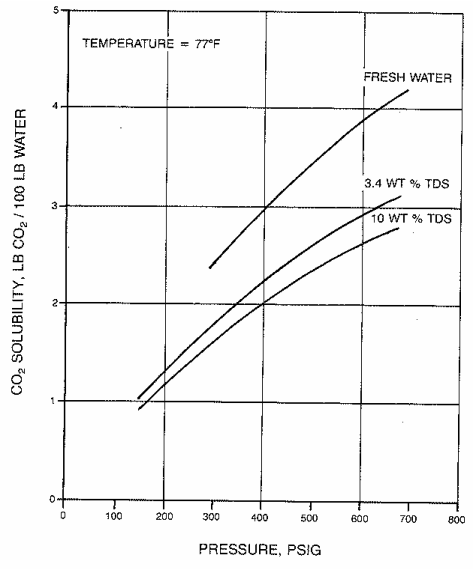

Figure 4-4: Effect of salinity on CO2 solubility in water (After [19])

To get a feeling about volume of CO2 that will not be available for miscible displacement, the following example from Ref. [12] explains:

Example: CO2 is to be injected into a reservoir at 1500 psia and 150 °F. Estimate the percentage loss of CO2 by solubility into water in the reservoir, assume that 1.0×10^6 scf of CO2 contacts residual water phase that is at a 25% saturation. Formation porosity is 0.20, and oil saturation is negligible. Assume that water is fresh and that water upon contact with CO2 water becomes saturated with CO2.

Solution: Calculate the volume of reservoir invaded by the CO2.

From Figure 4-5, density of CO2 (ρ_{CO_2}) at 1500 psia and 150 °F (65.56 °C) is 0.31 g/cm3

Convert density into field units; 1 g/cm3 = 62.4 lbm/ft3

$\rho_{CO_2} = 0.31\,\text{g/cm3}[(62.4\,\text{lbm/ft3})/(\text{g/cm3})] = 19.3\,\text{lbm/ft3}$

Since 1 lbm-mole of any gas at standard conditions (14.7 psia and 60 °F) occupies 379 scf, and 1 lbm-mole of CO2 is 44 lbm. Thus the mass of CO2 (m_{CO_2}) at standard conditions is:

$$m_{CO_2} = 1\times10^6 \text{ scf} / (379 \text{ scf/44 lbm}) = 1.16\times10^5 \text{ lbm}$$

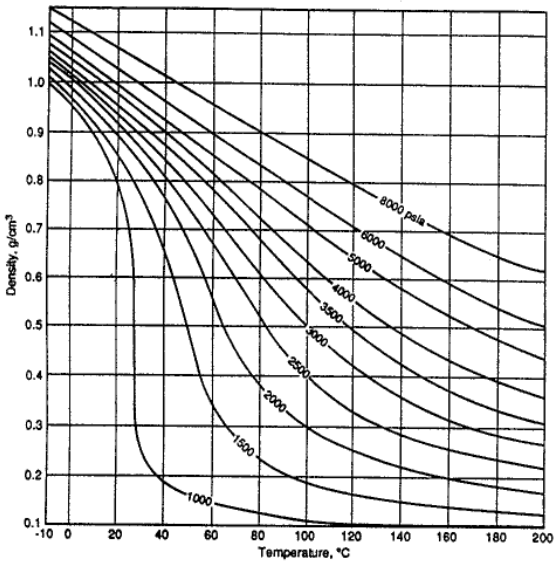

Figure 4-5: CO2 density vs. temperature at various pressures, (After [19])

Volume of CO2 at reservoir conditions (V_{iCO_2}) is calculated by dividing CO2 mass by its density at reservoir conditions;

$$V_{iCO2} = 1.16\times10^5 \text{ lbm}\left(\frac{1}{19.3 \text{ lbm/ft}^3}\right) = 6{,}010 \text{ ft}^3$$

The pore volume invaded by CO2 is calculated as;

$$\begin{aligned} V_P &= 6{,}010 \text{ ft}^3 / \phi S_{CO_2} \\ &= 6{,}010 \text{ ft}^3 / [0.20(1-0.25)] \\ &= 4.01\times10^4 \text{ ft}^3, \end{aligned}$$

Where; ø is the reservoir porosity, and S_{CO_2} is CO2 saturation

The mass of water in the pore volume contacted by CO2 is;

$$m_w = 4.01\times10^4\,\text{ft}^3\,\phi\,S_w\rho_{\text{H}_2\text{O}}$$
$$= 4.01\times10^4\,\text{ft}^3\times0.20\times0.25\times62.4\,\text{lbm/ft}^3$$
$$= 1.25\times10^5\,\text{lbm H}_2\text{O}$$

Where; S_w and ρ_{H_2O} are water saturation and density respectively

From Figure 4-3,

CO2 solubility ≈ 4.2 lbm CO2 / 100 lbm H2O

$$\text{and CO}_2\text{ loss} = \frac{4.2\ \text{lbm CO}_2}{100\,\text{lbm H}_2\text{O}}\times1.25\times10^5\,\text{lbm H}_2\text{O}$$
$$= 5{,}250\,\text{lbm}$$

$$\text{and percentage loss of CO}_2 = \frac{5{,}250}{1{,}16\times10^5} \approx 4.5\,\%\text{ of CO}_2\text{ injected}$$

If water was saline as it is the case of most formation waters, from Figure 4-4 if the water had a 3% to 10% total dissolved solids, only about 25% to 30% of the 4.5% will be lost, this means that the higher the salinity the less CO2 will be lost at a given pressure and temperature. The loss of injection CO2 from one side has a positive effect on the efficiency of the miscible process by collecting dead-oil droplets as mentioned earlier, however, on the other side from operational view point, more CO2 volumes are needed to inject a presumed solvent volumes

4.2 CO2/Rock Interaction

CO2 injection in petroleum reservoirs or aquifers for EOR or sequestration has received a great attention recently. Depending on time, thermodynamic conditions, fluid and rock compositions and the flow regime, CO2 injection can result in sever fluid/rock interaction.

Due to the high CO2 flow rates in the near wellbore region, the non equilibrium geochemical reactions may result in an unstable dissolution, thus dissolution fingers or “wormholes” are created, whereas in the far field region CO2 and water flow at reduced rate which results in uniform geochemical reactions which likely to result in a uniform pore structure modification [14]. Coupling of reaction and transport

"flow" phenomena controls the dissolution regime which ranges from wormholes near the injector to uniform dissolution in the far field.

The CO2/rock interaction affects pore bodies as well as the pore throats, and its direct cause is the chemical reaction between the carbonic acid formed by dissolution of CO2 into brine, and carbonates. Carbonates form the main body of rocks like limestone, dolomite, and anhydrite, whereas, the sandstones contain small amounts of carbonaceous material, primarily as cements, consolidating the sand grains and creating the pore structure [26].

When CO2 is injected in the reservoir, it contacts water, whether this water is flood-water or aquifer water, CO2 dissolves into brine forming carbonic acid (H_2CO_3) which dissociates to give acid that reacts with calcite present in carbonates (Calcium Carbonate, $CaCO_3$), as seen in the following chemical reactions:

$$CO_2 + H_2O \Leftrightarrow H_2CO_3 \Leftrightarrow H^+ + HCO_3^-$$
$$H^+ + HCO_3^- + CaCO_3 \Leftrightarrow Ca^{2+} + 2HCO_3^-$$

Where HCO3 is an intermediate form in the deprotonation of the carbonic acid

The acidity of the formed carbonic acid is not likely to be reduced as long as CO2 is injected, therefore this chemical reaction will continue resulting in precipitation or dissolution reactions, and consequently in formation damage or enhanced permeability, respectively, and thereby injectivity alteration.

In their experimental work on a carbonate cores, Egermann et al., [14] came to the conclusion that the flow rate, the composition of fluids initially present in the core, and brine composition are the major factors controlling dissolution/re-precipitation phenomena. Figure 4-6 shows wormholes and homogeneous alteration effects resulting from continuous acid injection.

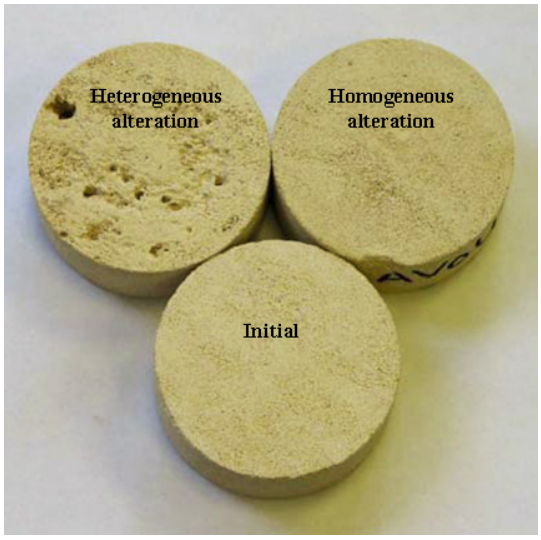

Figure 4-6: Effect of continuous acid injection on the dissolution regimes (After [15])

As a result of the pore structure changes due to chemical reactions, the petrophysical properties such as porosity and permeability will be modified accordingly. This means that other rock properties related to porosity and permeability such as relative permeability curves and capillary pressure curves are altered too. However to what extent?

Dissolution of CO2 into brine in a WAG displacement is different from that of carbonated water or "Fizz flood" injection, in the earlier two phases flow simultaneously, and therefore the acidity is not limited, while in the later only one phase flows and thus the acidity is gradually removed as dissolution proceeds.

As discussed in section (4.1), CO2 dissolves into brine and diffuses through water to contact trapped oil, this phenomenon takes place simultaneously with the dissolution process discussed in this section. Therefore the injected volume of CO2 might be divided into the following portions: one portion of the injected CO2 dissolves into brine forming the carbonic acid which reacts with the carbonate materials in pores and pore throats, another portion diffuses through water to reach, to swell, and to reconnect isolated oil droplets, while another portion miscibly displaces continuous oil phase. The first two portions are functions of time.

CHAPTER 5 WAG Process

The WAG process is a combination of two traditional techniques of enhanced oil recovery: waterflooding and gas injection [26]. As mentioned in CHAPTER 4 , at reservoir conditions, the viscosity of CO2 is very low related to that of either water or oil. This low viscosity results in an unfavorable mobility ratio i.e., >1. The mobility ratio is defined as the ratio of the mobility of the displacing fluid to that of the displaced fluid, or $M = \frac{\lambda_1}{\lambda_2}$, where λ_1 and λ_2 are the mobilities of the displacing and displaced fluids respectively.

$\lambda_1 = \frac{k_{r1}}{\mu_1}$ and $\lambda_2 = \frac{k_{r2}}{\mu_2}$, where k_{r1}, k_{r2} and μ_1, μ_2 are the relative permeabilities and viscosities of the displacing and displaced fluids respectively.

In practice a mobility ratio can be between 8 and 50 [12], [57]. The direct result of such unfavorable mobility ratio is viscous fingering and subsequently less volumetric sweep efficiency, Figure 5-1.

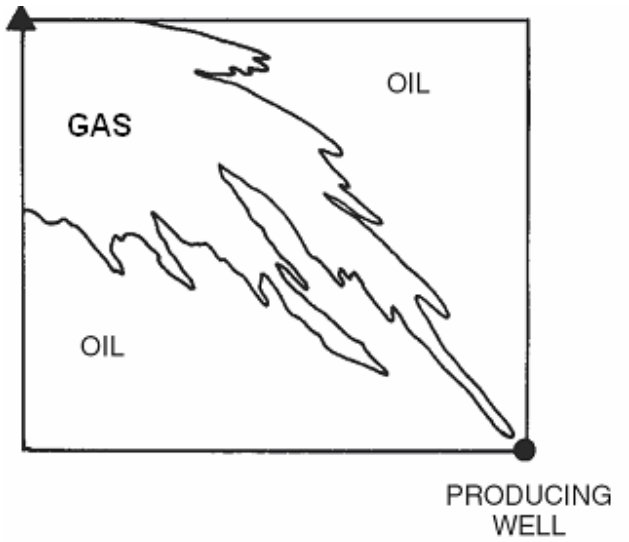

Figure 5-1: Schematic of viscous fingering

One method to overcome this problem is the injection of specified volumes (in practice called slugs) of water followed by gas in alternate manner, the flow of the two fluids water and gas simultaneously reduces relative permeability to each phase, and total mobility will be less than that of the injected gas alone, this means improvement to the mobility ratio. This method is named water alternating gas or WAG and it is in practice since Mobil conducted the first WAG project in North Pembina field in Alberta, Canada in 1957 [26].

WAG displacement can be a secondary process (i.e., water and gas are injected simultaneously without pre-waterflooding), or a tertiary displacement after water flooding. The ratio of water to gas can range from 0.5 to 4 volume of water per volume of gas at reservoir conditions [12], [26]. The size of gas slugs range from 0.1% to 2% PV. Reported cumulative injected CO2 can range from 15% to 30% HCPV, and in some reports it can be more or less than this range.

5.1 Laboratory Experiments

Laboratory experiments are used to simulate WAG process, these experiments start by saturating a core sample with 100% water, then oil is injected to displace water to the connate water saturation Swc (drainage). Water is injected to displace oil to its residual saturation Sorw (imbibition). Water and gas are injected simultaneously at a specified ratio (note, in field practices, solvent and water are injected alternately, however, because the size of the solvent slugs are usually small, they rapidly dissipate in the water approaching the simultaneous injection, however simultaneous CO2/water injection is not practical method to control mobility due to completion costs, gravity segregation, etc.,). Recoveries are measured by material balance. Sorw is strongly related to wettability. In strong water-wet rocks the injected water blocks oil and causes oil trapping and subsequently less recovery, whereas oil trapping is much less in oil-wet rocks, however, the overall recovery should be the same because of the solubility of CO2 in water as discussed in section

4.1. Trapping of oil by water works against the advantage of improved mobility in a WAG displacement.

5.2 Solvent to Water Ratio (WAG Ratio)

The efficiency of any WAG project is highly correlated to the WAG ratio which is the ratio of solvent slug to water slug in one full WAG cycle. The size of a slug is normally related to the Hydrocarbon Pore Volume, HCPV. For example, if WAG ratio is 0.5:1 and the slug of gas (solvent) is 7.5% HCPV then the slug of water is 15% HCPV. WAG ratio of 1:0 represents continuous gas injection, whereas 0:1 represents continuous water injection The solvent to water ratio is a very important parameter in WAG practices, because, if a small slug of water is injected then the solvent velocity will be higher and results in an unfavorable mobility ratio and subsequently fingering of solvent into the oil bank, on the other hand if the size of water slug is too large then water will move faster than the solvent resulting in increased oil trapping. Hybrid-WAG is a special type of WAG process, in which most of the CO2 available for injection is injected, followed by the remaining fraction divided into 1:1 WAG ratios, this scheme proved efficient.

Wettability dictates WAG ratio, it was proved experimentally that a water-wet rocks show an optimum WAG ratio of 1:0 which represents continuous gas injection, oil-wet rock on the other hand, have optimum WAG ratio of about 1:1, Figure 5-2, whereas in mixed-wet formations maximum recovery is strongly related to slug size in the case of CO2 secondary flooding than in the case of tertiary recovery [26], [25]. The oil recovery is adversely affected by mobile water in water-wet formations, but the effect of mobile water is small to negligible in mixed-wet and preferentially oil-wet [12].

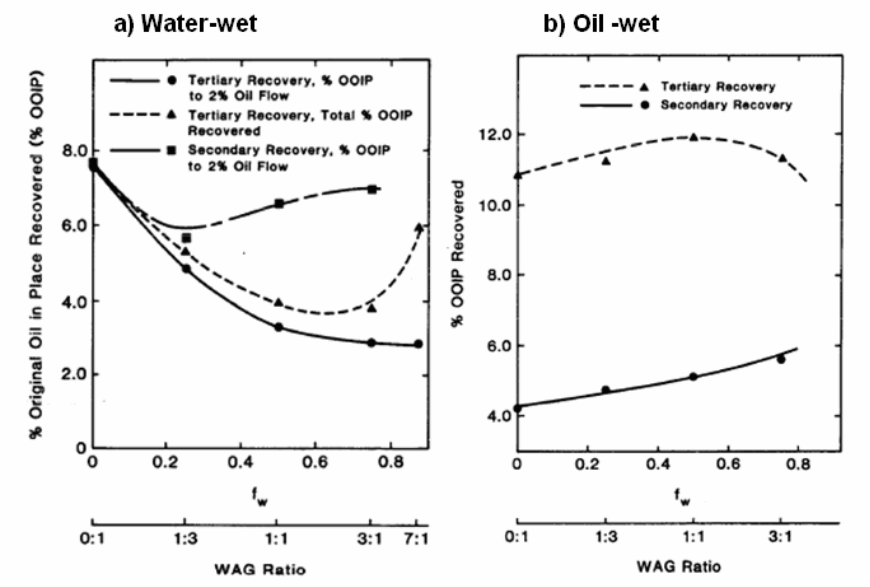

Figure 5-2: Extra oil recovery vs. WAG ratio for (a) water-wet, (b) oil-wet quarter-five-spot model, (After [25])

5.3 Oil Trapping by Water during WAG Displacement

Injection of water alternating with solvent or CO2 normally results in trapping of oil by water that would otherwise be contacted by the CO2, and the trapped oil remains blocked from the mobile flowing oil. The recovery of the trapped oil by CO2 is a time-dependent process [51]. That is the slower the displacement velocity the longer the time for mass transfer and diffusion.

There are different approaches as to estimate the trapped oil in a secondary or tertiary displacement, Shelton and Schneider [48] used oil relative permeability to estimate PV percent of trapped oil. They demonstrated that at a given k_{ro} the saturation difference between the drainage and imbibition curves represents the trapped oil which is the oil that may not be contacted by an injected solvent. From Figure 5-3 for example, at k_{ro}=10 percent, the trapped oil saturation is approximately 13 percent PV.

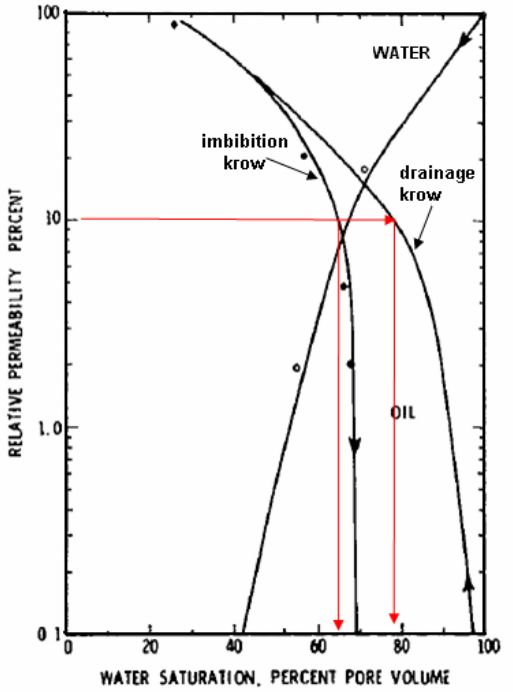

Figure 5-3: Relative permeability condition during miscible displacement, (After [48])

Another correlation may be useful in estimating blocked oil saturation proposed by Raimondi and Torcaso [42] for strongly water-wet rocks,

$$S_{or,wb} = \frac{S_{or}}{1 + k_{ro} / k_{rw}}$$

Todd et al. [57] modified this equation to account for the degree of oil-wetness by introducing the parameter α.

$$S_{or,wb} = \frac{S_{or}}{1 + \alpha k_{ro} / k_{rw}}$$

Where Sor is residual oil saturation after water flood, and $S_{or,wb}$ is after miscible displacement, and α is an empirical constant ranging from 1 to any higher value, for example a value of 1 represents a strong water-wet (i.e., strong oil blocking), whereas a value of 25 represents higher oil-wetness (weaker oil blocking), Figure 5-4. The terms trapping and blocking are used interchangeably.

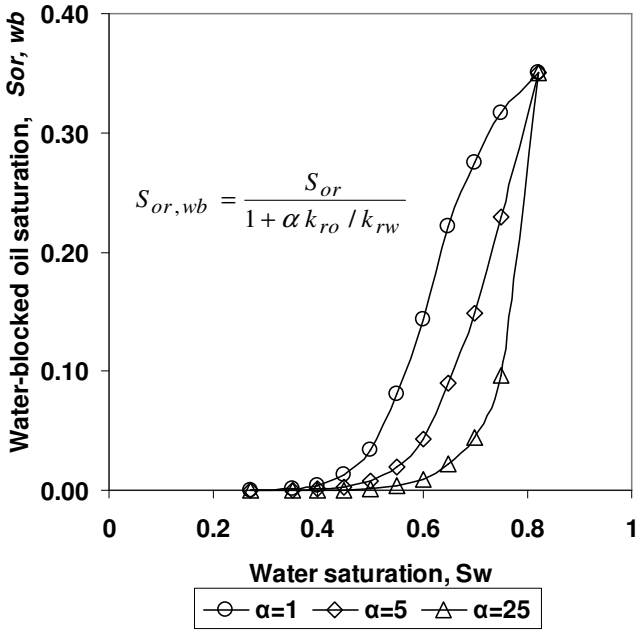

Figure 5-4: Example of water-blocking function: Sor=0.35, μw=1, μo=2, kro / krw is a function of water saturation

5.4 Wettability Alteration during WAG Displacement

Wettability is a controlling parameter that conditions any EOR process, oil blocking is strongly related to wettability [25]. In case of water-wet oil blocking by water is more pronounced, whereas in mixed-wet or oil-wet the effect is lesser to negligible [51]. However, in the case of water-wet, mixed-wet or oil-wet formations CO2 can eventually wet the pore surfaces at reservoir conditions, and occupies the small pores and it will be present in the large pores as a film on the rock surfaces. The presence of that film will affect the petrophysical properties such as relative permeability and capillary pressure curves [6]. This phenomenon adds another modification to relative permeability curves. Note, that the originally water/oil system, with respect to relative permeability, is the same as in a water flood process, however, during a tertiary process the system becomes water/oil/gas system with the same wettabiliy characteristics despite the change in relative permeability to water and oil. However if CO2 contacts the pore surfaces and

subsequently changes its wettabiliy the whole system will change, therefore CO2/rock interaction should be taken into account.

Due to the cyclic nature of the WAG displacement process, the water saturation increases during the water slug causing imbibition process, and decreases during the gas slug resulting in a drainage process [26]. This frequent change in the direction of saturation must necessarily have an impact on wettabiliy characteristics.

5.5 Injectivity Alteration during WAG Displacement

Besides the concerns about oil blocking by water, and loss of CO2 by solubility in brine, gas and water injectivity reduction is another concern in WAG process [46], although injectivity may be improved in some examples. John and Reid [26] presented a comprehensive review of the injectivity abnormalities. They addressed two major concerns; (1) the cause of unexpected low injectivity during gas injection, and (2) the reason for reduced brine injectivity after gas injection. These two concerns where observed in a number of WAG projects, Figure 5-5. They related the low injectivity of gas mainly to wettability alteration and three-phase effects

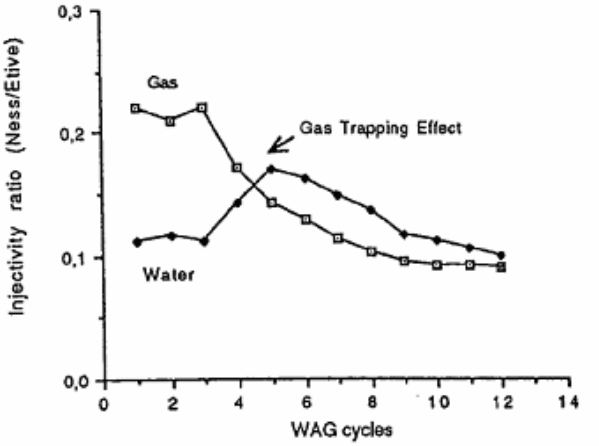

Figure 5-5: Injectivity ratio at water-gas cycles (After [52])

The problem with losing injectivity is translated into loss in reservoir pressure (i.e., high withdrawals, no replacement) which may affect miscibility and results in lower oil recovery. John and Reid [26] expected an average of 20% reduction of the water injectivity during WAG displacement. Practical attempts to overcome this concern include controlling mobility by decreasing WAG ratio, increasing injection pressure, and introducing additional wells.

Higher water injectivity during WAG process is attributed to combined effects of (1) high heterogeneity near wellbore such as layering and thief zones, (2) crossflow within the reservoir which increases communication between high-permeability streaks stacked above one another, (3) oil viscosity reduction by CO2, (4) penetration of CO2 into low-permeability zones, (5) channeling of CO2 through high-permeability zones, (6) solubility of CO2 in brine near the wellbore increases brine saturation [45], and dissolution of carbonates.

In some WAG applications, reduced water injectivity is observed, the reduction are attributed to (1) wettabiliy alteration which has a strong impact on fluid flow in porous media, (2) chemical effects such as formation of carbonic acid when CO2 contacts water, (3) dissolution, (4) precipitation, (5) particle migration.

CHAPTER 6 Model description

The goal of this thesis as mentioned was to study the effect of operating conditions during CO2 miscible displacement. Two models were considered, (1) a 1-D artificial model was considered in order to simulate to some extent slim-tube tests and to come up with general conclusions, and (2) then a real 3-D reservoir model was selected as a case study. A detailed description of the phase behavior is provided in CHAPTER 7 . A description of the EOS model is given in Appendix A.

The compositional simulator Eclipse 300 was used in simulating the models. Tuned EOS model based on PVT experiments on fluid samples from Sarir field was used for both models as well.

6.1 1-D Model

The 1-D linear model has 50 grid blocks, with 10×10×5 ft grid dimensions, (Figure 6-1). The model is homogeneous and isotropic, porosity is 15%, permeability is 50 mD. Layer thickness is 5 ft. The 500 ft long model is sufficient to simulate flow behavior from an injector placed in cell number 1 to a producer located in cell number 50. In a real reservoir model, the 500 ft length of the system is usually represented by the dimensions of one grid block.

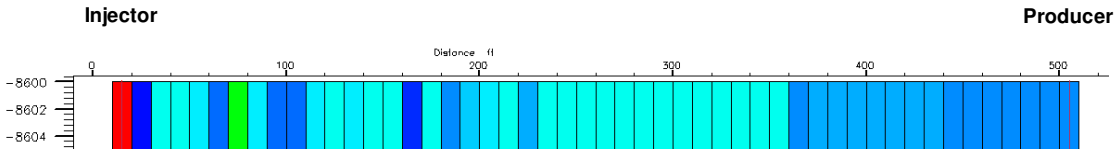

Figure 6-1: 1-D model shows saturation pressure profile between an injector and a producer (The Y and Z dimensions of the grid blocks are exaggerated for better visualization)

A two dimensional, 2-D, model was also considered, however, the problem was more complicated. Figure 6-2 depicts a wave of high saturation pressure in the center of the model. This is a gas slug flowing in the second layer of the model. Due to the complexity of the problem on a 2-D model it was decided to step back to a 1-D model.

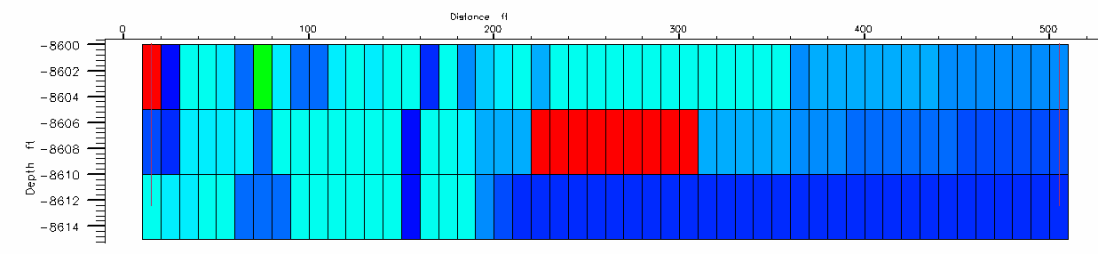

Figure 6-2: 2-D model shows saturation pressure profile between an injector and a producer

Oil-water and gas-oil relative permeability data used are those of Saturation Table no.1 from Sarir C-North model, see Appendix B.

For initialization, the top depth of the 1-D model was set at 8600ft and the bottom at 8605ft. To confine the slim-tube determined MMP which is approximately 3150 psia, the model was initialized at the reservoir temperature 225 °F and three pressures 3500, 3150 and 2500 psia at datum depth 8600 ft, so that miscibility is assured at 3500 and 3150, and to see how miscibility develops at pressures lesser than MMP, i.e., at 2500 psia.

The injection stream was 100% CO2. Based on the initialization pressures, the injection well was set to bottom-hole pressure targets of 3800, 3450, and 2800 psia, (i.e., Pinj=Pinit+300) whereas the producer was set to bottom-hole pressure targets of 3200, 2850, and 2200 psia respectively (i.e., Pprod=Pinit-300).

Continuous CO2 injection was considered, no mobile water is present in the model, and the water present in the model from the relative permeability is at Swc and

considered as part of the rock matrix. The simulations run for 149 days with 1 day timestep.

The following parameters were tracked along the displacement path, at 0.25, 0.5, 0.75, 1.0, 1.25 and 1.5 Hydrocarbon Pore Volumes injected.

PSAT	Saturation pressure, psia
PRESSU	Pressure, psia
VOIL	Oil viscosity, cp
DENO	Oil density, lb/cu-ft
XMFi	Oil component mole fraction of component i
YMFi	Gas component mole fraction of component i
ZMFi	Total mole fraction of component i

The mole fractions of CO2 and the sum of methane to hexane (XMF i) in the oil and the (YMF i) in the gas, and (ZMF i) total mole fraction are tracked. Additionally, total recovery versus HCPV injected was compared for different injection schemes.

6.2 Sarir C-North Field

The Sarir C-North field was selected for the compositional simulation as a case candidate for possible CO2 injection.

6.2.1 Background:

Sarir C-North (Concession 65) is one of the NNW – SSE trending reservoirs in the South Eastern part of the Sirte Basin approximately 500 km south of Benghazi Figure 6-3. It lies between the giant sarir C-Main Field (about 12 km to the south) and the Sarir L-Field , about 4 km to the north – west as shown in Figure 6-4.

C-North was discovered in 1963 by the discovery well C012, with oil – bearing interval between 8876 and 9043 ft KB in Lower Cretaceous sandstone. Production started in August 1967. In 1971 the field was nationalized and transferred to Arabian Gulf Exploration Company (AGECO). AGOCO has owned the field since 1982.

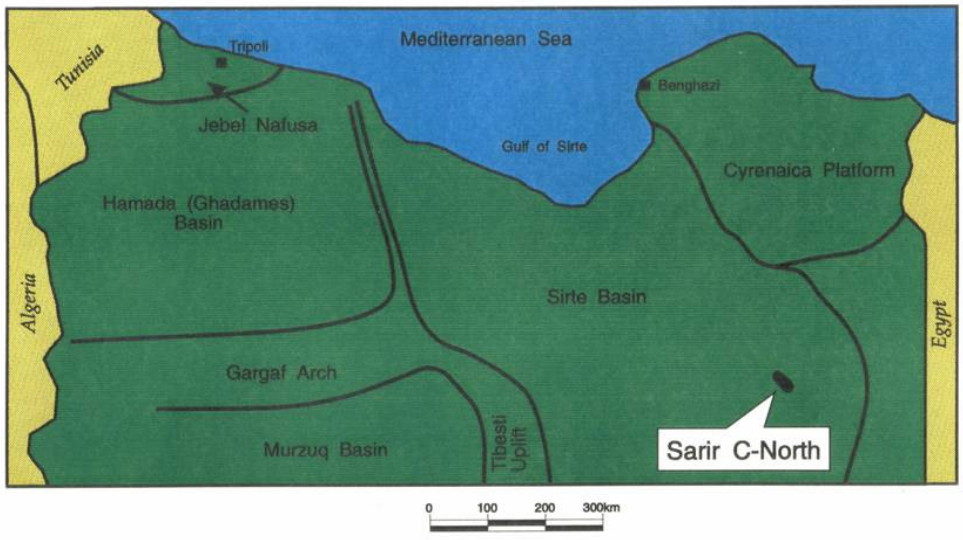

Figure 6-3: Sarir C-North in south east of Sirte basin, (From [1])

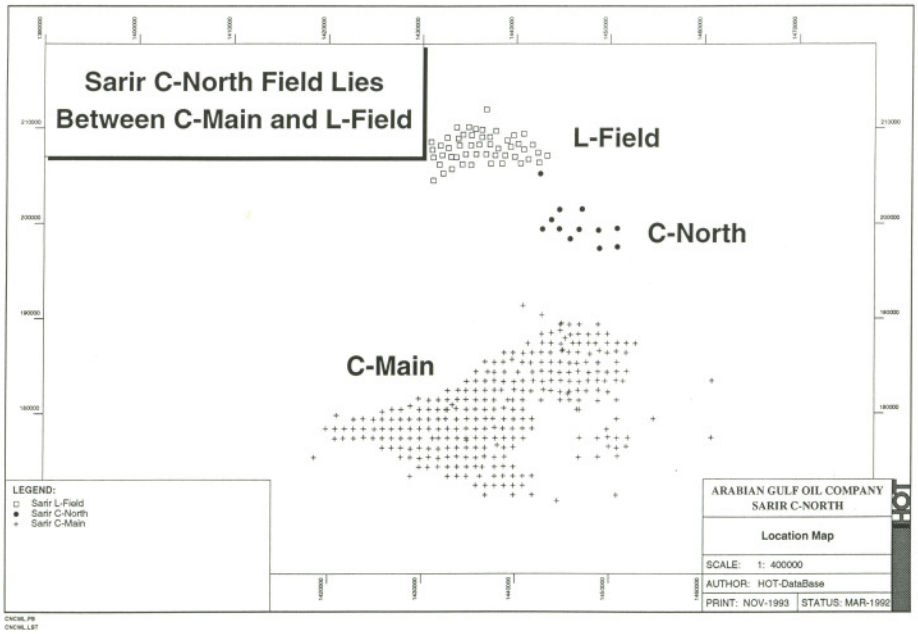

Figure 6-4: Sarir C-North is located between C-Main and L-Field, (From[1])

As of December 31, 2005, 18 wells including one replacement well (C019A) had been drilled in the Sarir C-North area. Five of them are non-productive and located outside of the main structure. Cumulative oil production from the field reached 36.1 MMSTB by the end of September 2005. Average oil production rate in 2005 was 4.2 MSTB/D. Because of the limited influx of water into the main productive zone, average water cut has remained low at 3.8%.

6.2.2 Geological Setting

In C-North, two stratigraphic units are oil–bearing: the Sarir Group and the Transgressive Sand (TGS). Based on petrophysical properties, the Sarir group is divided into 5AC, 5AB, and 5AA.

TGS: the composition of this member is marine reworking of continental facies and it is interpreted as transgressive shoreline deposit. This zone consists of a chaotic mixture of conglomerate, pebbly sandstone, silty sandstone, mosaic to nodular anhydrite, breccias (anhydrite matrix) and red silty shale/mudstone.

Member M5AA: is the highest part of Member 5, consists of well sorted medium to coarse grained quartz sandstone. Sandstone is locally interbedded with shaly sandstone and siltstone. The stacked character of these sandstone units suggests that this zone consists of a series of stacked fluvial channel sand bodies. The sandstone is comprised almost entirely of quartz, with minor amounts of kaolinite, illite, smecitite and anhydrite. Reservoir quality in this zone is generally good to excellent.

Member 5AB: consists of massively bedded thick red shale mudstone (simulation layers 5 and 7) with interbeds of clean massive sandstone, from less than 2 ft to 30 ft thick, this member is subdivided into to members 5AB1 and 5AB2.
The sand is showing a dominance of quartz, with minor kaolinite, illite and anhydrite. Reservoir quality in the sandstone units is good to excellent, although with some tighter streaks due to finer size and more abundant kaolinite.
The red shale and mudstone in this member represent distal overbank or flood-plain deposits, while the inter-bedded sandstones (Members M5AB1 and M5AB2) were formed as a result of meandering channel-fill deposits.

Member 5AC: is the lowermost unit consists of massively bedded shaly sandstone, red shale and mudstone, siltstone and minor clean sandstone. It represents proximal to distal overbank sequence. Clay minerals are chocking intergranular pores resulting in low reservoir quality. The OOIP in Member M5AC is located in transition zone and is considered as non-movable oil

6.2.3 Grid and Block Properties:

The model geometry as obtained from AGOCO has 97×73×14 grid cells in the X,Y and Z directions, however, except for layers 8 to 11 other layers where significantly coarse for use in monitoring displacement behavior between injectors and producers which is our target, therefore vertical refinement for some zones was necessary. The

areal extension of 500×500 ft was preserved. In the vertical direction, the simulation model was initially subdivided into 14 zones, based on the Flow Zone Indicator concept “FZI”.

(TGS) is represented by zone1
M5AA is represented by zones 2, 3, 4
Thick shale (mudstone) by zone 5
M5AB2 is represented by zone 6
Thick shale (mudstone) by zone 7
M5AB1 is represented by zones 8, 9, 10, 11
M5AC is represented by zones 12, 13, 14

The stratigraphic thickness of each of the zones 1, 2, 3, 4 and 6 where subdivided further into 15 ft height, using a 2 ft minimum cell thickness. Thus, the model dimensions become 97×73×42, and the total number of grid cells is 297402 cells, using minimum pore volume and ignoring cells outside the proven area the number of active cells is 73959.

Zone 1 was subdivided into 8 simulation layers (1 to 8), zone 2 into 8 simulation layers (9 to 16), zone 3 into 7 simulation layers (17 to 23), zone 4 into 7 simulation layers (24 to 30), and zone 6 into 3 layers (32 to 34), Table 6-1. Properties of the coarse zones where downscaled to the corresponding simulation layers.

Table 6-1: Zone division

Zone	Output grid layer	Input grid top layer	Input grid base layer
Zone 1	1	1	1
Zone 1	2	1	1
Zone 1	3	1	1
Zone 1	4	1	1
Zone 1	5	1	1
Zone 1	6	1	1
Zone 1	7	1	1
Zone 1	8	1	1
Zone 2	9	2	2
Zone 2	10	2	2
Zone 2	11	2	2
Zone 2	12	2	2
Zone 2	13	2	2
Zone 2	14	2	2
Zone 2	15	2	2
Zone 2	16	2	2
Zone 3	17	3	3
Zone 3	18	3	3
Zone 3	19	3	3
Zone 3	20	3	3
Zone 3	21	3	3
Zone 3	22	3	3
Zone 3	23	3	3
Zone 4	24	4	4
Zone 4	25	4	4
Zone 4	26	4	4
Zone 4	27	4	4
Zone 4	28	4	4
Zone 4	29	4	4
Zone 4	30	4	4
Zone 5	31	5	5
Zone 6	32	6	6
Zone 6	33	6	6
Zone 6	34	6	6
Zone 7	35	7	7
Zone 8	36	8	8
Zone 9	37	9	9
Zone 10	38	10	10
Zone 11	39	11	11
Zone 12	40	12	12
Zone 13	41	13	13
Zone 14	42	14	14

6.2.4 Relative Permeability and Capillary Pressures:

No laboratory core measurements were available, therefore correlations were used to estimate relative permeability and capillary pressure curves. These curves were validated against Sarir C-Main measured core data.

6.2.4.1 Relative Permeability

Relative permeability: Drainage oil-water relative permeability was calculated using Sigmund and McCaffery modification of Corey's relative permeability models, the calculated drainage relative permeability is presented graphically in 0.

The model for oil relative permeability is:

$$k_{ro} = k_{ro}(S_{wi})\frac{\left(S_o^N\right)^{no} + A\left(S_o^N\right)}{1+A}$$

$$S_o^N = \frac{1 - S_w - S_{orw}}{1 - S_{wi} - S_{orw}}$$

$k_{ro}(S_{wi})$ = end point relative permeability to oil

S_o^N = normalized oil saturation

no = oil saturation exponent

A = constant used to match data at low oil saturation

S_w = water saturation

S_{wi} = end point water saturation

S_{orw} = residual oil saturation after water-flooding

The model for water relative permeability is:

$$k_{rw} = k_{rw}(S_{orw})\frac{\left(1 - S_o^N\right)^{nw} + B\left(1 - S_o^N\right)}{1+B}$$

Where:

$k_{rw}(S_{orw})$ = end point relative permeability to water

nw = water saturation exponent

B = constant used to match data at low water saturation

The resulting relative permeability curves correctly account for capillary, viscous and gravity forces affecting water and oil relative permeability in Sarir mixed-wet reservoir [1].

The model for gas relative permeability:

Drainage gas-oil relative permeability was calculated using Corey's approximation and Wyllie and Gardner method for cemented Sandstone, 0:

Wyllie and Gardner:

$$k_{ro} = (S_o^N)^4$$

$$k_{rg} = (1 - S_o^N)^2 (1 - S_o^{N\,2})$$

Corey's correlation:

$$k_{ro} = (1 - S_g^N)^4$$

$$k_{rg} = (S_g^N)(2 - S_g^N)$$

where S_o^N and S_g^N are normalized oil and gas saturations respectively.

6.2.4.2 Capillary Pressure Curves

Capillary pressure data were calculated using integrated rock and log derived saturation data suggested by Skelt and Harrison based on the work of Thomeer, the

general form of the functions relating hydrocarbon saturation S_h to height above FWL h is:

$$S_h = 1 - S_w = a \exp\left[-\left(\frac{b}{h+d} \right) \right]^c$$

The equivalent expression related to capillary pressure is:

$$S_h = 1 - S_w = a \exp\left[-\left(\frac{b}{P_c + d} \right) \right]^c$$

The terms a, b, c, and d are either constants, or they may be functions of rock properties

6.2.5 PVT Properties:

One bottom-hole sample from C012 was analyzed, however oil viscosity was not measured. Sarir C-North crude is very similar to C-Main crude with low viscosity, density and wax content, low bubble point pressure, GOR and formation volume factor; therefore a fully analyzed sample from Well C-116, Sarir C-Main was used in the compositional simulation as discussed in Appendix (A)

CHAPTER 7 CO2 - Oil Phase Behavior

Accurate determination of minimum miscibility pressure (MMP) is very important criteria in achieving high recovery. In this chapter the MMP of the Sarir oil was estimated from eight correlations, and results were compared with the slim-tube measured MMP. Also a new MMP correlation is developed using parameters related to the oil properties, CO2 properties and the reservoir conditions.

7.1 Sarir Miscibility Conditions

In May 1984, two slim-tube miscibility tests were performed on a subsurface fluid sample collected from the Sarir C-Main field, the tests were conducted using CO2 as the injection gas at reservoir pressure 3300, and also 2500 psig, both at reservoir temperature 225 ˚F. The fluid composition is listed in Table 7-1. The slim-tube characteristics were: 40 ft long, 0.176 in (ID) and 37.5% porosity. Reservoir fluid sample properties: Pb=715 psig at 225˚F, GOR=162 SCF/STB, Oil FVF=1.207 BBL/STB at Pb, oil gravity=36.5 API at 60˚F and gas gravity=1.015 (air=1.000).

Table 7-1: Fluid composition

Component	Mole %	Weight %	Density @ 60˚ F, g/c.c	API	Mole Weight
CO2	01.12	00.27			
N2	01.05	0.16			
C1	10.82	0.96			
C2	04.34	0.72			
C3	08.22	2.01			
iC4	02.22	0.72			
nC4	06.41	2.07			
iC5	02.86	1.14			
nC5	03.54	1.42			
C6	04.45	2.12			
C7+	54.97	88.41	0.8644	32.0	290

Recoveries from both tests were 90 and 78 percent at one pore volume respectively, Figure 7-1. According to the definition of MMP as 90% recovery at 1.2 PV

injected, it was clear that CO2 is miscible with the reservoir fluid sample at reservoir conditions (i.e., 3300), but immiscible at 2500 psig, and from interpolation MMP is approximately 3150 psig. However the reservoir pressure in September 2007, in the subject well, is 2415 psig at datum depth. The average pressure for the field as a whole is about 2700 psig, that means at the time of commencement of such CO2 flooding program, the reservoir pressure will certainly be about 2000 psig.

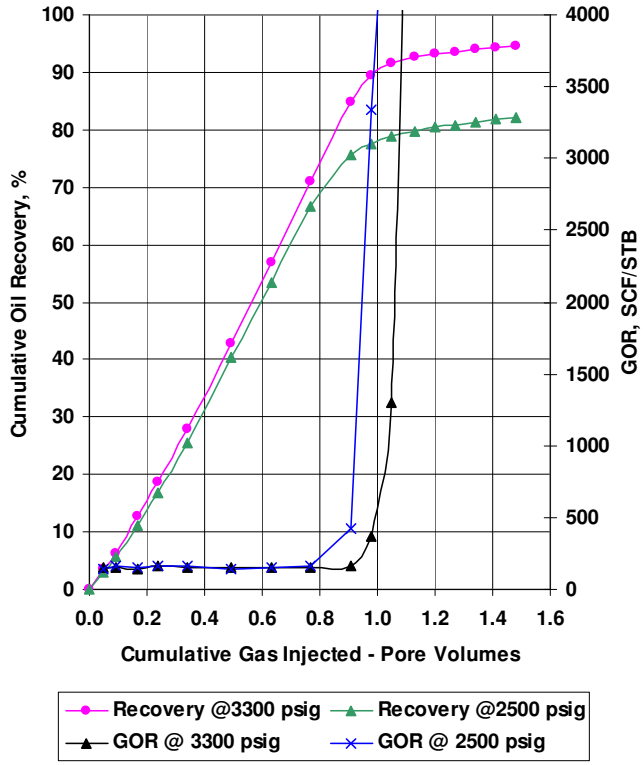

Figure 7-1: Experimental slim-tube test @ 3300 and 2500 psig

In order to come up with an approximate estimation to the MMP for design purposes, there are correlations that can reasonably predict MMP. Among others, common CO2 MMP correlations were used to estimate miscibility conditions.

Table 7-2 summarizes the parameters required for the following correlations:

Table 7-2: Input parameters for MMP correlations

Reservoir temperature, ˚F	225
Reservoir pressure, psig	3300
Oil M_{C7+}	290
Oil M_{C7+} corrected*	254.29
Oil M_{C5+}**	254.88
Reservoir fluid gravity, g/cc	0.842
Mole percent of C_1 and N_2	11.87
Watson factor, *Kw*	11.71
Reservoir fluid sample M	192.32
M_{CO2}	44
CO_2 critical temperature, ˚F	87.89
CO_2 critical pressure, psia	1070.6

*** For Glasø correlation**
**** Average not measured**

Benham et. al. correlation [3]:

Although Benham et al. correlation is proposed for rich-gas miscible-displacement processes, however, from their charts, Holme and Josendal found out that a mixture of 59 mole percent methane, and 41 mole percent propane, is equivalent to CO2. Therefore CO2 MMP estimated from Benham et al. correlation will be identical to that predicated by Holem and Josendal

Yellig and Metcalfe correlation [62]:

The correlation parameters are: Temperature only.

Holm and Josendal correlation [23]:

The correlation parameters are: Temperature, C5+ content, C5 through C30 content and CO2 density. However, due to the exponential behavior of the correlation at C5+ molecular weights higher than 220, and the reservoir temperature of 225 ˚F, although the correlation was derived at 165 ˚F, it predicts MMP with a reasonable accuracy.

The Cronquist correlation [19]:

The correlation parameters are: Temperature ˚F, C5+ mole weight, and mole percent of methane and nitrogen.

$$MMP = 15.988T^{\alpha}$$

Where:

$\alpha = (0.744206 + 0.0011038M_{C5+} + 0.0015279MPC_1)$, T is reservoir temperature in ˚F, M_{C5+} is the reservoir fluid C5+ molecular weight, and MPC_1 is the mole percent of methane and nitrogen

Johnson and Pollin correlation [29]:

The correlation parameters are: oil gravity, oil molecular weight, reservoir temperature and injection gas composition.

$$MMP - P_{C,inj} = \alpha_{inj}\left(T_{RES} - T_{C,inj}\right) + I\left(\beta M - M_{inj}\right)^2$$

Where: $P_{C,inj}$ is injection gas critical pressure, psia, T_{RES}, and $T_{C,inj}$ reservoir temperature and injection gas critical temperature respectively in deg. Kelvin, M and M_{inj} are oil and injection gas molecular weight respectively, the constant β has the value 0.285, and for pure CO2, α_{inj} =18.9 psia/K. The characterization index I is a function of density and molecular weight and it can approximated as a function of Watson factor K_w from the following formula:

$$I = 2.22K_w - 25.84 + 0.66K_w^{-2}$$

Where:

$$Kw = 4.5579M_{C7+}^{0.15178}\gamma_{C7+}^{-0.84573}$$

Glasø correlation [20]:

Glasø found out that the solubility of CO2 is similar to the solubility of a mixture of 58% methane and 42% propane), and used the following equation for MMP estimation if intermediates (i.e., C2 to C6) content exceed 18 mole %:

$$MMP = 810 - 3.404 M_{C7+} + (1.7 \times 10^{-9} M_{C7+}^{3.730} e^{786.8 M_{C7+}^{-1.058}}) T$$

Where M_{C7+} is corrected to the 11.95 K_w factor using C7+ properties

Alston et al. correlation [2]:

Alston et at. correlation is an extension to the Holm and Josendal correlation, the correlation parameters are: temperature, oil C5+ molecular weight, volatile oil fraction (C1 and N2), intermediate oil fraction (C2, C3, C4, H2S and CO2), and the composition of CO2. For pure CO2, the correlation is:

$$p_{CO_2-\mathrm{LO}} = 8.78 \times 10^{-4} (T_{RES})^{1.06} (M_{C5+})^{1.78} (x_{vol} / x_{\mathrm{int}})^{0.136}$$

p_{CO2-LO} is MMP for CO2 with live oil, TRES is reservoir temperature in ˚F, MC5+ is pentane plus molecular weight, and x_{vol}/x_{int} is the reservoir oil volatile to intermediate mole fraction ratio

Sebastian et al. correlation [47]:

This correlation accounts only for impurities in CO2 stream, and uses CO2 MMP for the pure CO2 stream as an input estimated from other correlations, therefore it is not applicable for pure CO2.

Orr and Silva correlation [40]:

Correlation parameters are: weight fractions of C2 through C37 if available, pressure and temperature:

$$w_{iC2+} = \frac{w_i}{\sum_{2}^{37} w_i}$$

$$\log k_i = -0.04175 \times C_i + 0.7611$$

$$F = \sum_{2}^{37} k_i \cdot w_{iC2+}$$

$\rho_{MMP} = -0.524 \times F + 1.189$

when F <1.467, and

$\rho_{MMP} = 0.42$

when F > 1.467

where: W_{iC2+} is the normalized weight fraction, C_i is component carbon number, K is a weighting factor, and F is the weighted composition parameter to which the density of CO2 at MMP is a function

In this example, calculated F = 3.035, thus ρ_{MMP} =0.42

Eakin and Mitch correlation [13]:

The input parameters are solvent composition, oil C7+ fraction molecular weight and the pseudo-reduced temperature. For pure CO2:

$P_r = MMP / P'C$

$T_C = T / T'_C$

Where: P'_C and T'_C are CO2 critical pressure and temperature respectively

$$\ln P_r = \ln\left(MMP / P'_C\right) = 0.01221 M_{7+} - 0.0005899 M_{7+}^{3/2} / T_r$$

Results

Table 7-3 summaries MMP as calculated from common correlations. The absolute average error AAE is calculated as: $AAE = \frac{\left|MMP_{measured} - MMP_{calculated}\right|}{MMP_{measured}}$:

Table 7-3: Results of MMP calculated from eight common correlations

	Correlation	MMP	AAE
		[psia]	[%]
	Slim-tube test	3150*	
1	Yellig and Metcalfe	2800	11.1
2	Holm and Josendal	3387	7.5
3	Cronquist	4560	44.8
4	Johnson and Pollin	2529	19.7
5	Glasø	3326	5.6
6	Alston et al.	4817	52.9
7	Orr and Silva	2800	11.1
8	Eakin and Mitch	3598	14.2

*** interpolated for 90% recovery at 1.2 PV injected at 3300 and 2500 psig**

Discussion

Most researchers use slim-tube determined MMP to generate and/or calibrate their correlations, and/or tune EOS models. However, a slim-tube test is a simplified one dimensional experiment, and most of the factors affecting a real gas injection process whether miscible or immiscible are minimized. A slim-tube test is usually conducted at pressures greater than the bubble point pressure, Pb, and if the real reservoir pressure is lower than the Pb, Yellig and Metcalfe [62] suggested using the Pb as MMP, this suggestion was denied later by Monroe [37] et al. and John and Orr [28]

It is well established that MMP is an important screening factor for the selection of solvent type, and thus the operating conditions, nevertheless one can notice the following:

1. No industry agreement upon definition of the slim-tube determined MMP other than the general definition, that it is the lowest pressure at which miscibility can be achieved. Even the criterion used in slim-tube tests vary.
2. Correlations developed from published MMP's should adopt specific criteria to be consistent.
3. No standard apparatus is used for MMP determination, although Yellig and Metcalfe [62] suggest the slim-tube apparatus as an industry standard.
4. Characteristics of the slim-tube apparatus (length, ID, permeability) vary from one lab to another, and flow rates are different. Although it was stated [29] that miscibility is independent of the transport problems. There should be standard limits.
5. No standard method or correlation for MMP below Pb. Some authors state that MMP is at least equal to Pb, others noticed that miscibility or near miscibility can be achieved even below bubble point pressure.
6. Inclusion of C6 in the definition of the intermediate fraction is another point of disagreement.

7. Estimated MMP for Sarir field sample with 8 different correlation along with the slim-tube measurements showed that three correlations [20], [23], [40] predicted MMP with acceptable accuracy. Two correlations [2], [19] failed to predict MMP and three correlations [13], [29], [62] displayed medium deviation

7.2 A New Correlation

A new and easy correlation is developed which takes into account the properties of CO2 and the oil. The correlation parameters are: reservoir temperature, CO2 density, molecular weight of C5+, and Watson characterization factor Kw.

7.2.1 Correlation Parameters

Twenty five published experimental data were used to observe the effect of four parameters on MMP. Figure 7-2 shows the strength of the correlation between MMP and temperature, molecular weight of C5+, density of CO2 at MMP, and Watson characterization factor.

It is evident that temperature is the strongest correlation factor therefore it is a fundamental parameter in any MMP correlation. CO2 density at MMP is also a strong correlation parameter. The reason is that it represents the solvency strength of CO2 at supercritical conditions. The degree of supercriticality “represented as density” plays a pronounced role in miscibility development. The correlation is developed using CO2 density at measured MMP, and for prediction of MMP the CO2 density may be estimated from Figure 7-3 (b) at MMP derived from Yellig and Metcalfe correlation, Figure 7-3 (a), which uses temperature as the only correlation parameter. The C5+ molecular weight is another strong correlation parameter, because CO2 mainly is miscible in this fraction of the crude oil. The effect of methane on MMP is insignificant, as indicated by several authors, for example Monroe et al. [37] attributed the insensitivity of one-dimensional displacement to the presence of methane to the observation that methane strongly

preferentially partition into the more mobile vapor phase and concentrates in the leading edge of the transition zone so that the injection CO2 when it comes in contact with the hydrocarbon mixtures does not see methane, this explains why efficiency and MMP of 1-D CO2 injection processes is insensitive to the presence of methane in the oil composition as indicated by Yellig and Metcalfe [62]. Holm and Josendal [22] observed that the presence of methane in the oil does not significantly affect MMP, but inversely affect the over-all efficiency of the process. Nghiem and Li [38] confirmed the observation of Holm and Josendal by means of a compositional simulation. Finally, the Watson characterization factor Kw which is an indicator of the degree of paraficinity showed negative correlation.

A product "A" is excellently correlated to the experimental MMPs, as seen in Figure 7-4.

The correlation introduces MMP as a logarithmic function in the product A.

$$MMP = 998.92 \times \mathrm{Ln}(A) - 134.56$$

where:

$$A = \frac{T_{RES}^{1.5} \times \rho_{CO2}^{1.5} \times Mw_{C5+}}{K_w \times 1000}$$

$$Kw = 4.5579 M_{C7+}^{0.15178} \cdot \gamma_{C7+}^{-0.84573}$$

$$T_{RES} = \deg F$$

$$\rho_{CO2} = \text{g/cc} @ MMP \, derived \, from \, Yellig \, and \, Metcalfe$$

7.2.2 Accuracy of the Correlation

The accuracy of the correlation, as shown in Figure 7-5 and Table 7-4, is very good. The correlation predicted Sarir MMP with 3% deviation.

For example, the predicted MMP for Sarir oil is calculated as follows;

T_{RES}=225 °F,

First estimate of MMP from Yellig and Metcalfe is 2800 psi, and CO2 density @ MMP=0.42 g/cc, Mw_{C5+} =254.88, Kw=11.7

So, the product $A = \frac{T_{RES}^{1.5} \times \rho_{CO2}^{1.5} \times Mw_{C5+}}{Kw \times 1000}$

$$A = \frac{225^{1.5} \times 0.42^{1.5} \times 254.88}{11.71 \times 1000} = 20$$

$$MMP = 998.92 \times \ln(A) - 134.56$$

$$MMP = 998.92 \times \ln(20) - 134.56 = 2858\,psi$$

Absolute Average Error is $\frac{|2858 - 3150|}{3150} \times 100 = 9.3\%$

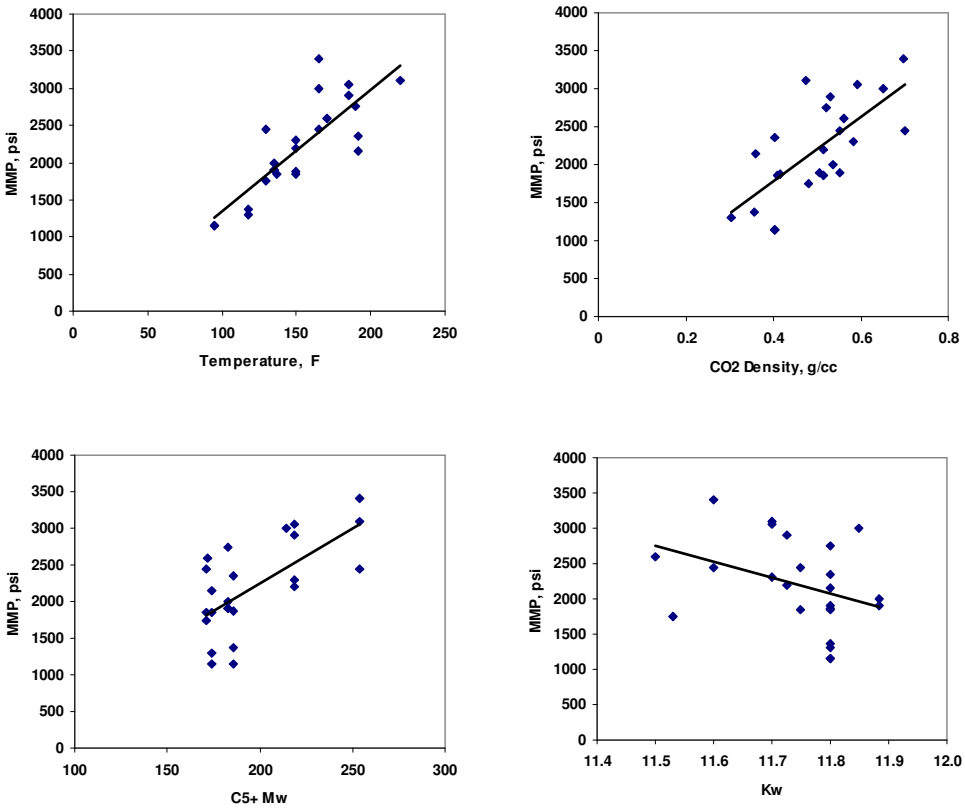

Figure 7-2: Correlation parameters vs. MMP

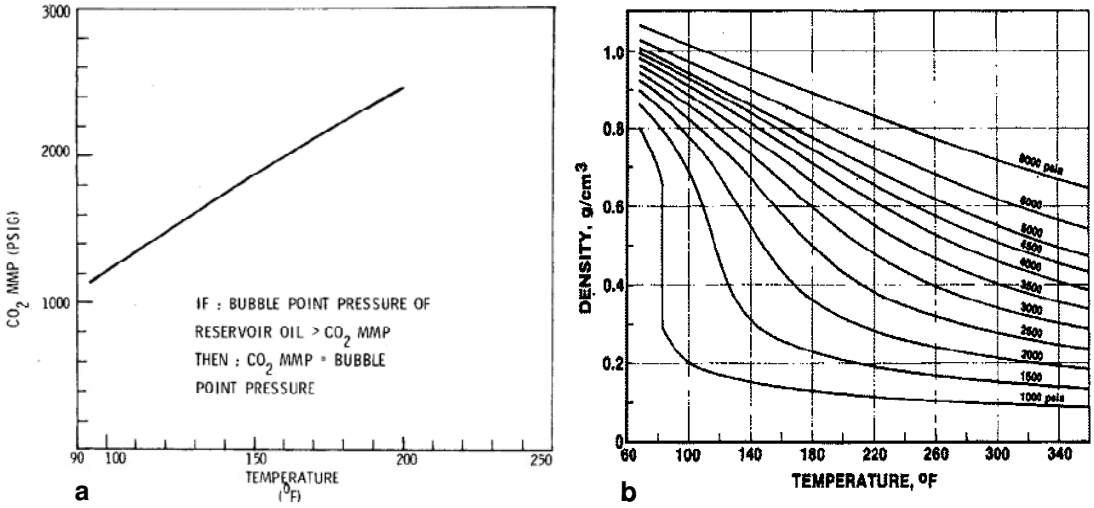

Figure 7-3: (a)Yellig and Metcalfe CO2 MMP correlation, (After [62]) and (b) CO2 density vs temperature, (After [23])

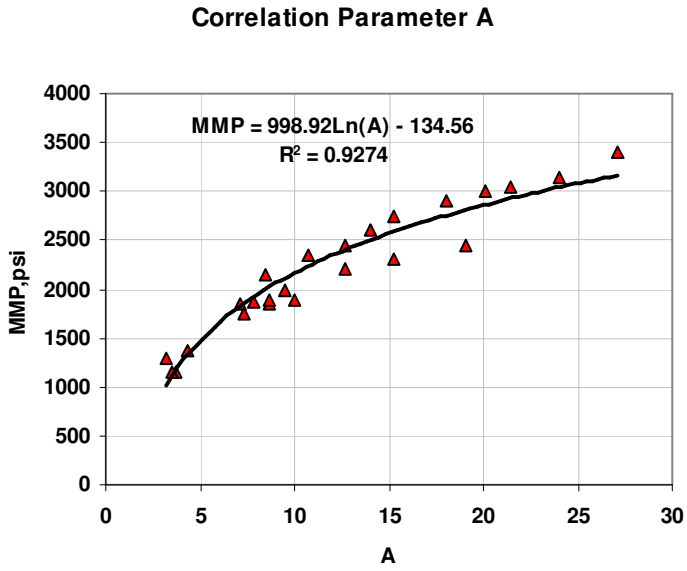

Figure 7-4: MMP as a function of the product A

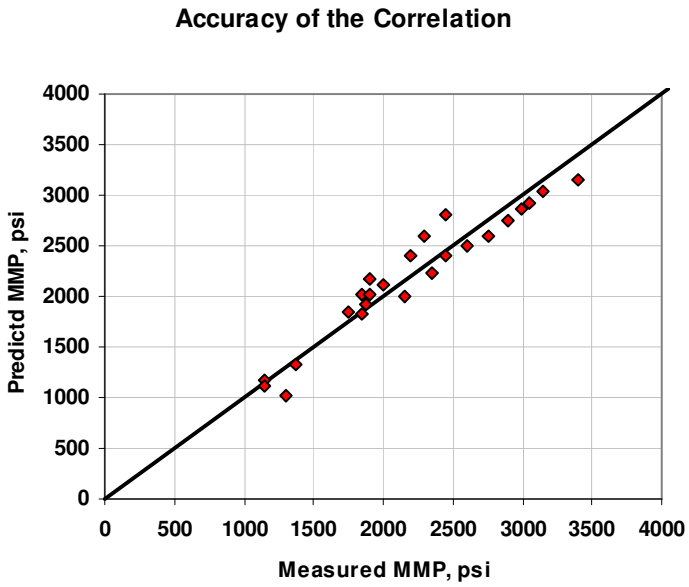

Figure 7-5: Comparison of measured MMP from developed correlation and experimental MMP obtained from slim-tube tests

Table 7-4: Input parameters for the new correlation

Ref.	Measured	T	CO2* density	C5+ Mw	Kw	A	Calculated	Deviation
	MMP, psi	°F	g/cc				MMP, psi	AE %
[23]	1850	137	0.515	171	11.75	8.62	2018	9.1
[23]	1900	135	0.553	183	11.80	10.00	2166	14.0
[23]	2300	150	0.582	219	11.70	15.27	2588	12.5
[23]	2450	130	0.701	254	11.60	19.05	2809	14.7
[23]	2450	165	0.552	171	11.75	12.65	2400	2.0
[23]	2600	171	0.561	172	11.50	14.01	2505	3.6
[23]	2750	190	0.521	183	11.80	15.27	2589	5.9
[23]	3000	165	0.651	214	11.85	20.10	2863	4.6
[23]	3050	185	0.592	219	11.70	21.45	2928	4.0
[23]	3400	165	0.698	254	11.60	27.06	3160	7.1
[1]	3150	225	0.465	254	11.70	23.19	3006	3.0
[62]	1150	95	0.403	186	11.80	3.73	1181	2.7
[62]	1375	118	0.356	186	11.80	4.29	1321	4.0
[62]	1875	150	0.417	186	11.80	7.80	1917	2.2
[62]	2350	192	0.403	186	11.80	10.73	2236	4.9
[62]	1150	95	0.403	174	11.80	3.50	1115	3.1
[62]	1300	118	0.305	174	11.80	3.20	1022	21.4
[62]	1850	150	0.408	174	11.80	7.07	1818	1.7
[62]	2150	192	0.360	174	11.80	8.49	2000	7.0
[22]	1750	130	0.480	171	11.53	7.31	1853	5.9
[22]	1900	135	0.505	183	11.88	8.67	2023	6.5
[22]	2000	135	0.537	183	11.88	9.51	2115	5.8
[22]	2200	150	0.515	219	11.72	12.68	2403	9.2
[22]	2900	185	0.529	219	11.72	18.08	2758	4.9

*CO2 density is calculated from EOS at reservoir temperature and measured MMP

CHAPTER 8 Numerical Modeling of Supercritical CO2 Injection

This chapter describes the simulation results performed on a 1-D and 3-D models.

8.1 CO2 Injection into 1-D Model

Results of the CO2 injection in the 1-D model are presented in line plots. These results describe the change of oil properties and composition at six different hydrocarbon pore volumes injected (≈ 0.25, 0.50, 0.75, 1.00, 1.25, 1.50 HCPV) versus dimensionless distance, $\sum_{i=1}^{n} \Delta x \Big/ x$, where n is the number of blocks, Δx is the grid x-dimension equals 10 ft, and x is the distance from injector to producer equals 500 ft. Also comparison of oil recovery vs. HCPV injected to simulate slim-tube experiments is presented. The above arrangement is used for three initialization pressures confining the miscibility conditions, 3500, 3150, 2500 psi, where the measured slim-tube MMP is 3150 psi at 225 °F.

Figure 8-1 clearly shows that at MMP or higher pressures recovery is almost identical at all HCPVs injected, while at 2500 psi miscibility has not strongly developed, however the ultimate recovery is very much the same. The Adaptive Implicit Method (AIM) using Eclipse 300 compositional simulator backed by Peng-Robinson EOS was used to model the behavior of 11 components namely; CO2, C1, C2, C3, C4, C5, C6, FRC1, FRC2, FRC3, and FRC4. For details of the EOS, see Appendix A.

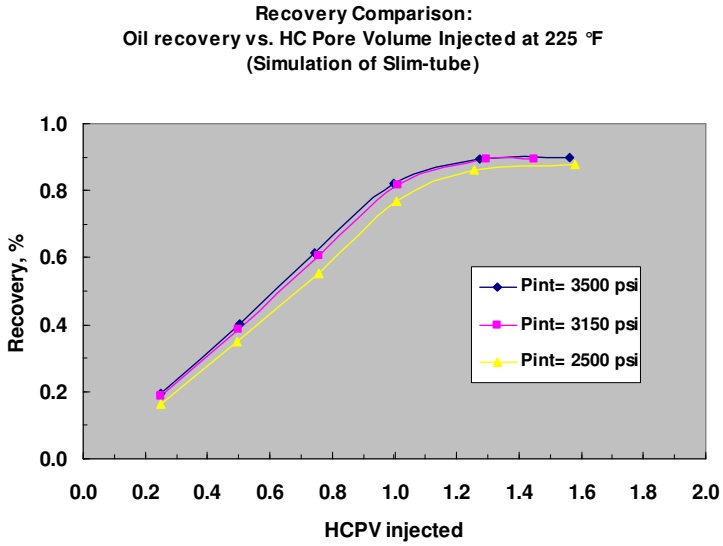

Figure 8-1: Comparison of recovery vs. HCPV injected for Cases 1, 2, and 3

8.1.1 Case-1, Pinit=3500 psi, T=225 °F

Figure 8-3 through Figure 8-10 in detail describe development of phase properties along the injection path. This case represents a first contact miscible displacement. The measured MMP (3150 psia) is considerably lower than the initial pressure (3500 psia) as well as the injection pressure (3800 psia).

Saturation Pressure

When the oil is undersaturated, the injected CO2 dissolves into the oil causing the bubble point pressure to increase. The system remains a single phase as long as the reservoir pressure is greater than the new bubble point (or saturation pressure). This is exactly the case of Sarir oil. The oil is undersaturated, and its measured bubble point is 715 psi. Very interesting is the observation of the advancing of the saturation pressure and its effect on oil viscosity and density. The advancing saturation pressure was like a wave of a constant height which gets wider progressively as it advances until breakthrough. After breakthrough of CO2, saturation pressure exceeds the reservoir pressure in most of the grid blocks, nevertheless some grid blocks remain undersaturated, and some blocks exhibit

lower saturation pressure sometimes even lower than the original. The increase in saturation pressure strongly affects oil properties

Oil Viscosity

Viscosity is an important property of crude oils, which significantly affects displacement efficiency, therefore one of the means of EOR is to reduce crud oils viscosity. The viscosity is a direct function of pressure, temperature and composition. During CO2 injection, the increase in CO2 content in the oil reduces the oil viscosity. In Figure 8-3 at 0.25 HCPV injected, oil viscosity increased slightly above the initial value (from 1.63 to 1.74 cp) although the CO2 content in the saturation pressure wave is higher than in the original oil in place. This observation looks surprising at the first glance, but the reason can be explained as follows: the increase in CO2 content should intuitively decrease oil viscosity, on the other hand the increase in the average reservoir pressure from 3500 (for Case-1) to around 3700 psia due to injection should naturally increase oil viscosity because viscosity is a function of pressure, however, the increase in block pressure had a stronger effect than the effect of CO2 content in the advancing front at this HCPV injected. Therefore, when combining the two effects the result is higher oil viscosity. After breakthrough of CO2, the oil viscosity was very low due to the high CO2 content.

Oil Density

Oil density is also a function of pressure, temperature and composition. The general behavior of the oil density was the same as for the oil viscosity. Density increased and decreased based upon CO2 content and block pressure.

Fluid Composition

The oil composition along the injection path as well as for the produced fluids has not deviated from the original composition. Only the CO2 content increased but the

proportionality between OOIP components was the same. This is a clear evidence that the initialization pressure 3500 psia is higher than MMP of the system. Figure 8-4 through Figure 8-9 shows component mole fractions in the vapor, liquid as well as in the total composition for the eleven components, and also for groups of light, intermediate, and heavier components i.e., CO2, C1, C2-C6, and C7+.

The effect of numerical dispersion is considered by simulating Case-1 using 500 cells with 1 ft Δx. Figure 8-2 shows a comparison between the normalized mole fractions of methane, C1, and carbon dioxide, CO2. It is clear that the 500 cell model results in a smaller transition zone and more stable displacement than the 50 cells model. In the literature [4], a model of approximately 200 cells is sufficient to model any compositional effects. The studied model (i.e., 50 cells) was fine enough to serve our purpose of simulating slim-tube test.

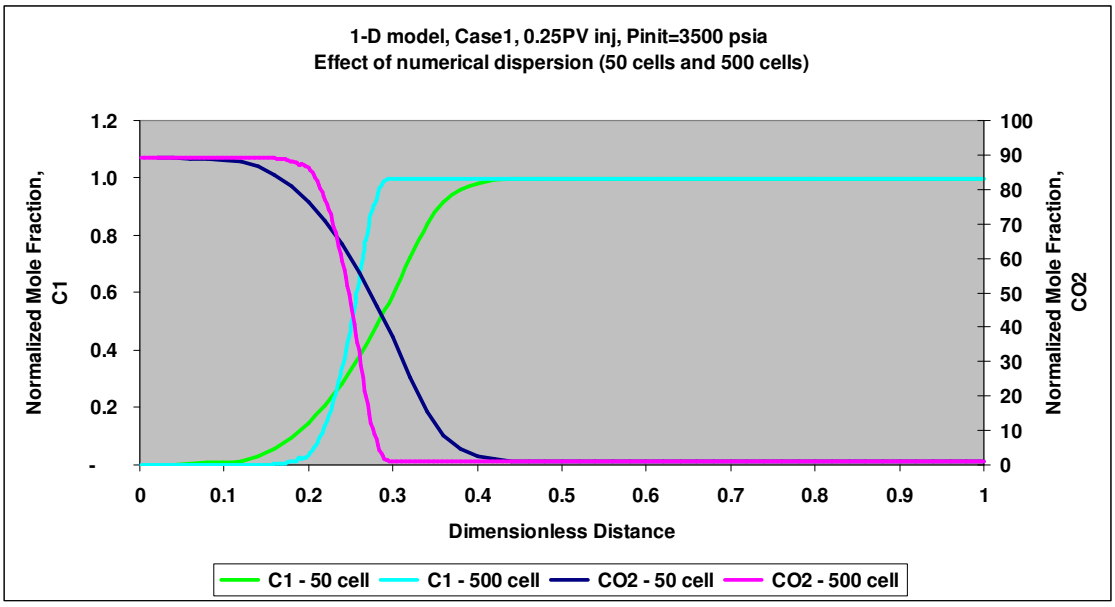

Figure 8-2: Effect of numerical dispersion on a 1-D model with 50 and 500 cells

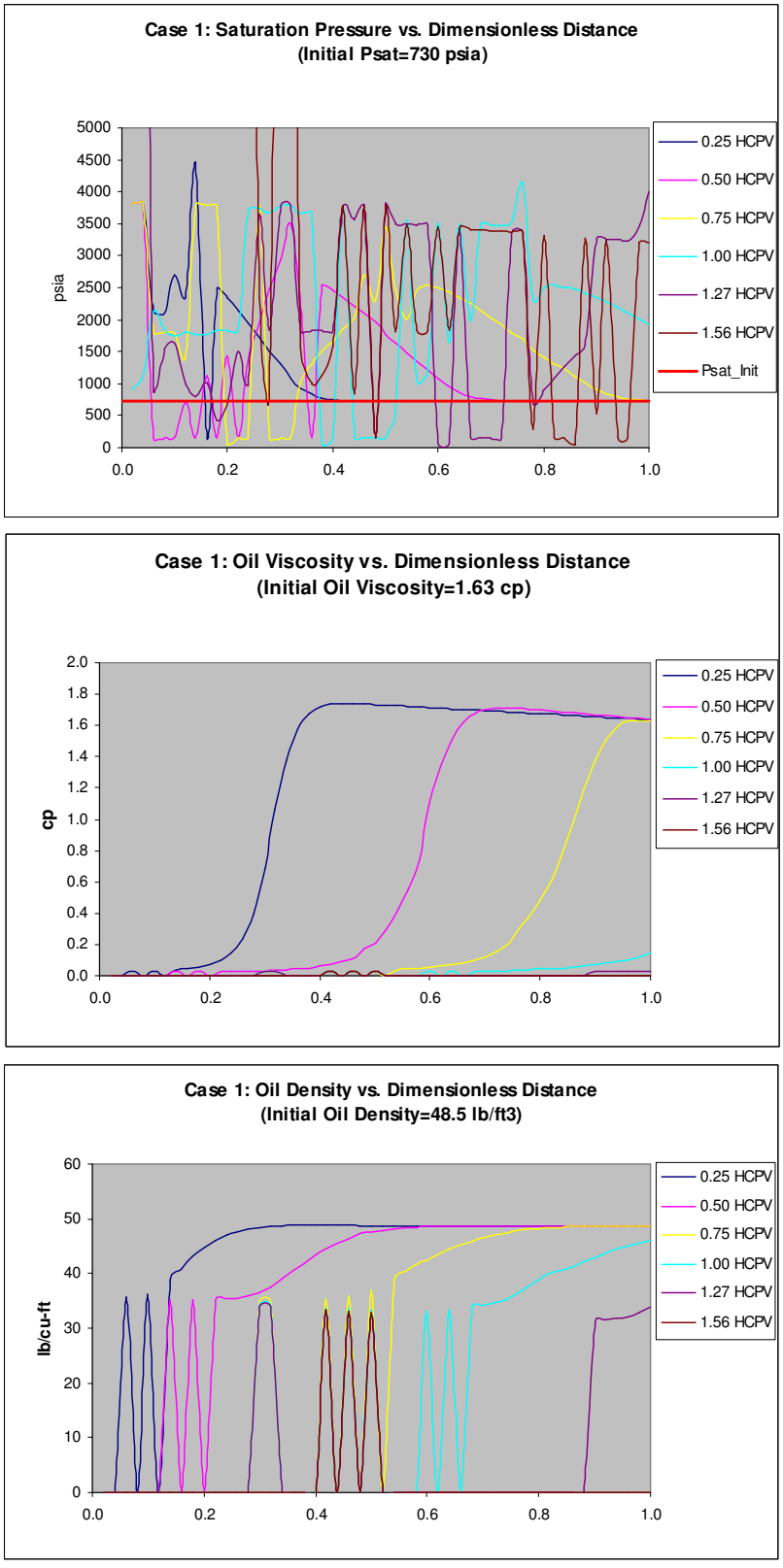

Figure 8-3: Case 1, Comparison of basic properties vs. distance for different HCPV injected

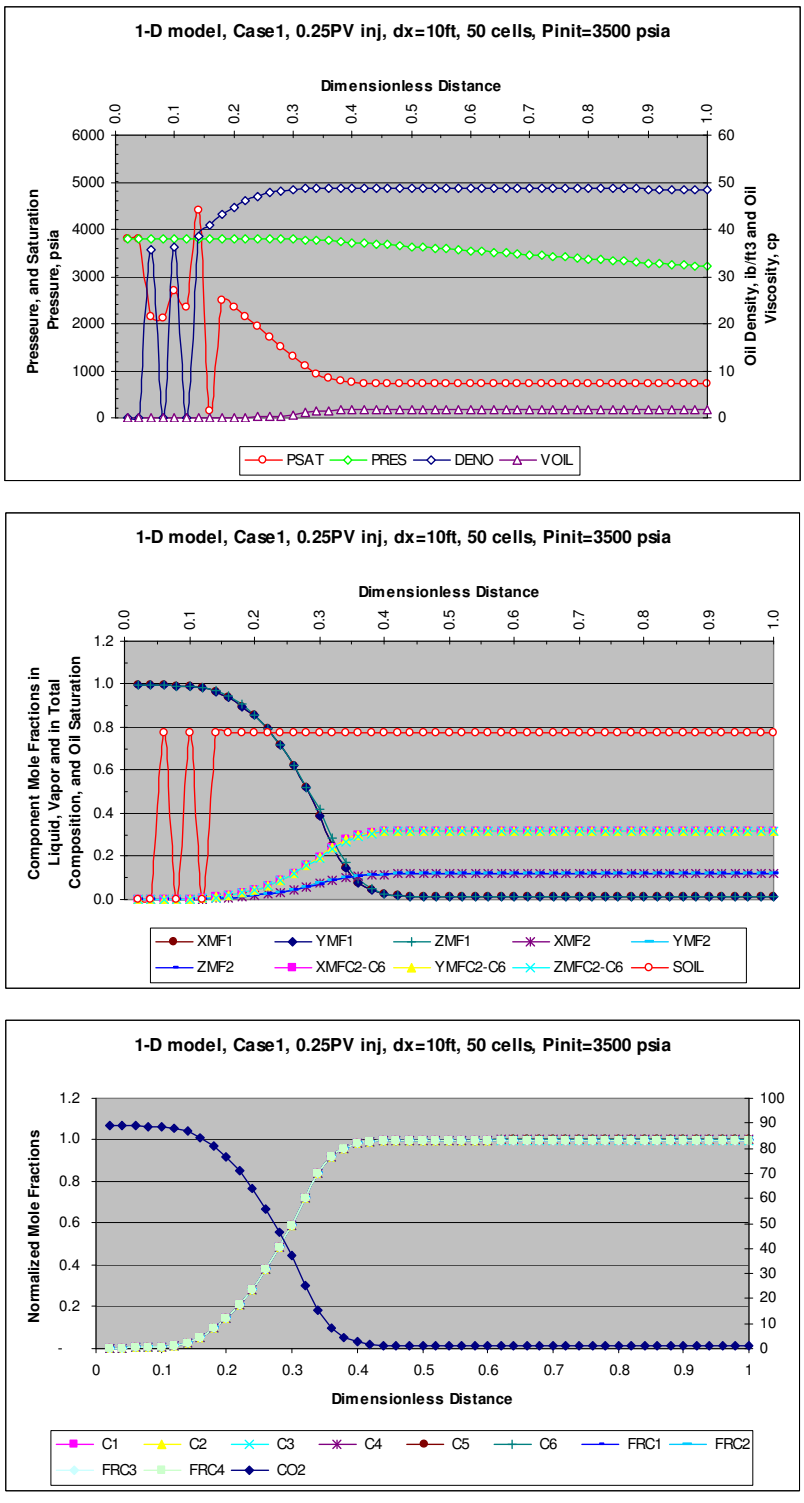

Figure 8-4: Case-1, 0.25 HCPV injected

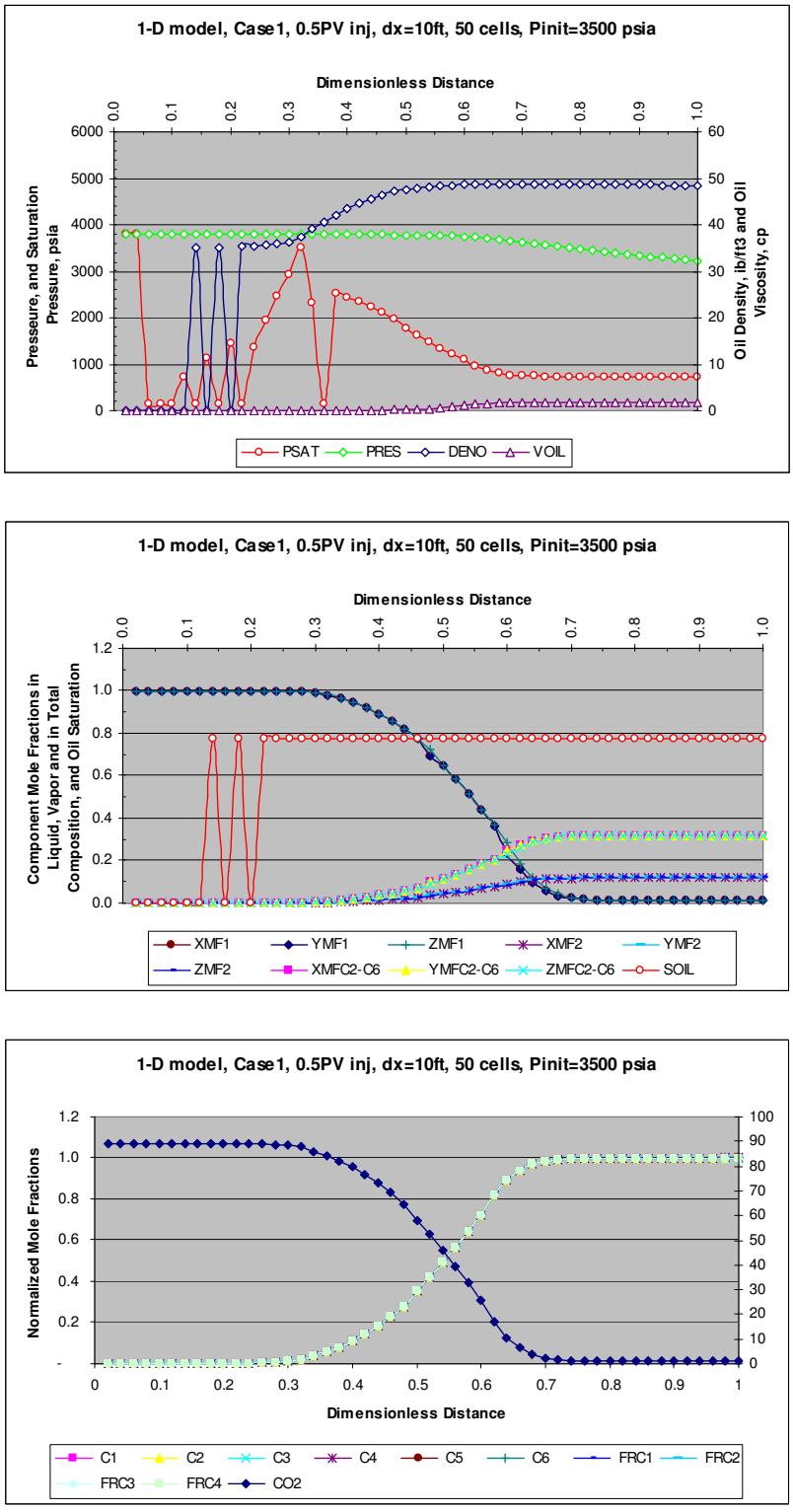

Figure 8-5: Case-1, 0.5 HCPV injected

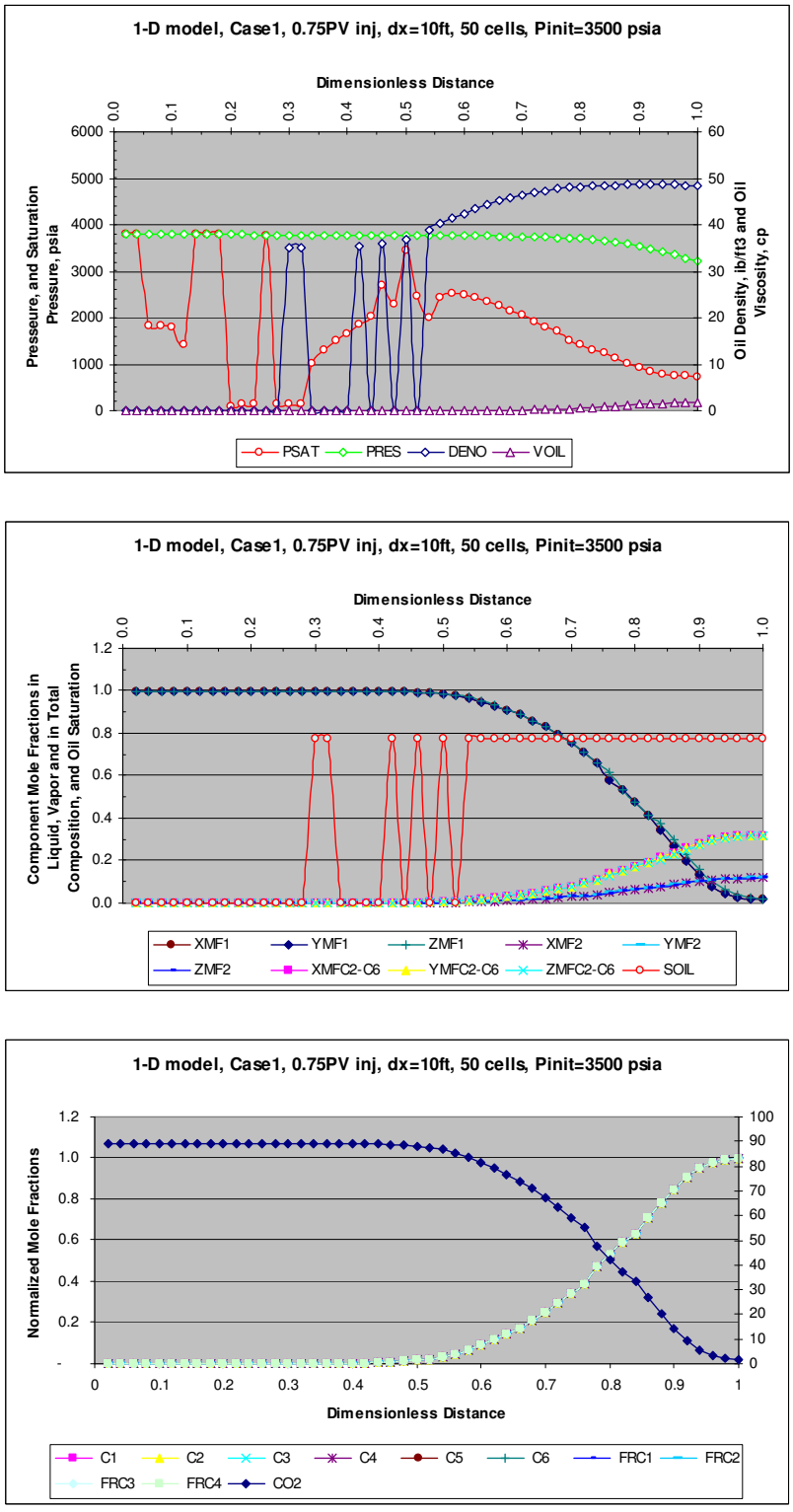

Figure 8-6: Case-1, 0.75 HCPV injected

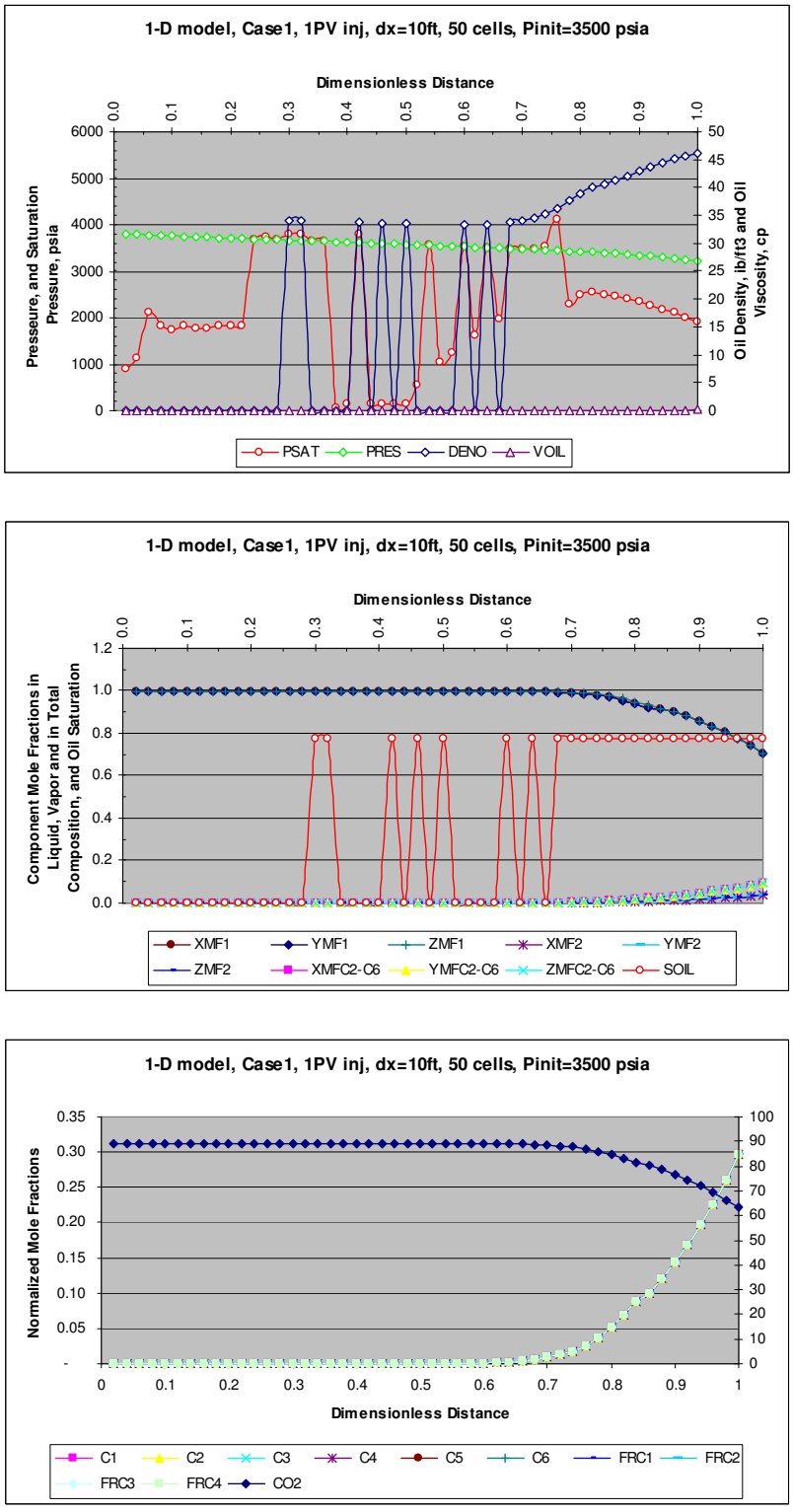

Figure 8-7: Case-1, 1 HCPV injected

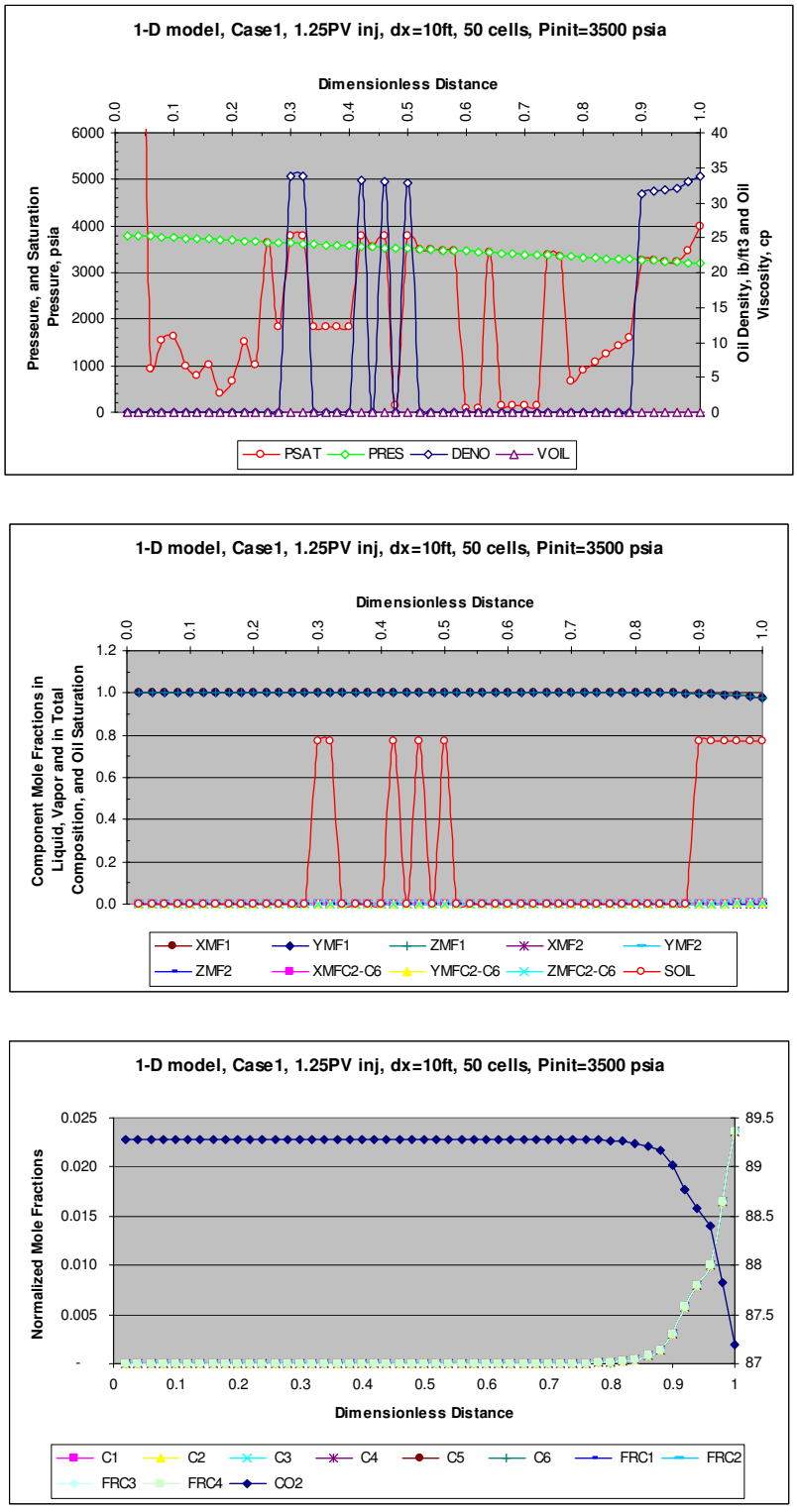

Figure 8-8: Case-1, 1.25 HCPV injected

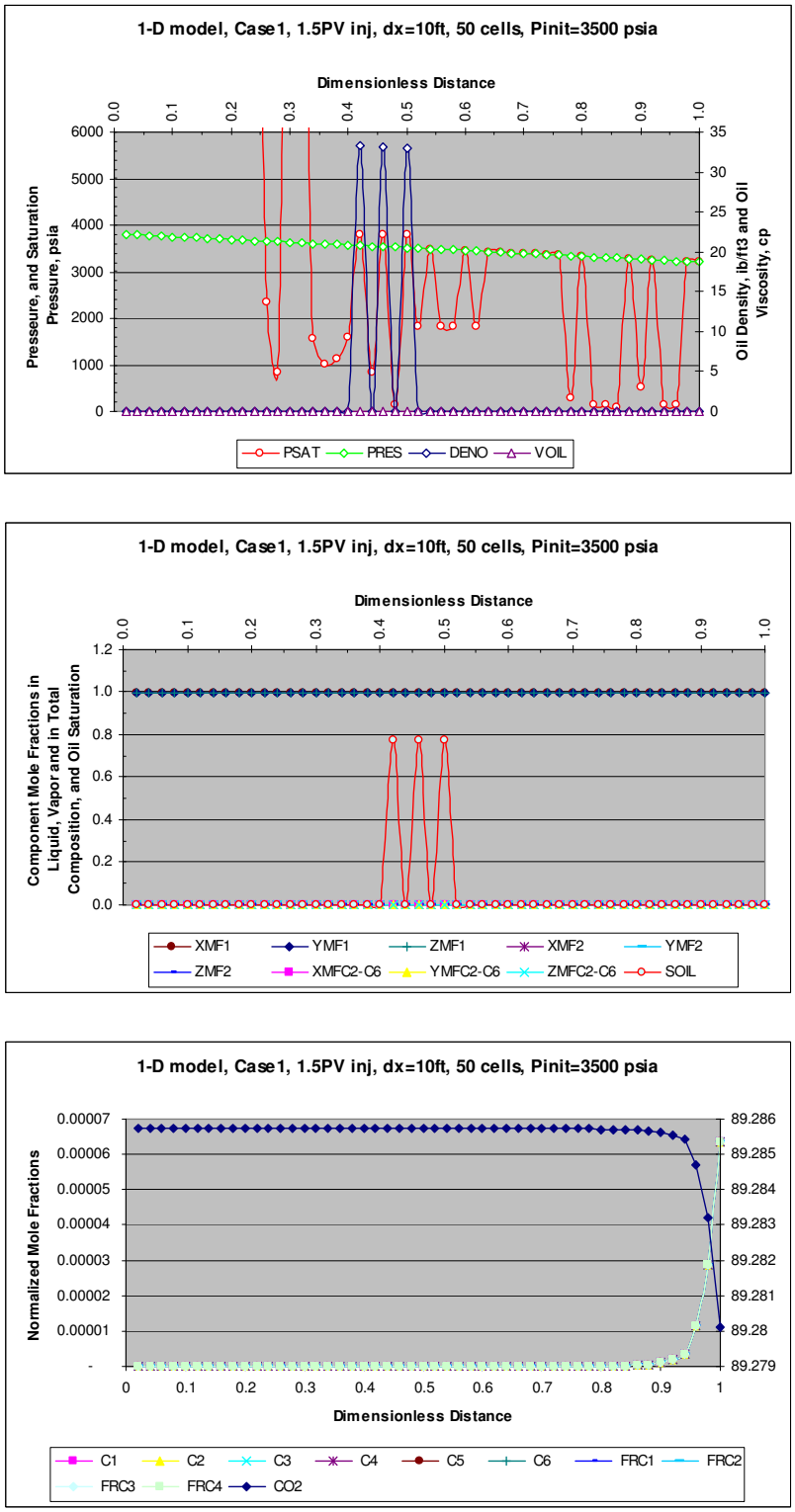

Figure 8-9: Case-1, 1.5 HCPV injected

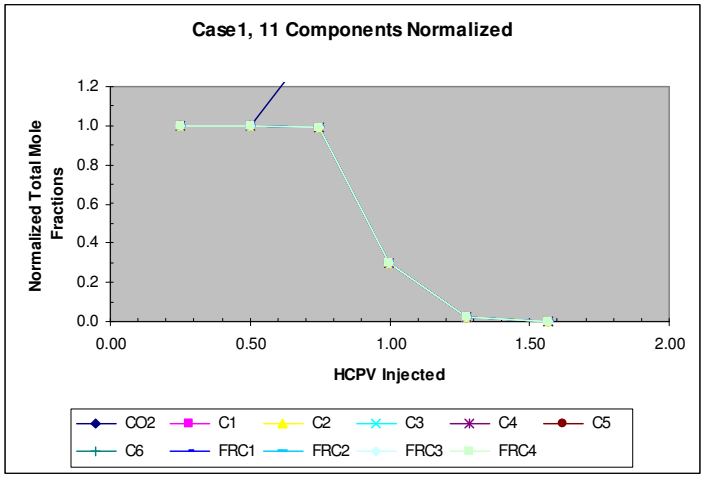

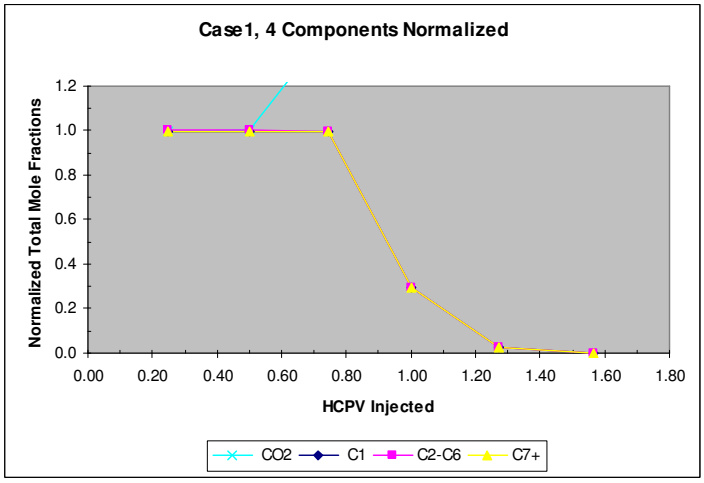

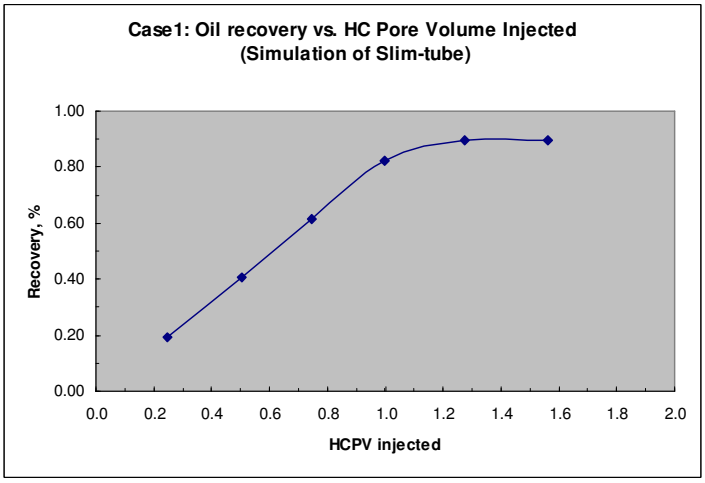

Figure 8-10: Case-1, Recovery vs. HCPV injected

8.1.2 Case-2, Pinit=3150 psi, T=225 °F

Case-2 was initialized at MMP (3150 psia), which is measured experimentally by slim-tube test and also estimated from other correlations. Results of Case-2 are generally identical to Case-1. Except in highly depleted cells, the saturation pressure in Case-2 reached a maximum at about 2500 psia. This is the same as in Case-1. Oil viscosity, density and produced fluid composition as well as composition movement along the injection path are comparable to Case-1.

Case-2 is a multiple contact miscible displacement. The mechanism by which miscibility is developed is a combined vaporizing/condensing gas drive mechanism.

Figure 8-11 through Figure 8-18 show the development of miscibility for the 6 different HCPVs injected.

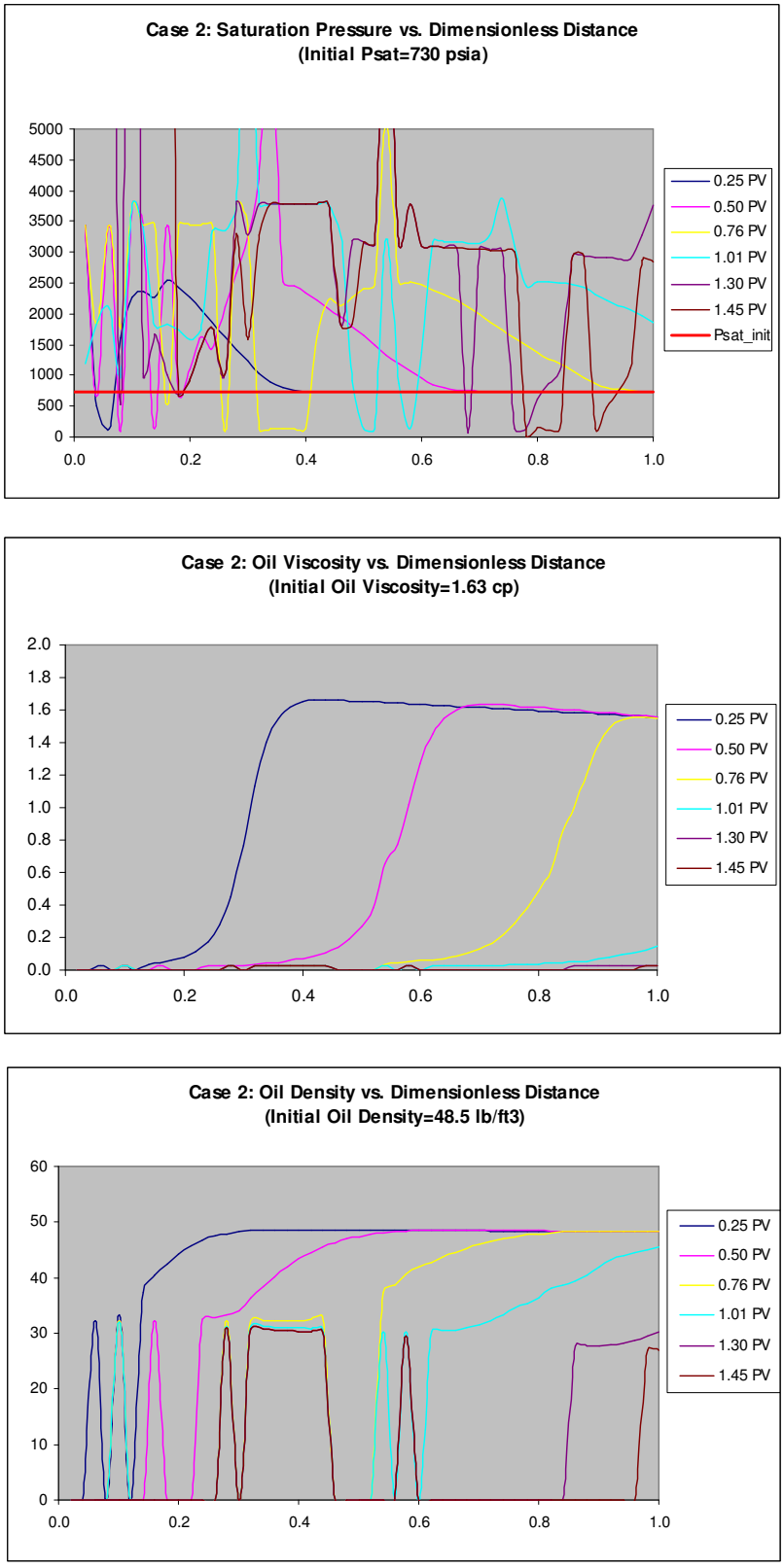

Figure 8-11: Case 2, Comparison of basic properties vs. distance for different HCPV injected

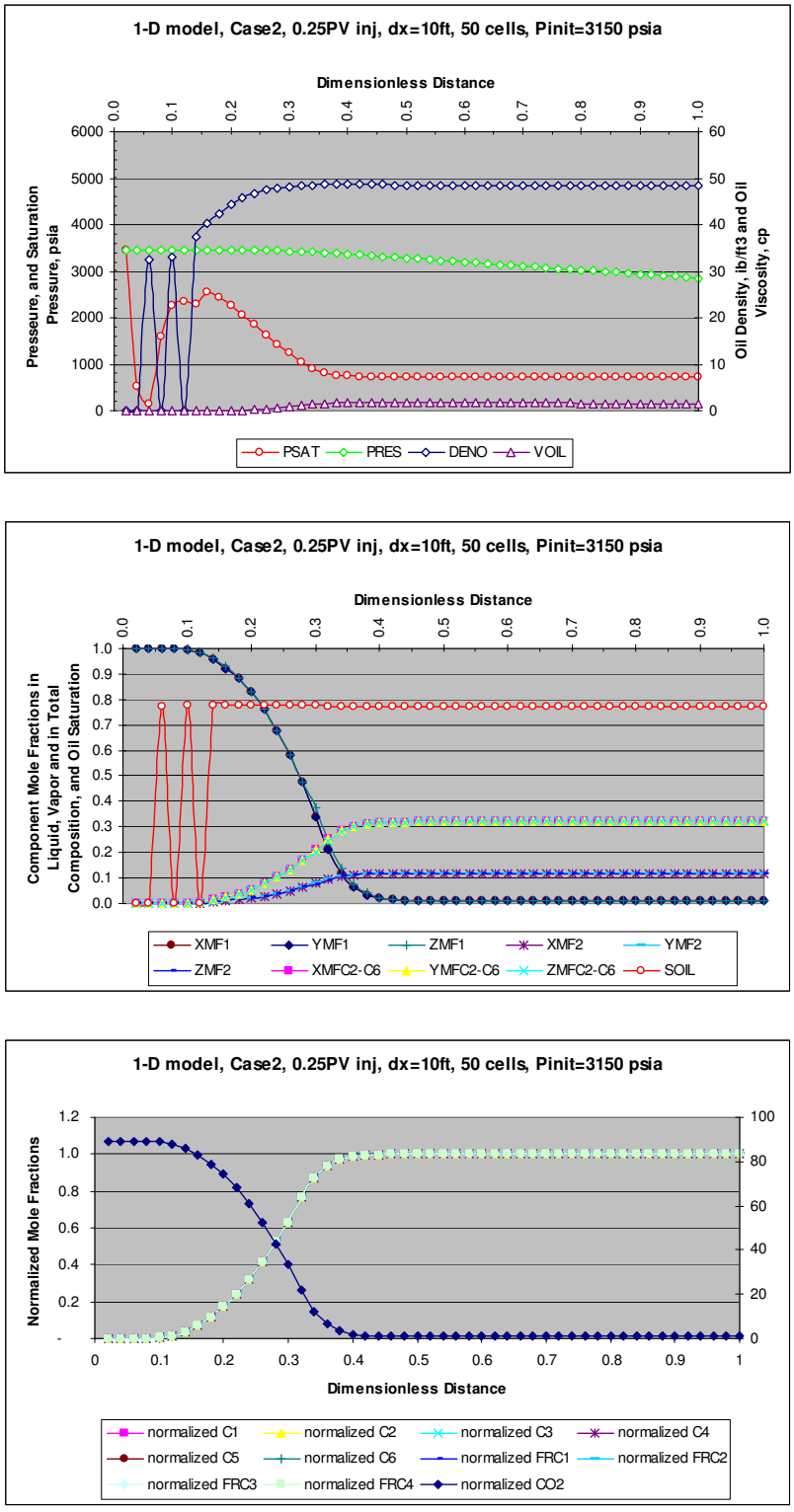

Figure 8-12: Case-2, 0.25 HCPV injected

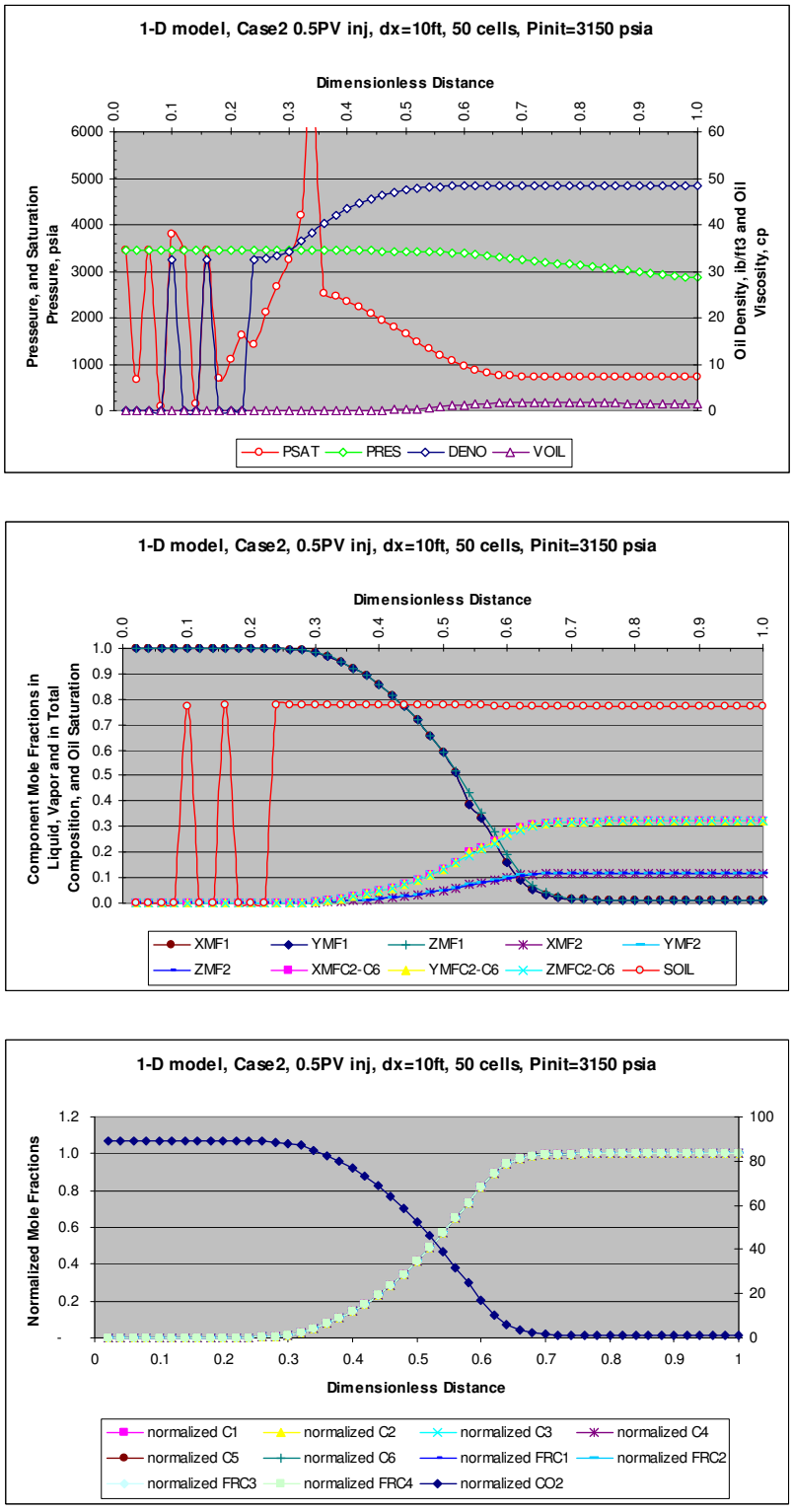

Figure 8-13: Case-2, 0.5 HCPV injected

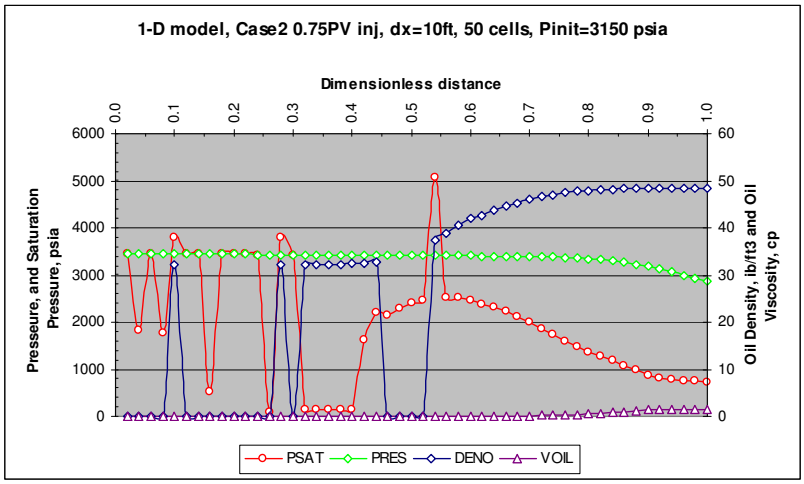

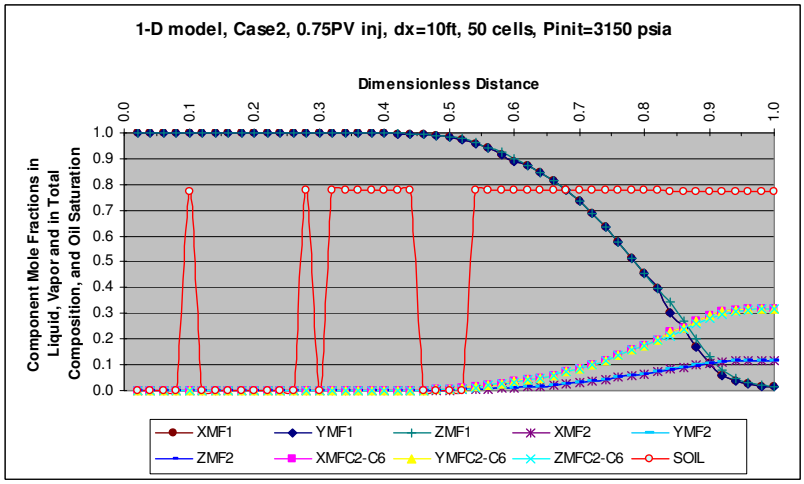

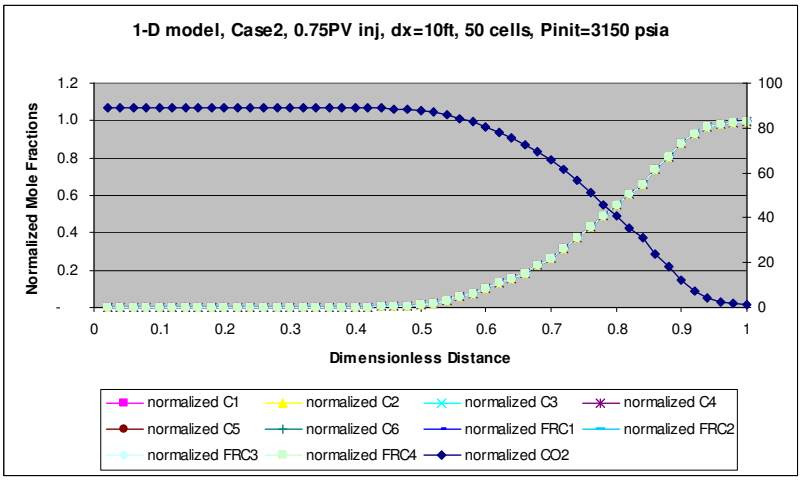

Figure 8-14: Case-2, 0.75 HCPV injected

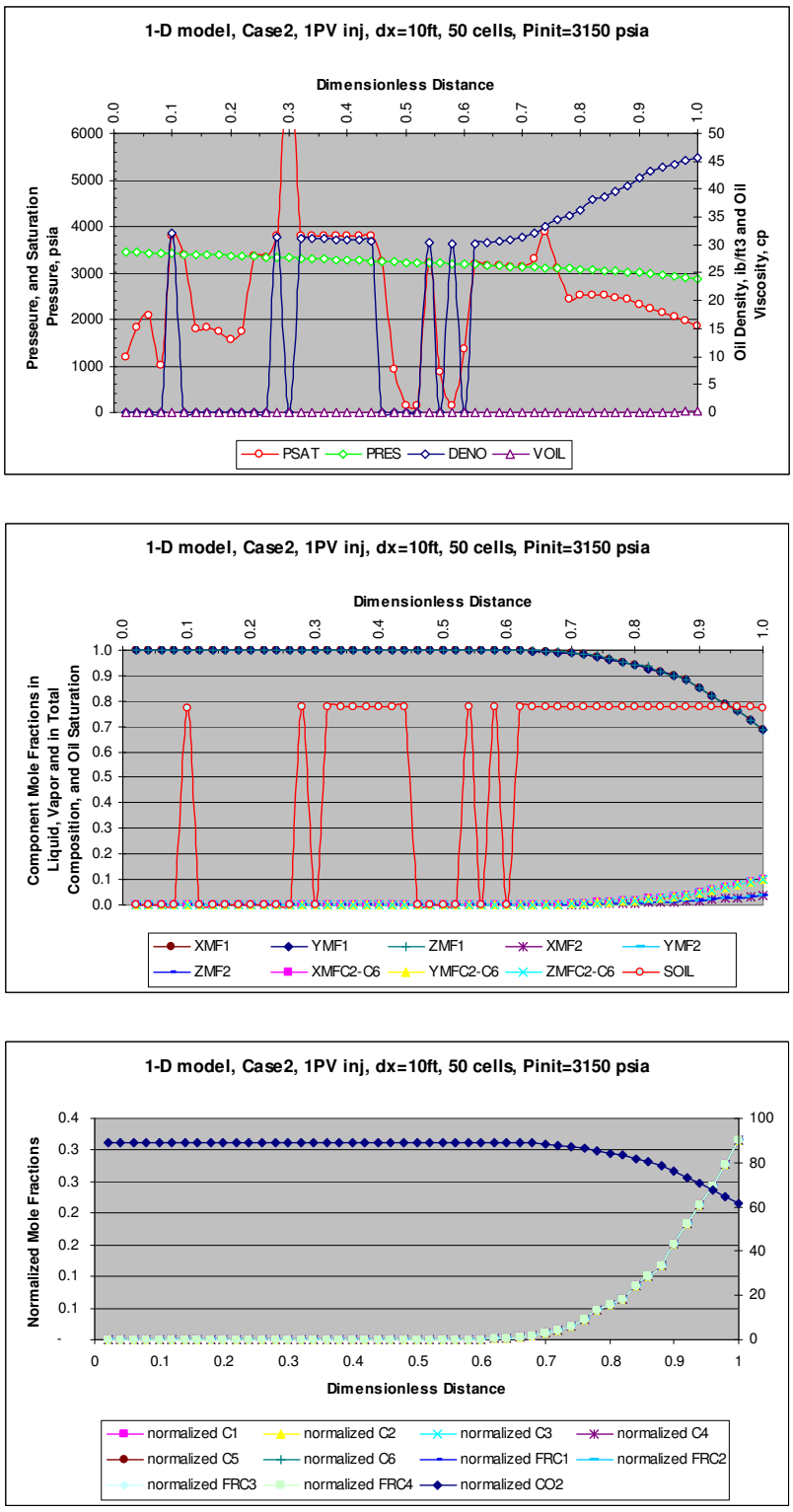

Figure 8-15: Case-2, 1 HCPV injected

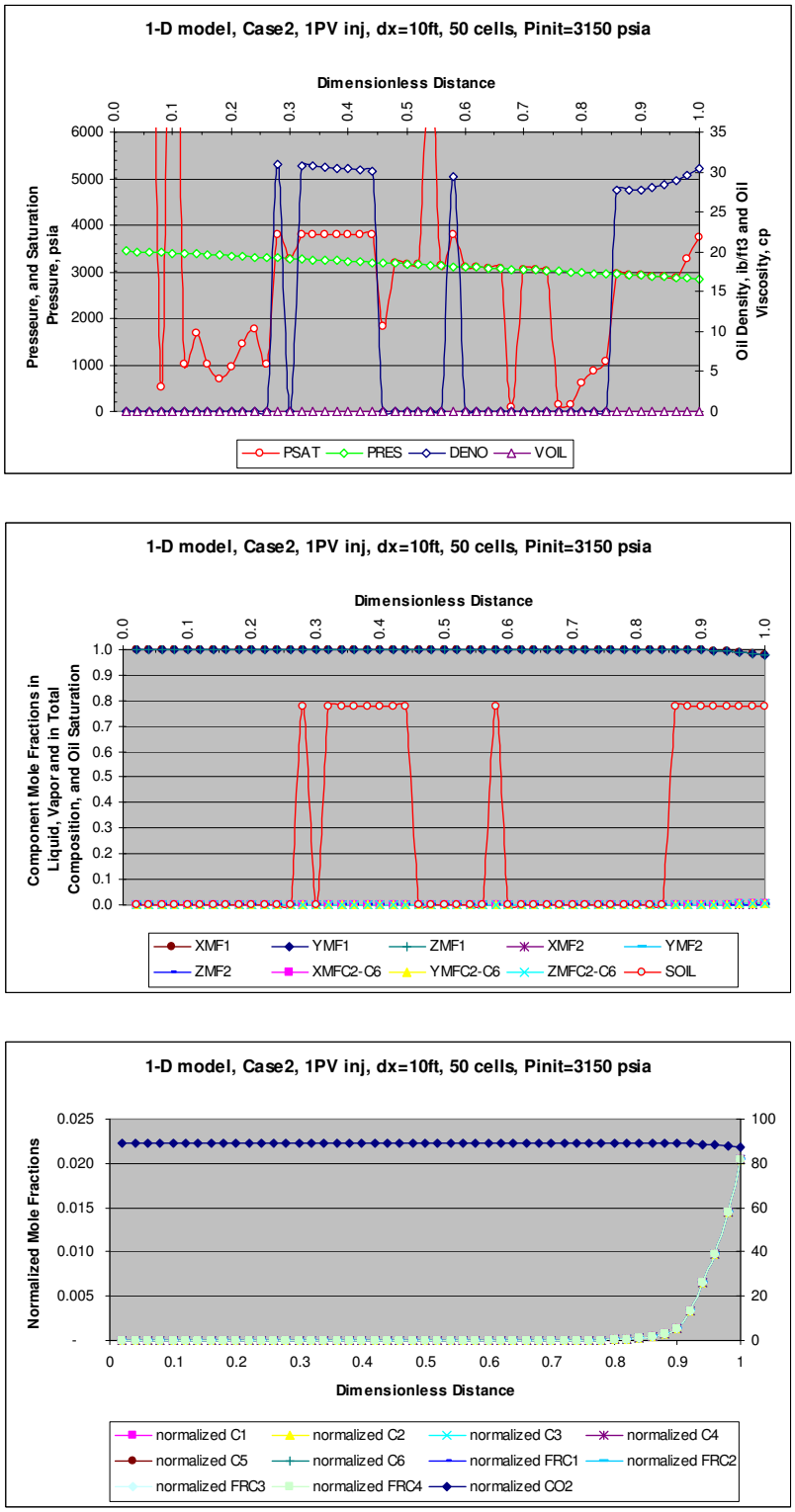

Figure 8-16: Case-2, 1.25 HCPV injected

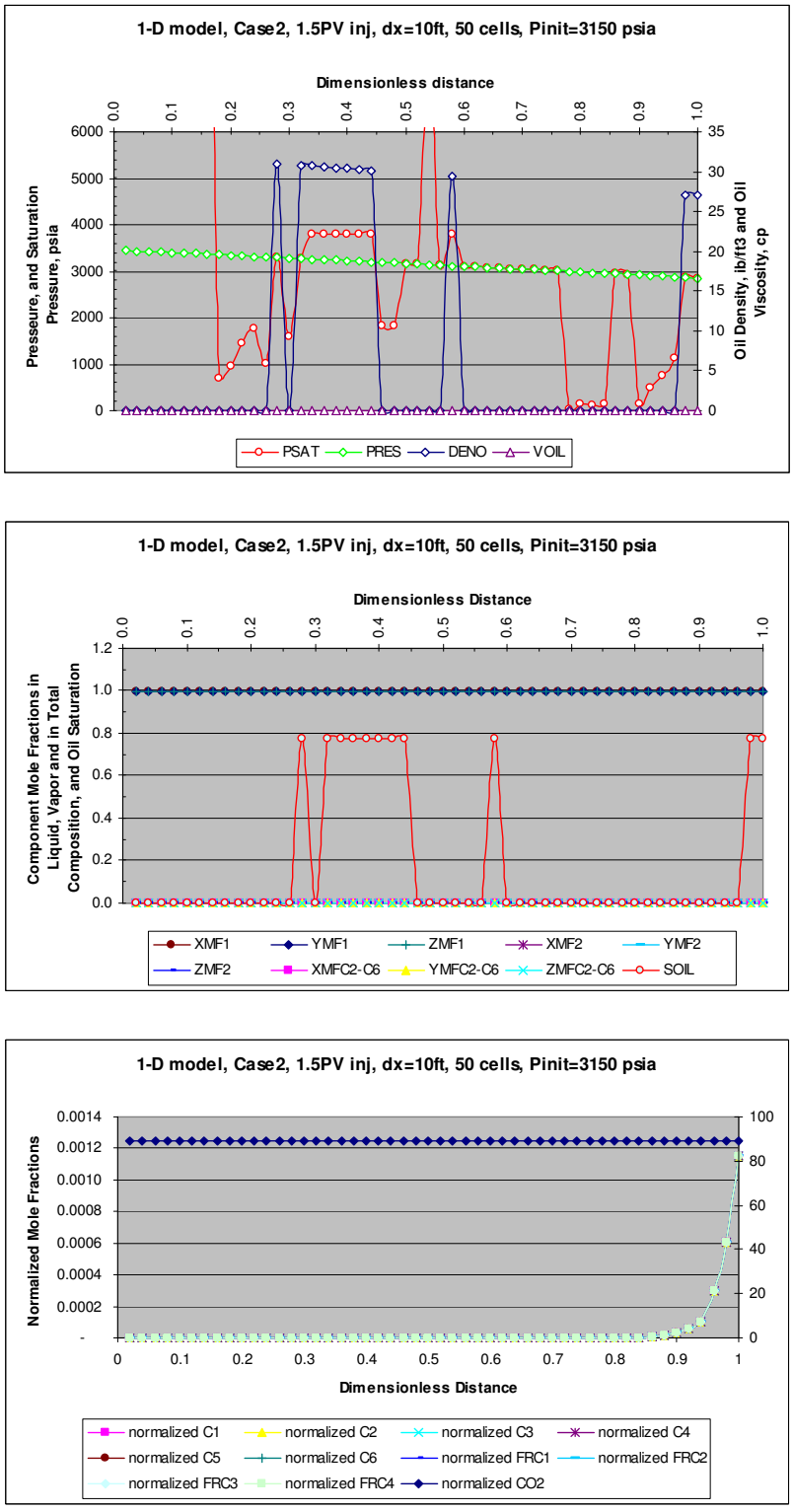

Figure 8-17: Case-2, 1.5 HCPV injected

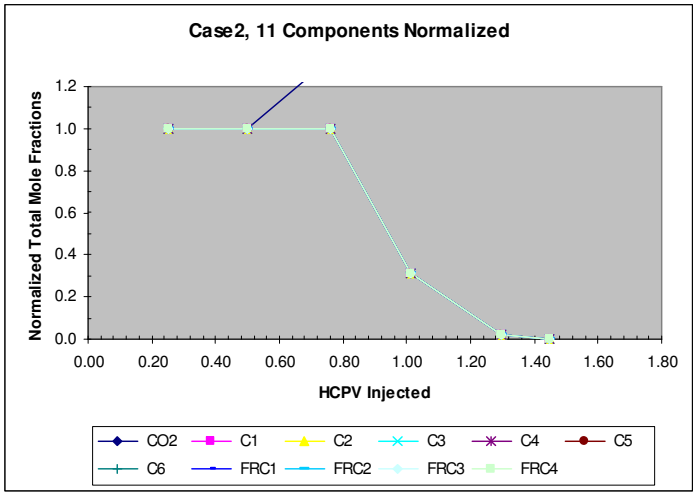

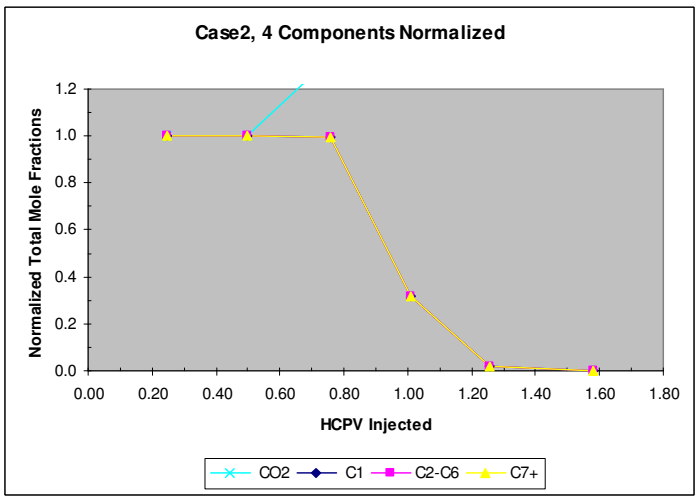

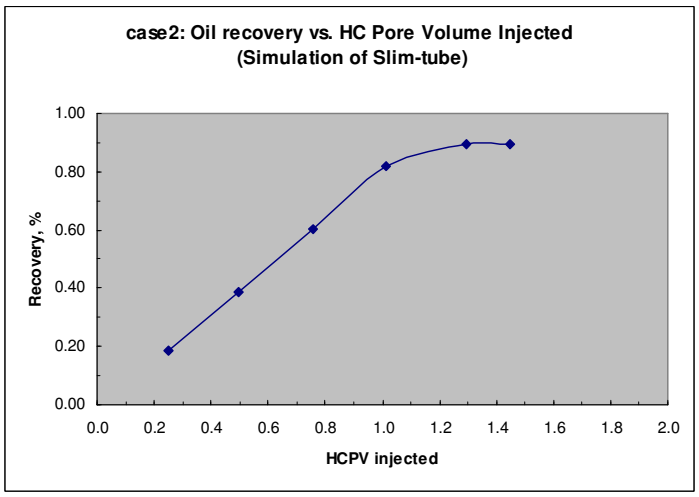

Figure 8-18: Case-2, Recovery vs. HCPV injected

8.1.3 Case-3, Pinit=2500 psi, T=225 °F

Case-3 was initialized at 2500 psia which is below slim-tube measured MMP. Results of this case are shown in Figure 8-19 through Figure 8-26.

The saturation pressure versus pore volume injected again takes wave shaped behavior until 1 HCPV injected. After 1 HCPV the pattern is destroyed, and the cells that are not yet fully swept are characterized with saturation pressures higher than the reservoir pressure, also the saturation pressure is equal to the reservoir pressure for oil saturation greater than 0.

The oil viscosity and density behavior is similar to that of Case-1 and Case-2.

The normalized fluid composition after 1 HCPV injected is a distinguished character of Case-3, because proportionality between OOIP components is lost. In Case-1 and Case-2 the proportionality at all HCPVs injected was maintained, see Figure 8-24 through Figure 8-26. The change in the oil composition along the 1-D model after 1 HCPV injected is related to the decrease in the content of the light hydrocarbons and increase in the content of the heavier components, essentially FRC1, FRC2, and FRC3. The reason is the development of a vaporizing miscibility process.

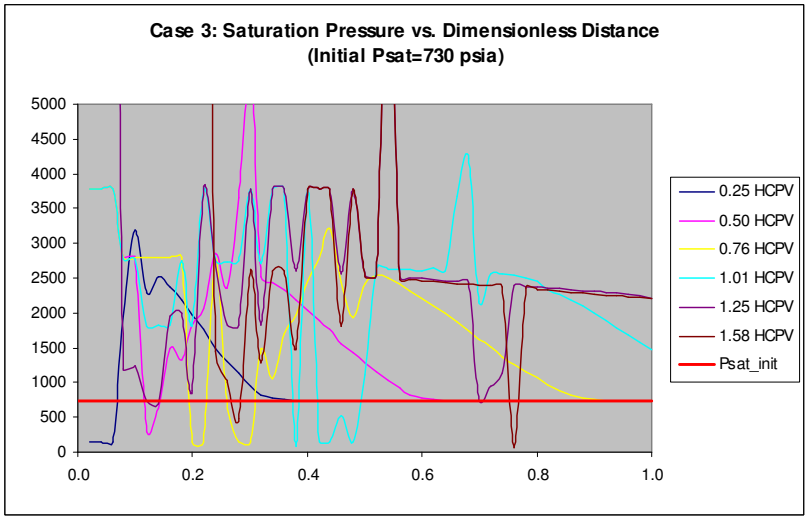

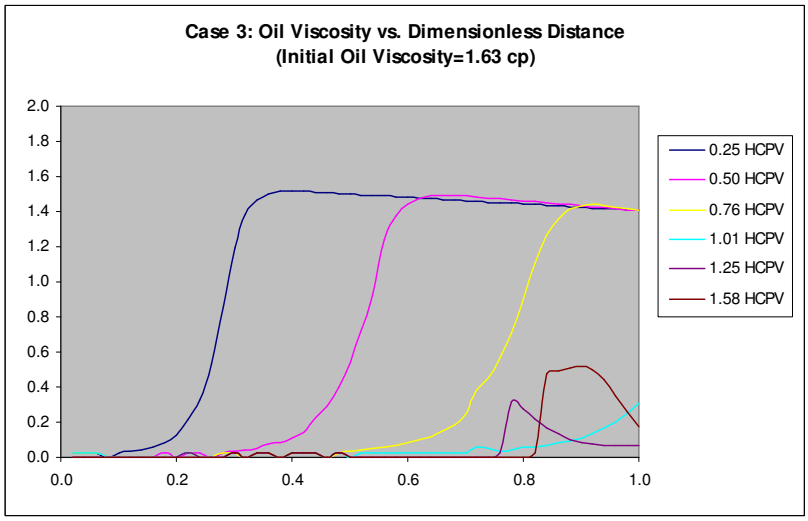

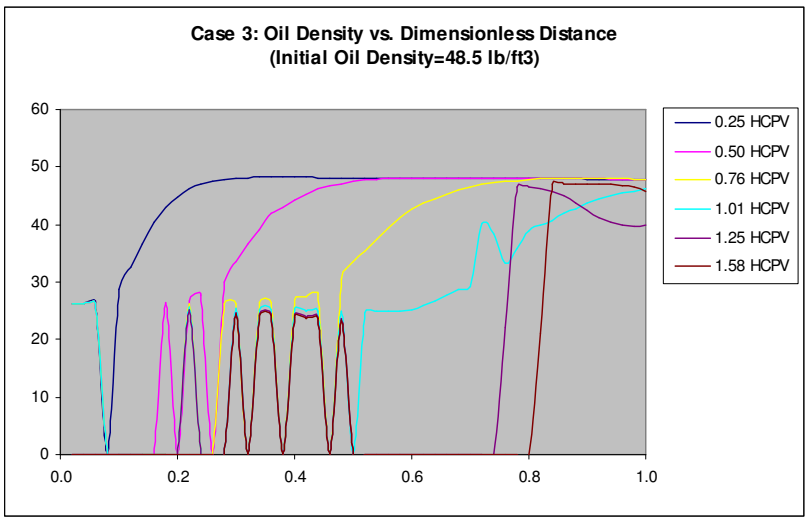

Figure 8-19: Case 3, Comparison of basic properties vs. distance for different HCPV injected

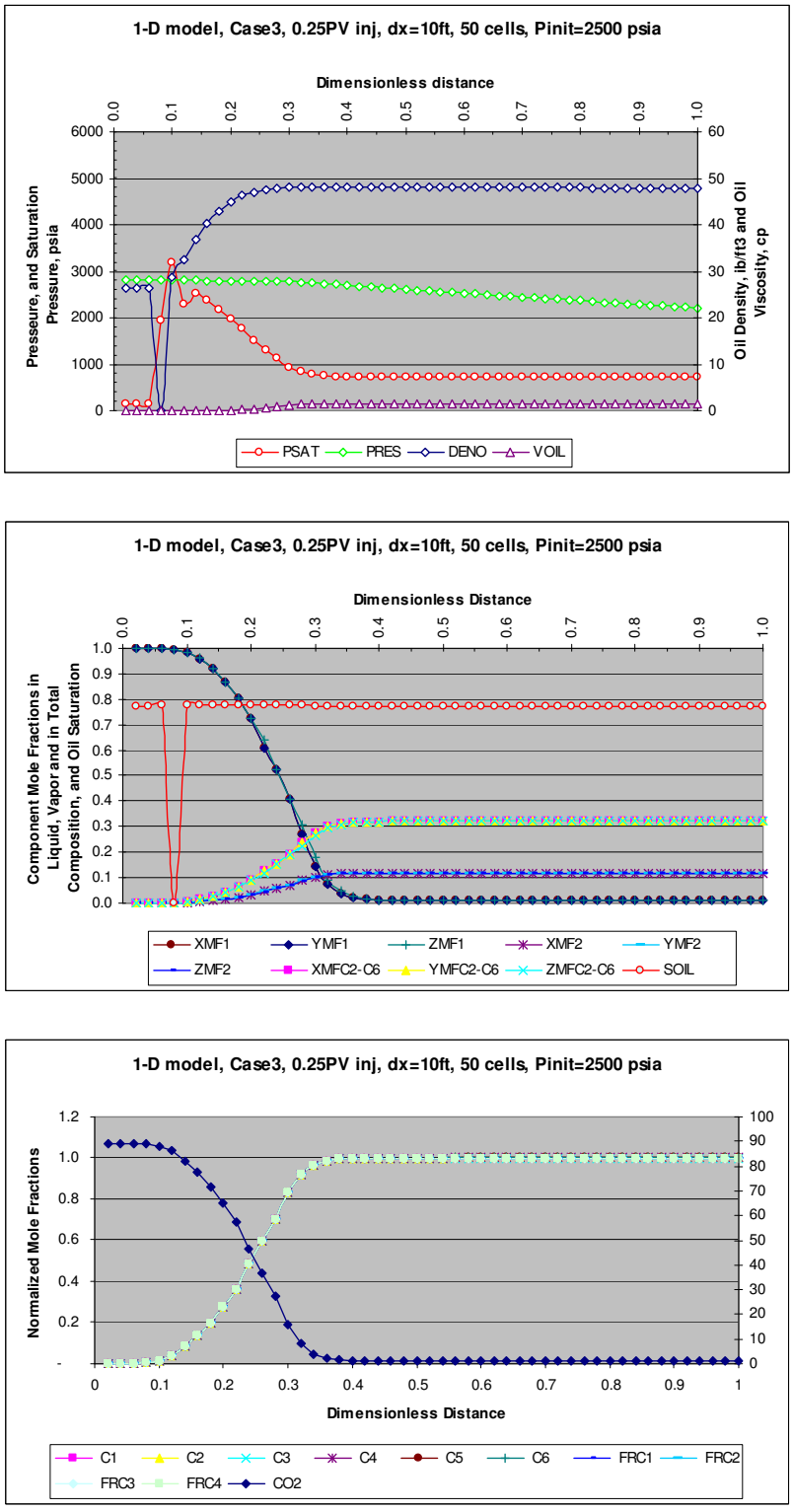

Figure 8-20: Case-3, 0.25 HCPV injected

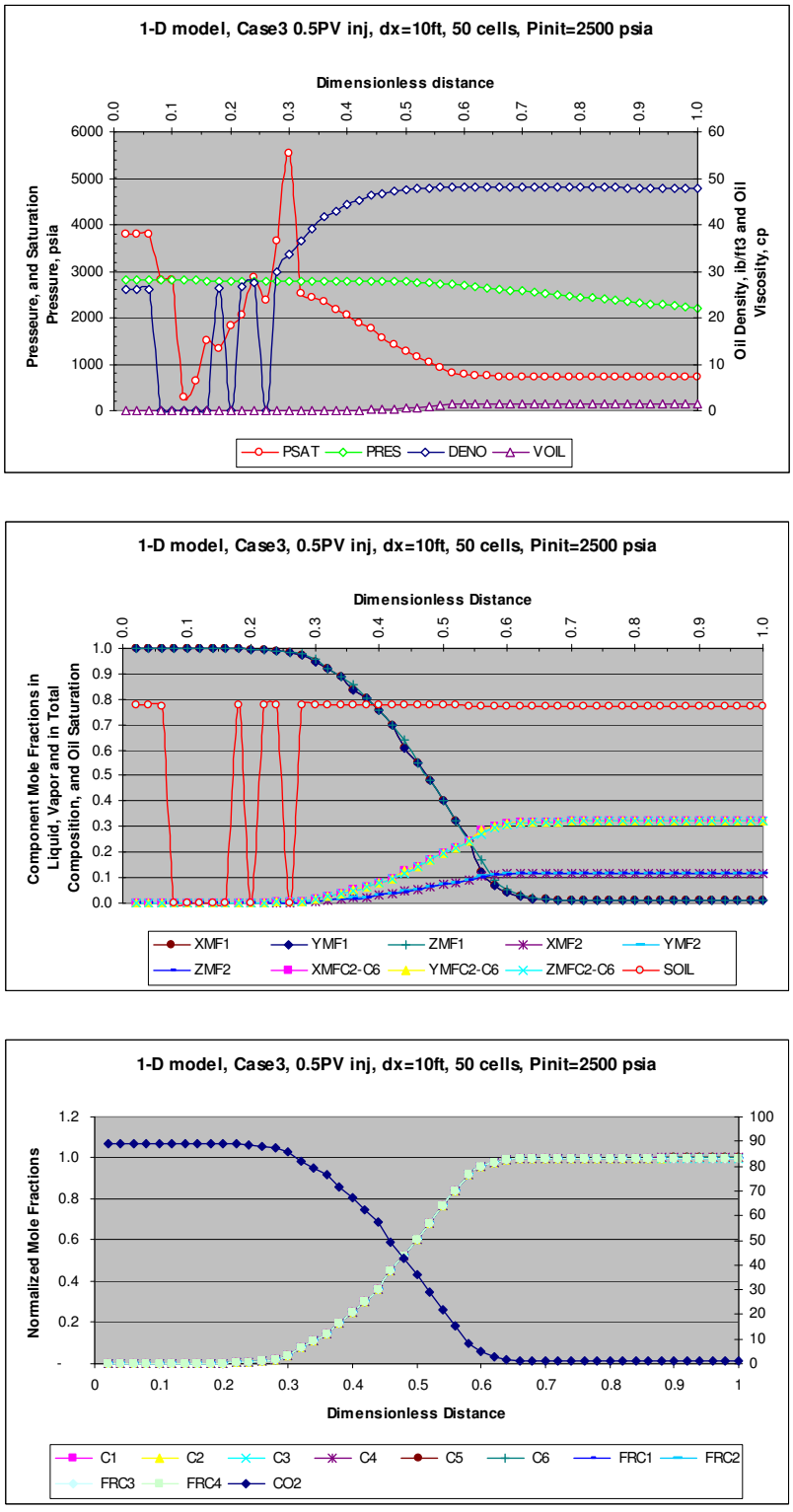

Figure 8-21: Case-3, 0.5 HCPV injected

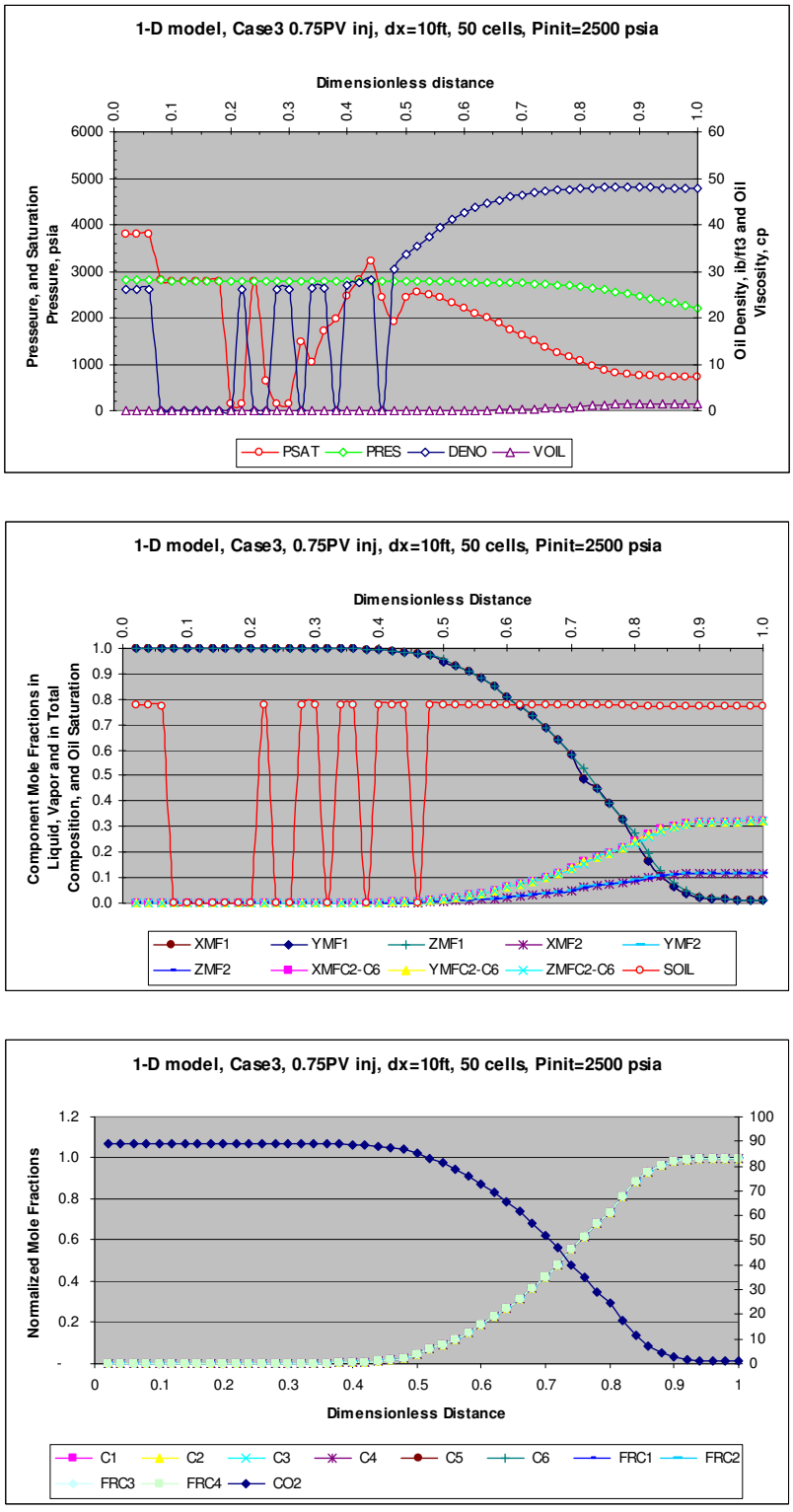

Figure 8-22: Case-3, 0.75 HCPV injected

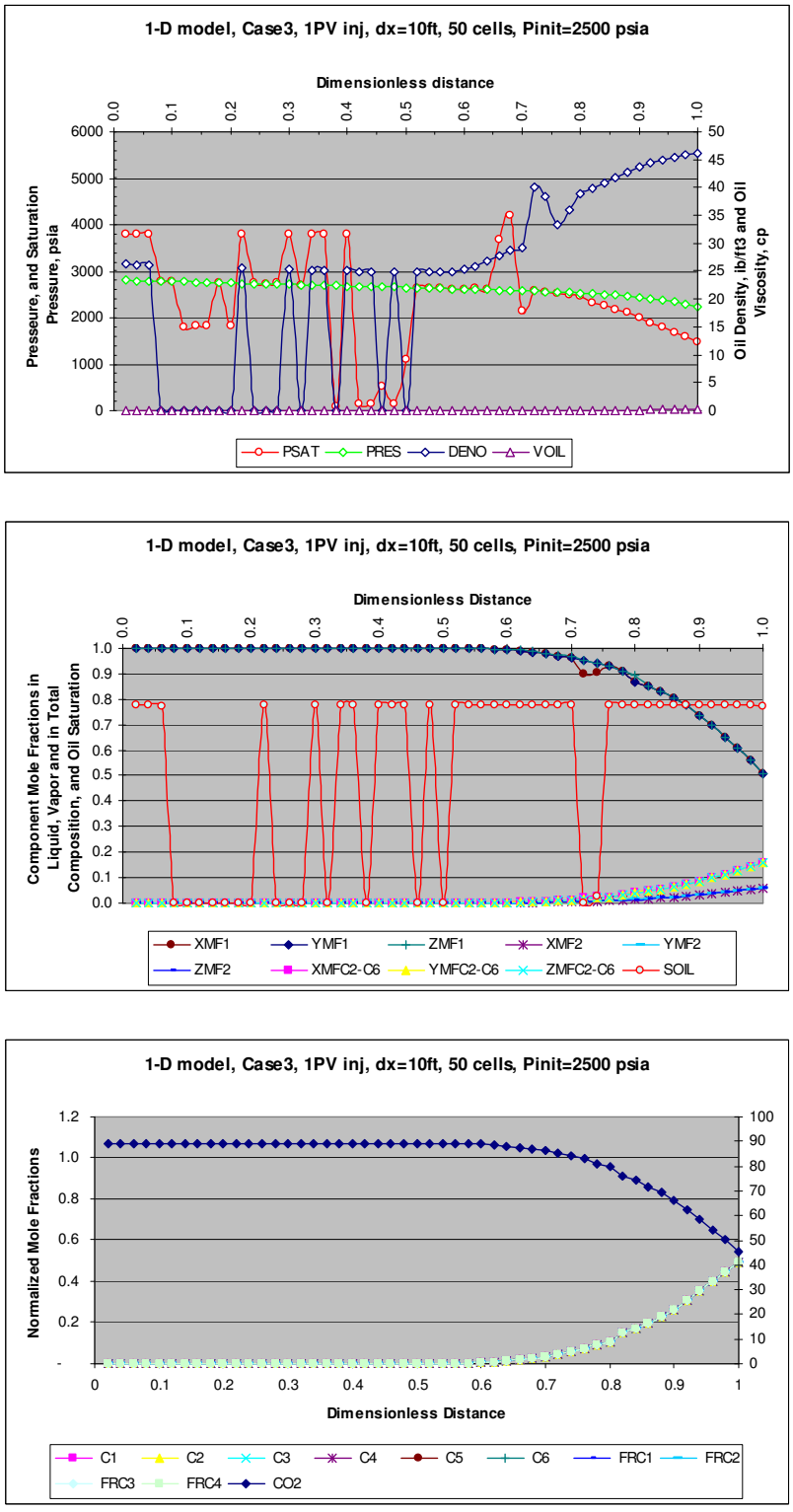

Figure 8-23: Case-3, 1 HCPV injected

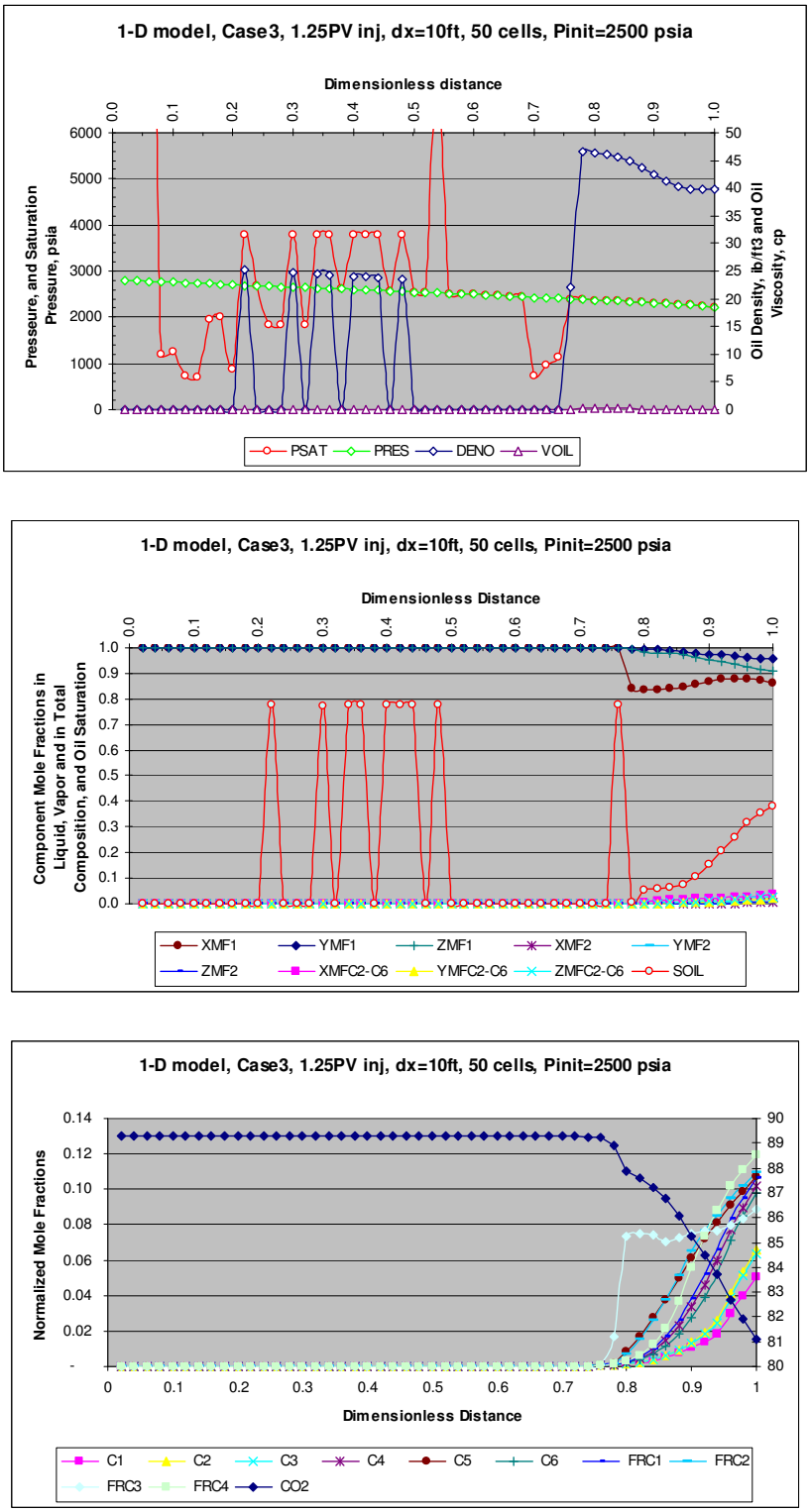

Figure 8-24: Case-3, 1.25 HCPV injected

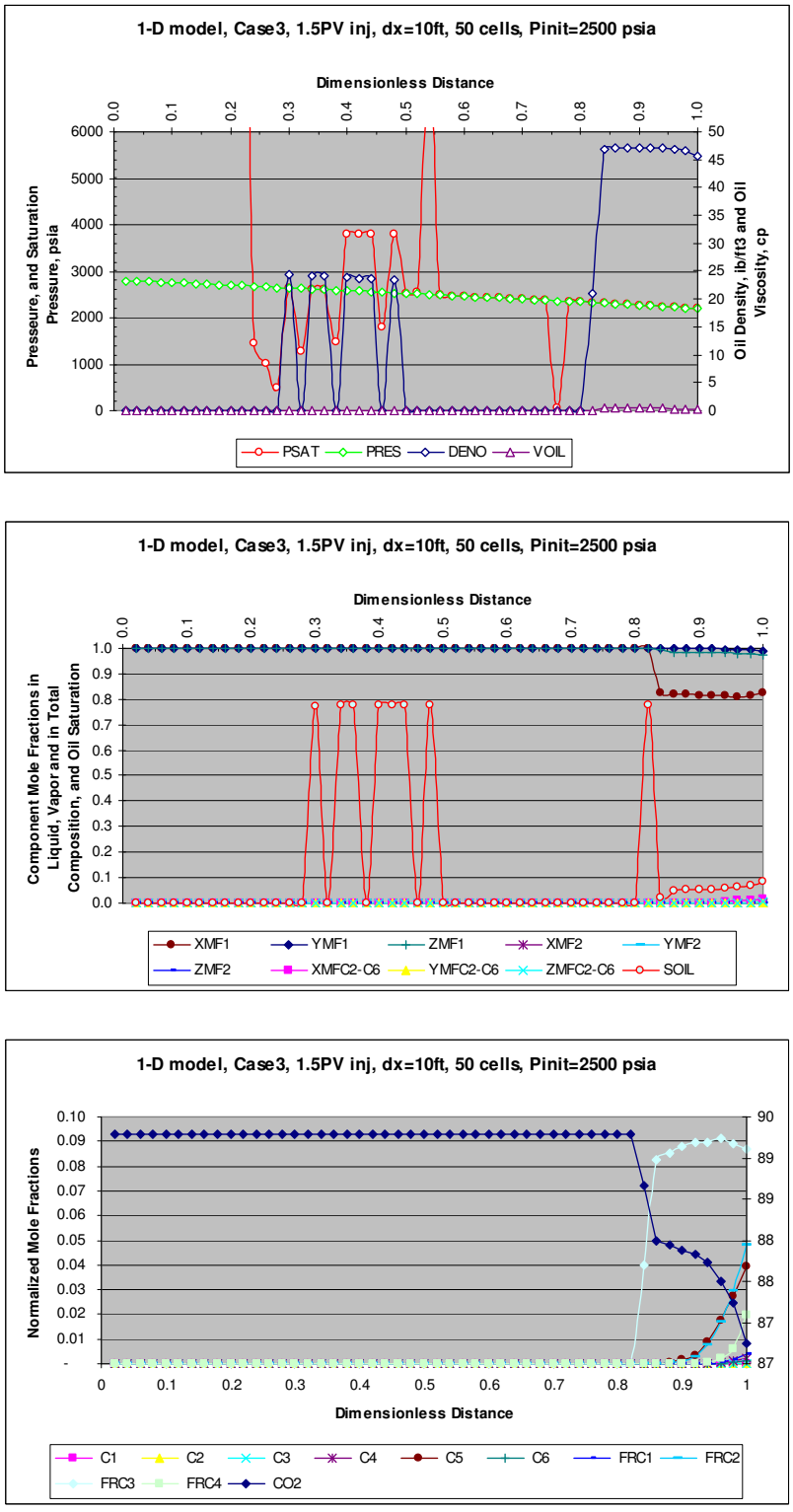

Figure 8-25Case-3, 1.5 HCPV injected

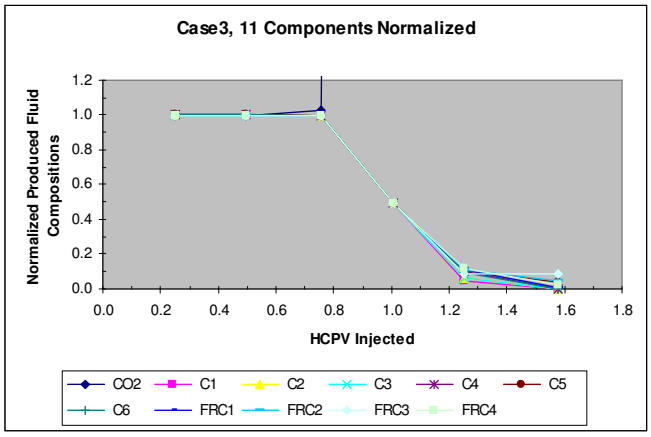

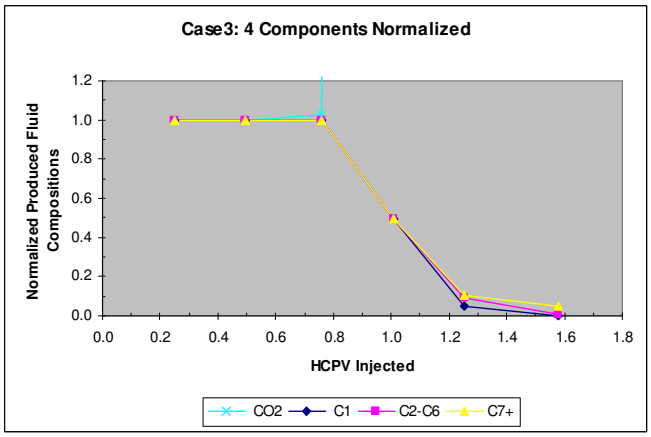

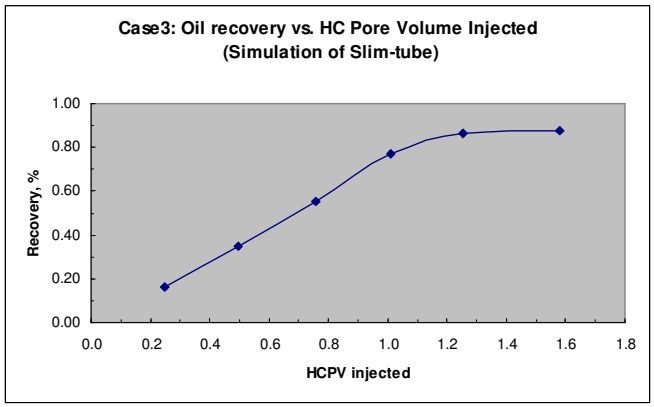

Figure 8-26: Case-3, Recovery vs. HCPV injected

8.2 CO2 Injection into Sarir C-North

Model initialization resulted in the following OOIP distributed. For confidentiality reasons, the OOIP of the individual members are shown as percentage from the field OOIP

Table 8-1: Original oil in place (OOIP) distribution

Member	% of OOIP
M5AA	81.81
M5AB2	11.26
M5AB1	6.93
Total	**100.00**
M5AC	Transition Zone

Because M5AA contains most of the OOIP (81.81%) any water or gas injection will naturally target this member. OOIP in M5AC is considered as non/movable oil, and M5AB1&2 are more heterogeneous than M5AA. More over these two members (M5AB1&2) are partially supported by a limited aquifer which results in slow water encroachment, therefore M5AA by all criterion is the best candidate for future water and/or gas injection.

Lateral extension of M5AA covers the entire top view of the reservoir, however most of the oil is accumulated in the fault blocks located along the east-west direction, yet small oil banks are distributed in the adjacent fault blocks as well. Figure 8-27 depicts M5AA fault blocks of interest. Any future drilling whether for production or injection will target M5AA region plus those of M5AB 2&1 just underneath. For the academic research only M5AA FIP region is consider as shown in Figure 8-27 which includes layers 1 to 30 in the simulation model.

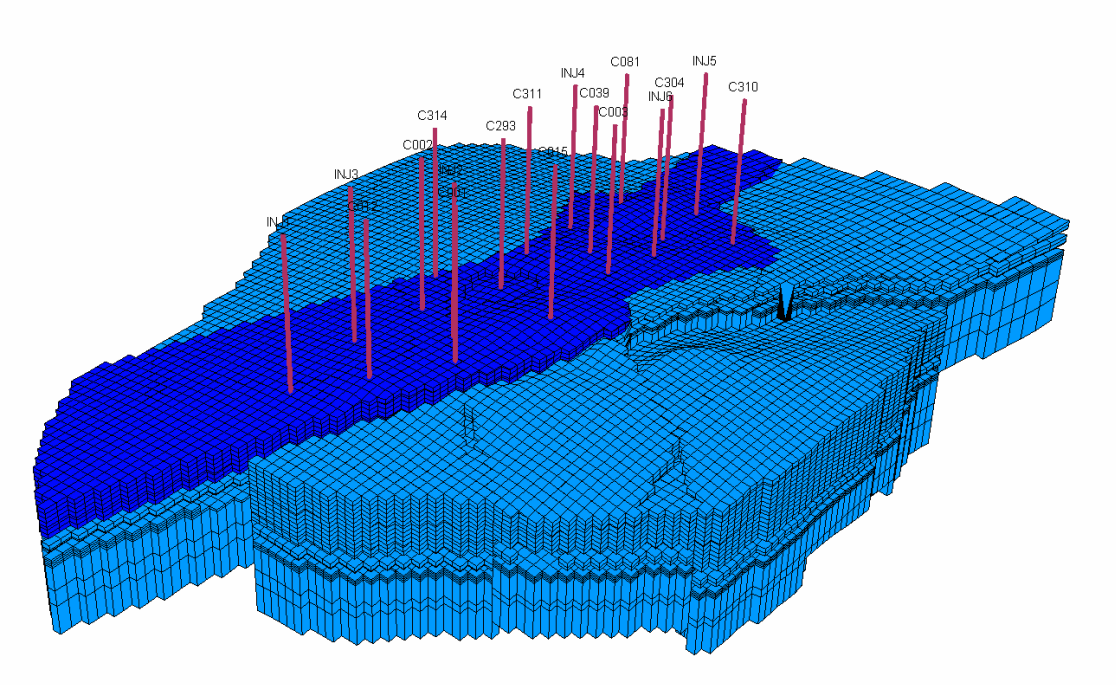

Figure 8-27: M5AA FIP region

It was clear that the field is underdeveloped, consequently three more producers namely C001, C002 and C003 as well as six injectors namely INJ1 to INJ6 were introduced right at the beginning of the simulations.

8.2.1 Effect of Initialization Pressure, (Without History)

The model was initialized at datum depth of 8500 ft and at the same pressures as for the 1-D model which confine the minimum miscibility pressure (ie., 3500, 3150, 2500 psia), and the same reservoir temperature 225 °F. Three runs of continuous CO2 injection were performed for 2000 days each.

Again, like in the 1-D model, the injectors were bottom-hole pressure constrained at BHP equals the initial pressure plus 300 psia, whereas the producers were bottom-hole pressure constrained at BHP equals the initial pressure minus 300 psia, and producers were shut-in if GOR exceeds 4000 SCF/STB (initial GOR=156 SCF/STB). The reason why the maximum GOR was set to 4000 SCF/STB is due to

the laboratory swelling test shown in Figure 8-28 where 4000 SCF/STB represents dew point.

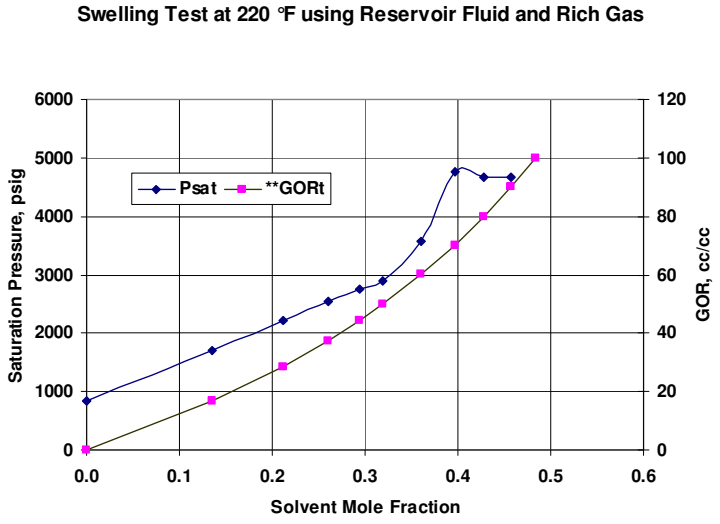

Figure 8-28: Laboratory CO2 swelling test for Sarir

Cumulative Oil Production

Figure 8-29 and Figure 8-30 shows a comparison of the total oil production after 2000 days of continuous CO2 injection at three different initial pressures. One additional case of continuous water injection is also shown on Figure 8-29. The water injectors were bottom hole pressure constrained to 4000 psi to allow for maximum water injection. The maximum oil production resulted from the initial pressure of 2500 psig, then 3150 psia and finally 3500 psia, this result can be related to pressure functions: oil viscosity and density, Table 8-2. The continuous water injection was by far the worst scenario of all.

Table 8-2: Oil properties at initialization pressures

Initial pressure, psia	Oil viscosity, cP @ Pinit and 220 °F	Oil density, lb/cu-ft @ Pinit and 220 °F
3500	1.7543	48.787
3150	1.6739	48.595
2500	1.5227	48.204

The variation in viscosity vs. pressure results in an unfavorable mobility ratio and relatively early breakthrough at higher pressures, this result seems inconsistent with the principle of the advantage of the injection at or above MMP, and one may ask why these effects are not seen in a slim-tube test? And the answer could be related to the fact that slim-tube test is a simplified experiment which ignores many real flow effects like gravity, heterogeneity, fingering …etc. It can be concluded that if flooding using CO2 or any injection gas suffers from unfavorable mobility ratio then it is evident that at higher pressures this problem is more pronounced. Table 8-3 shows viscosity and density of CO2 however at the same conditions.

Table 8-3: CO2 properties at initialization pressures

Initial pressure, psia	CO2 viscosity, cP @ Pinit and 220°F	CO2 density, lb/cu-ft @ Pinit and 220°F
3500	0.0429	32.746
3150	0.0391	29.767
2500	0.0318	23.201

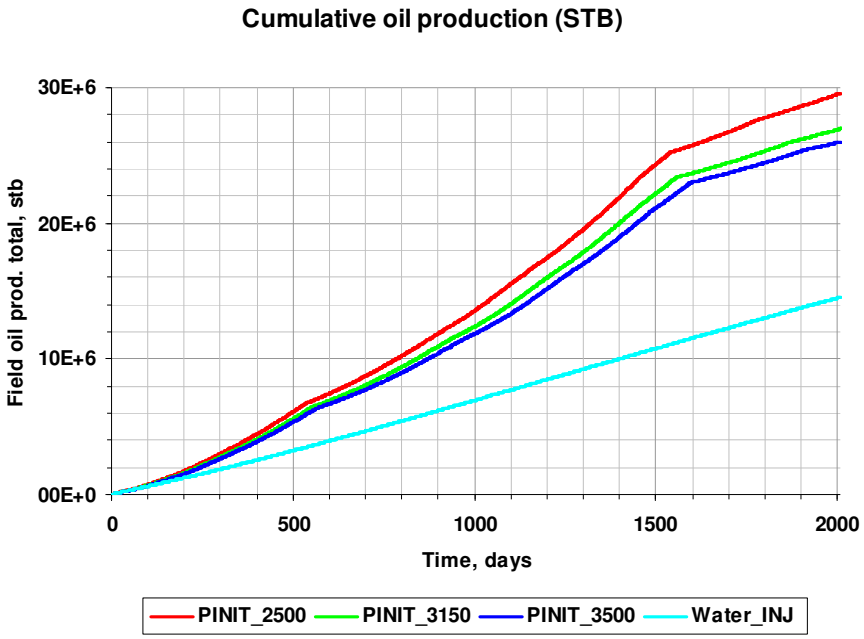

Figure 8-29: Cumulative oil production (STB) after 2000 days

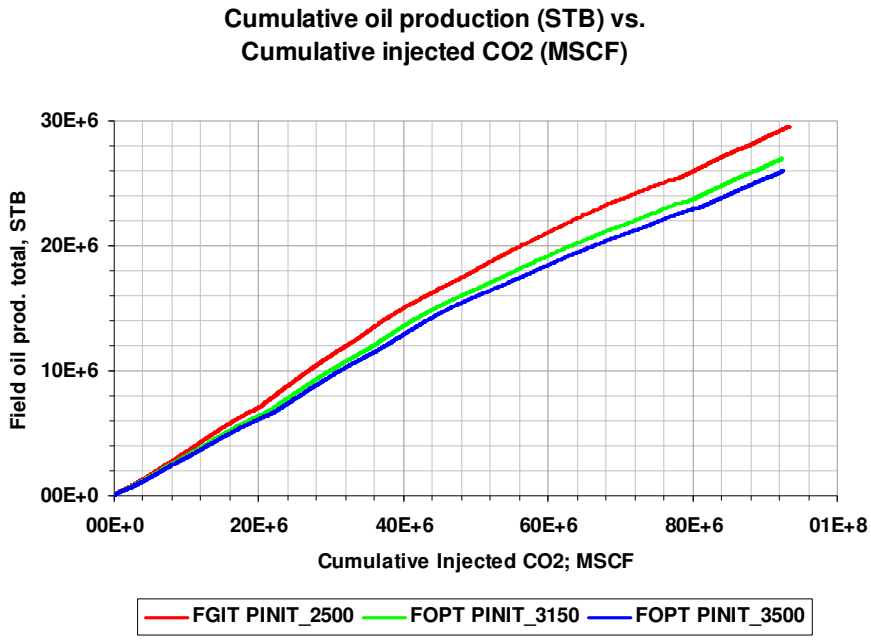

Figure 8-30: Field recovery vs cum. injected CO2

Near wellbore effects and behavior such as saturation pressure, in the region of high pressure around an injector and low pressure surrounding a producer can not be depicted by a coarse simulation grid block with dimensions like for example 500×500 ft, these effects are typically studied in the lab, yet the overall performance of a CO2 injection process can be traced and interpreted as recovery efficiency. More laboratory research is required to better understanding of near wellbore and phase behavior effects during gas injection process.

The efficiency of CO2 flood is not only linked to its ability to extract intermediate components but also to reducing oil viscosity and also to its diffusivity in water to collect isolated oil droplets. If miscibility conditions are favorable then this is an extra advantage of CO2 to other solvents. The studied oil sample was highly undersaturated, the GOR was 156 SCF/STB. Therefore it was difficult to see free CO2 flowing in the model, the solvent is immediately dissolved in the undersaturated oil and the system remained a single phase, the extreme case where CO2 could be seen is at high injection rates.

8.2.2 Injection Schemes, (After History Match)

Sarir C-North geological model, production data as well as SCAL and PVT data were used. The model was initialized at datum depth of 8200 ft, and at the initial pressure of 3890 psi, and history matched from June 1967 to Sep. 2005. Then a series of sensitivities were performed to determine optimum CO2 injection rate, and slug size for WAG parameters. Three Cases were considered, a continuous CO2 injection, a WAG process and a continuous water injection process. The three injection schemes were run and compared to verify recovery as a result of the flooding process. The forecasted schemes lasted ≈ 15 years: 1 Oct. 2005 – 1 Aug. 2020.

Three new producers namely C001 to C003 as well as the six injectors namely INJ1 to INJ6 were introduced right at the beginning of the predictions, i.e., Oct. 2005.

The injectors were given a constant injection rate, whereas the producers were bottom-hole pressure constrained at BHP equal to the last simulated history matched pressure, and producers were shut-in if GOR exceeds 4000 SCF/STB (initial GOR=156 SCF/STB).

Optimization of CO2 injection rate

Six sensitivity runs were performed at CO2 injection rate of 500, 1000, 1500, 2000, 2500 and 3000 MSCF per well per day. Figure 8-31 shows field recoveries at various injection rates. It was clear from the individual well performance that the optimal injection rate is between 2000 and 2500 MSCF/well/day. Three wells were shut-in due to GOR limit. Although in the overall field performance the 3000 MSCF/well/day produced the maximum cumulative oil production. The continuous CO2 injection did not support the reservoir pressure, Figure 8-32.

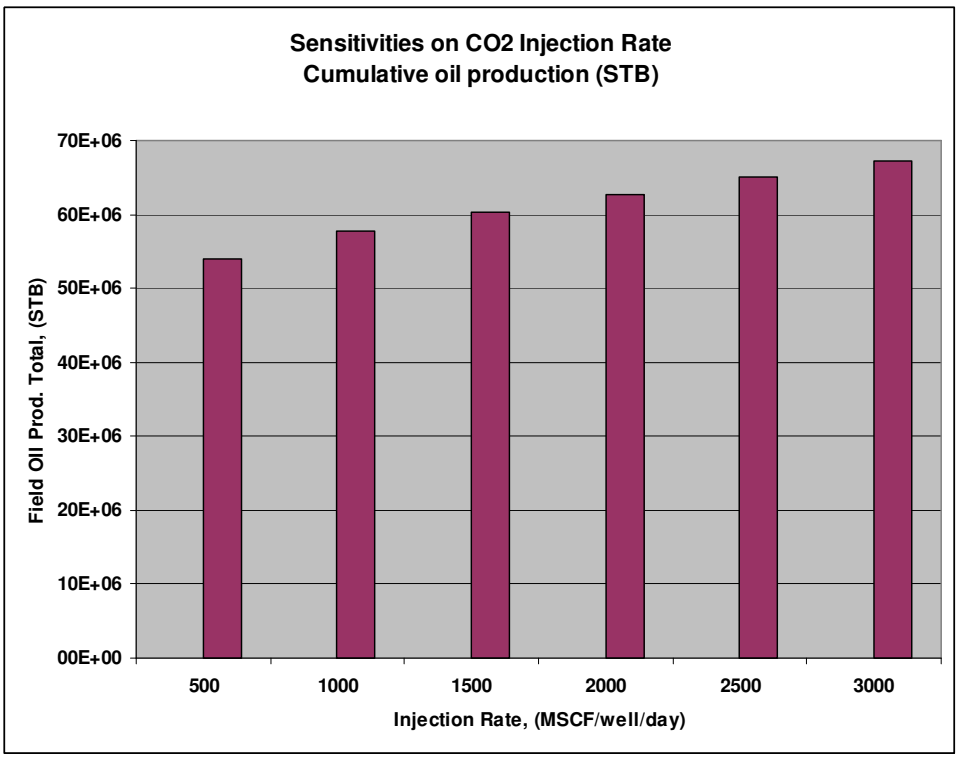

Figure 8-31: Sarir Field, Optimizing CO2 injection rate

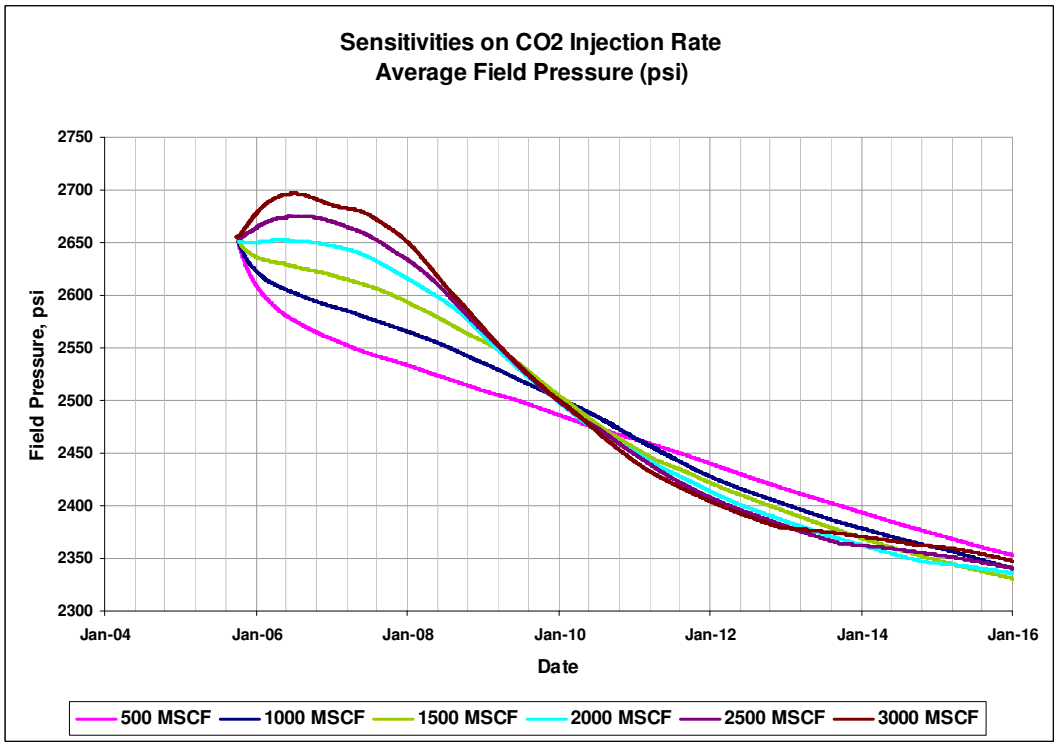

Figure 8-32: Sarir field, field pressure

Continuous CO2 Injection

The average reservoir pressure at the end of the history match (Sept. 2005) was approximately 2656 psia at datum level of 8200 ft, see Figure 8-32. Reservoir pressure in M5AA at the end of the history match was relatively low (approximately 2200 psi). Therefore, pressure maintenance using water injection was implemented for 5 years (1 Oct. 2005 – 1 Oct. 2010) with injection rate of 1000 STB/well/day which represents about 8 % of HCPV in M5AA region. Then continuous CO2 injection was implemented for the rest of the prediction period i.e., 10 years.

Water Alternating CO2, (WAG)

The WAG displacement was based on the sensitivity carried out for the optimum CO2 injection rate, and assuming 10% HCPV CO2 slug size, 1:1 WAG ratio and performing the process in six cycles.

Table 8-4 summarizes WAG parameters i.e., WAG ratio, slug size and duration needed for cycling gas and water.

Table 8-4: WAG parameters calculation

Input:	
M5AA HCPV (stb)	152,682,000
Water inj. rate (rb/well/day)	1,000
Gas inj. rate (scf/well/day)	2,500,000
Start of prediction	30.09.2005
End of prediction	30.07.2020
No. of inj. wells	6
CO2 slug size, % HCPV	10%
WAG rtio 1:	1.0
No. of cycles	6

Output:	
Water slug size (cum.) stb	15,268,200
Gas slug size (cum.) stb	15,268,200
Cum. time, day	5,418
WAG period, day	3,592
Water inj. before WAG, day	1,826
Field water inj. rate, rb/day	6,000
Cum. time of water inj., day	2,545
Bg, rb/scf @ 2200 psia and 225 °F	0.000972
Field gas inj. rate, scf/day	15,000,000
Field gas inj. rate, rb/day	14,580
Cum. time of gas inj., day	1,047
Gas cycling every, day	175
Water cycling every, day	424

Continuous water injection

With all parameters fixed, this scenario is a continuous water flood. No CO2 is introduced to the model. Table 8-5 shows the parameters of the injection schemes.

Table 8-5: Injection scheme parameters

Scheme	no. of Inj wells	Water Inj. Rate (STB/well/day)	CO2 Inj. Rate (MSCF/well/day)	GOR limit (MSCF/STB)	Cum. Water inj. (% HCPV)	Cum. CO2 inj. (% HCPV)
continuous	6	*1000	2500	4	7.18	34.3
WAG	6	1000	2500	4	17.18	10.0
Continuous water injection	6	1000	0	-	22	0

* Pressure support during the first five years after history

Results

Results of the flood performance of the three injection schemes are presented as line plots comparing recovery for the field under different flooding schemes. Only the prediction period is shown. The first five years are identical for all runs because only water was injected for pressure maintenance with the same rates in the same wells. It is shown in Figure 8-33 that for Sarir C-North under the above mentioned operating conditions and constraints and well spacing it is evident that a continuous CO2 injection ranked top as far as field recovery is concerned then WAG and finally water injection. Continuous CO2 injection results in less water production, Figure 8-34 . No economics are involved, however the economic analysis may favor one method over another. Nevertheless, it is evident that both continuous CO2 injection and WAG result in a more efficient displacement and better recovery over continuous water injection.

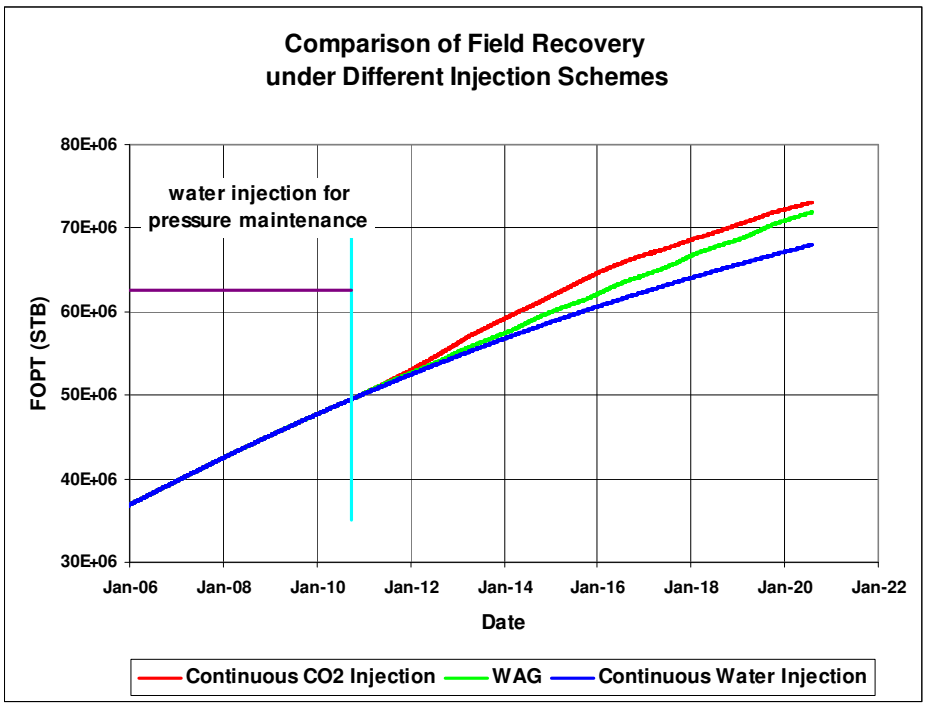

Figure 8-33: Sarir field, comparison of field recovery

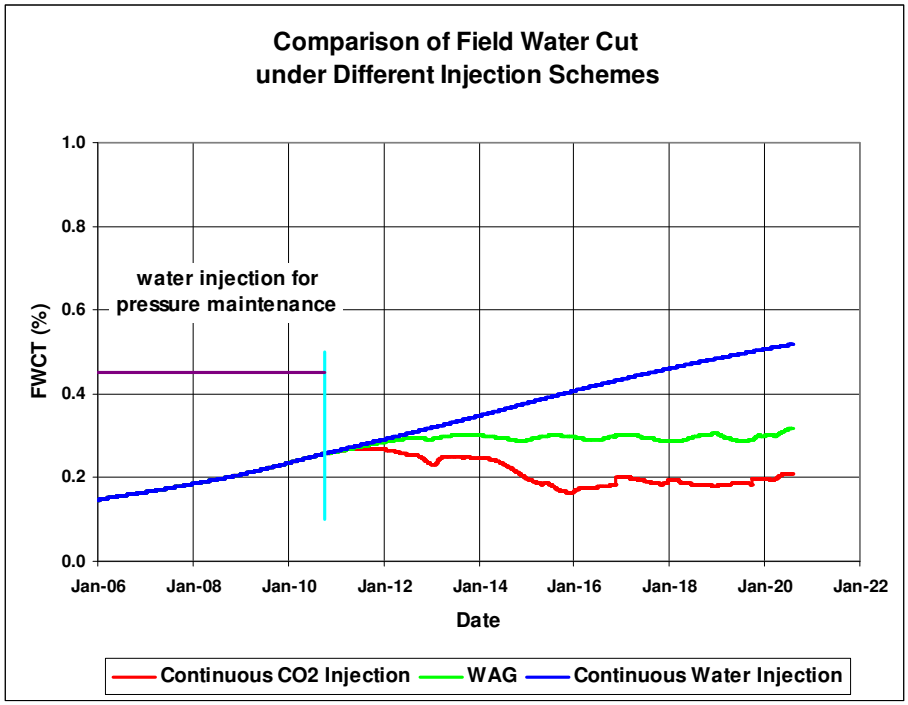

Figure 8-34: Sarir field, comparison of water cut

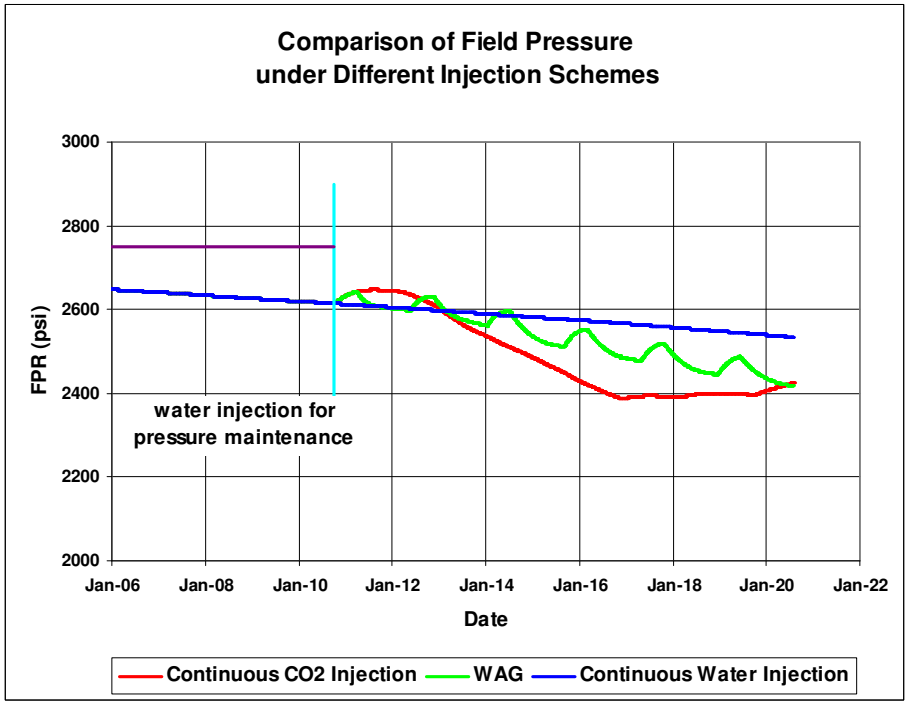

Figure 8-35: Sarir field, comparison of reservoir pressure

CHAPTER 9 Operational Problems and Associated Risks

CO2 injection either as a continuous gas injection or WAG operation is usually accompanied with operational problems. Examples of such problems are; early breakthrough in production wells, reduced injectivity, corrosion, hydrate formation etc. The Health Safety Environment, HSE, and associated risks on the human life and society during the different phases of CO2-flood projects must be taken into account and consideration

9.1 Operational problems

In the production life of an oil field, some operational problems are anticipated, and these problems are more serious during WAG process than in a pure gas or water injection processes because the injection fluid must be changed frequently. The operational problems can occur in both the injection and production wells, as well as in the surface facilities including compressors, pipelines separators etc.

The direct result of unfavorable mobility ration is fingering and early gas breakthrough, as discussed in CHAPTER 5 . Fingering or channeling is caused not only by unfavorable mobility ratio but also by the reservoir heterogeneity and especially high permeable layers [7].

The most significant effect of CO2 on the surface facilities, wellbore casing and down-hole tools is corrosion. The reason is that these tools and equipments are not designed for such type of operations. In fact these tools and equipments are designed to handle primary and secondary recovery processes using water injection, unless if CO2 is found in high concentrations in the reservoir. CO2 dissolves into water forming Carbonic acid, H2CO3, which is the direct cause of corrosion.

$$CO_2 + H_2O \Leftrightarrow H_2CO_3 \Leftrightarrow H^+ + HCO_3^-$$

$$H^+ + HCO_3^- + CaCO_3 \Leftrightarrow Ca^{2+} + 2HCO_3^-$$

If the cementation is not resistant to H2CO3 Carbonic acid will interact with the cement behind the casing dissolve part of it causing channeling of CO2 behind the casing. Corrosion control methods include:

- Changing/modifying operating parameters (e.g., flow rate, temperature, remove water)
- Applying organic coating or use of liner to isolate metal from corrosive environment
- Use of corrosion-resistant materials e.g., 13% Cr, duplex stainless steels either in a sold form or cladding on carbon steel
- Use of nonmetallics e.g., fiber-reinforced plastics

Scale formation during WAG process is also expected. The formation of scale stresses the pipelines and can lead to failure. Scaling also causes casing failure. Chemical treatments such are scale inhibitors are used to control or prevent scale depositions.

The change in the operating conditions especially temperature in the injector results in hydrate formation which causes plugging of the injector and freezing of the wellhead during cold weather [53]. The formation of hydrate usually can be controlled with methanol solvent treatment.

The change in temperature between the injected fluids (water and gas) during WAG process may result in stress-related tubing failures [34]

9.2 Associated Risks

Carbon Dioxide (CO2) is a colorless, odorless non-flammable gas and is the most prominent Greenhouse gas in Earth's atmosphere. CO2 density is 1.53 relative to air. CO2 causes a high risk of loss in human life at concentrations of 150,000 ppm,

thus human exposure to elevated levels of CO2 can be hazardous in two ways: by a reduction in the oxygen content of the ambient air causing suffocation or through direct CO2 toxicity [10].

9.2.1 Risk Associated with Surface Pipeline Network

Use of CO2 for EOR or sequestration includes risks on the human health and environment. Risk management of CO2 storage is of a great importance to avoid environmental problems and man's life. Potential risks associated with the plant and aboveground facilities for separating, compressing and transporting CO2 to the injection site, and possible failures of the engineered system are: pipeline rupture, pipeline puncture (i.e., releases through a small hole), and rupture of the wellhead injection equipment. Accidental releases from the pipeline or wellhead, although infrequent, could potentially affect the general public in the vicinity of a release.

Transporting huge volumes of CO2 from the capturing locations or CO2 reservoirs incorporates the risk of failure in the transport lines and consequently CO2 leakage this risk results in severe and deadly consequences on the human life as well as the environment. One technique to the reduce safety hazards is to "over engineering" CO2 pipelines particularly those close to human dwellings and also "marking" the gas with a chemical to make any leaks more readily detected [27]

9.2.2 Risk Associated with Underground Storage

The capture and storage of CO2 in geological reservoirs is now considered to be one of the main options for achieving deep reductions in greenhouse gas emissions [27]. These geological formations contained the hydrocarbon accumulations for millions of years, therefore they should be able to store the injected volumes of CO2. This statement appears correct, but in fact it ignores the changes that tock place in the geological formations during the period of production such as (1)

change in the local stresses because of pressure decline due to production, (2) reduced degree of consolidation of the rocks due to water encroachment, and (3) decrease in the tightness of the seal that the cap-rocks provided during the production period of the reservoir. So, characteristics of the geological formations that contained the hydrocarbons for millions of years are not necessarily the same as the current characteristics, and no guarantee that CO2 will remain in the same formations and do not leak to surface or adjacent formations, especially in faulted reservoirs. This discussion however, is for the case where CO2 is injected for sequestration, but for the case where CO2 is injected as an EOR fluid then storage is not the objective, in fact CO2 will be re-produced and re-injected in a cyclic manner. Only the portion that dissolves in the formation water will be lost which is normally in the range of 5% depending on pressure, temperature and salinity of the formation water, as explained in the example given in CHAPTER 4 . The information available about the depleted hydrocarbon reservoirs, the number of wells already exist, the storage capacity and the known initial pressure give them an advantage to be candidates for CO2 sequestration compared to other possible alternatives, yet the risk induced by the injection of CO2 in terrestrial storage is significant and risk assessment must be a prerequisite for any CO2 injection process regardless of the objective of injection EOR or sequestration. Good engineering and geotechnical information included in the reservoir modelling and combining these with identification of features, events and processes that may influence the integrity of the reservoir is the way to assure stability of the bearing formations.

The Saline formations and aquifers are also good potential ground storage. They are geographically wide distributed and they have huge storage capacities. The main risk associated with these formations is the unavailability of information, for example, the initial formation pressure which may be exceeded during the injection phase will lead to the risk that the injection will crack rock layers and CO2 leaks to the surface. Coal-beds have high storage capacity. Coal-beds absorb CO2 and emit methane which can be recovered. CO2 storage under the ocean is also an area of research, however the effect of CO2 on the organic life due to the increase in the

acidity (reduced PH) and possible CO2 migration to the see level are clear risks that have an enormous impact on marine life.

9.2.3 Monitoring

Monitoring CO2 related risks associated with surface leakage due to migration from underground storage to the surface including casing leaking, cement failure or through cap-rock seal failures, faults, fractures or wells is an extremely important to assure prevention of negative consequences on the environment and eliminate any danger on human life. Monitoring includes gathering information on leakage of CO2 from existing injection sites and natural releases. The information to be collected for analogy between injection sites and natural releases include: description of the zone with CO2, physical characteristics of the seals and porous zones, information on shallow groundwater and surface water, nearby faults, numbers of nearby wells, the amount of CO2 released from leakage or a natural event, the conditions present at that time, and any known effects. Gathering of all these data is an essential step for risk analysis

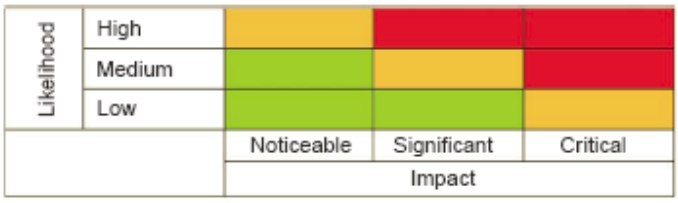

Figure 9-1: Risk categories (After [30])

Once risks are identified, they are categorized according to their impact on health, safety and environment and likelihood, Figure 9-1.

In summary, three scenarios could potentially cause acute effects: upward leakage through the CO2 injection wells; upward leakage through the deep oil and gas wells; and upward leakage through abandoned or poorly constructed wells. Six scenarios could potentially cause chronic effects: upward leakage through cap-rock and seals by gradual failure; release through existing faults due to effects of increased pressure; release through induced faults due to effects of increased

pressure (local overpressure); upward leakage through the CO2 injection wells; upward leakage through the deep oil and gas wells; and upward leakage through abandoned, or poorly constructed wells.

Monitoring can be summarized in the following categories:

- Groundwater monitoring: continuously checks quality of drinking water from shallow aquifers
- Wellhead monitoring: delivers data on CO2 composition, injection pressure, and temperature
- Measurement of soil CO2 flux
- Crosswell electromagnetic measurements display images of CO2 saturation distribution
- Measurements of surface CO2 flux

9.2.4 Injection Well Risk Assessment

To assure a long-term wellbore integrity and safe CO2 injection process, the following requirements on CO2 injector wells must be considered:

1. The right selection for casing and cementation to assure durability of the casing and cement that is used to isolate the annulus and reduce the risk of failure
2. The integrity of cement jobs must be proved by tests and logs, e.g., CBL, and remediate any weakness in the cement sheath to assure long-term integrity for the full life of the wellbore
3. Well completion has to be withstand mechanical, chemical and thermal demands
4. Emergency Shutdown (ESD) must be installed on the well head
5. Subsurface Safely Valve (SSSV) must be installed
6. Sensors (sensible to CO2, H2S) linked to ESD and SSSV
7. Monitoring CO2 concentrations

CHAPTER 10 Conclusions and Future Work

10.1 Conclusions

Flow problems during supercritical CO2 injection are discussed. CO2 minimum miscibility pressure correlations were reviewed and a new correlation was developed. The saturation pressure, viscosity and density along the path between an injector and a producer as well as recovery were investigated.

The following conclusions summarize the output from this research:

1. This research has practical aims for CO2 injection in Libyan mature oil fields, especially for the Sirte basin crude oils, as well as academic observations. The academic questions addressed in this research were not discussed in the literature in this detail.
2. Near wellbore effects and fluid behavior such as saturation pressure, in the region of high pressure around an injector and low pressure surrounding a producer, can not be depicted by a coarse simulation grid block, these effects are best studied in a the lab, yet the overall performance of a CO2 injection process can be traced and interpreted as recovery efficiency.
3. The efficiency of CO2 flood is not and should not be linked only to its ability to extract intermediate components but also to its direct effect on the oil properties by swelling and reducing oil viscosity, and also to its diffusivity in water to collect isolated oil droplets, however when miscibility conditions are favorable then this is an additional advantage of CO2 to other solvents.
4. The supercriticality of CO2 is the reason for its lower MMP as compared to other hydrocarbon solvents.
5. For highly undersaturated oils, such as the studied sample, it was difficult to see free CO2 flowing in the model at low injection rates. The solvent is

immediately dissolved in the highly undersaturated oil and the system remained a single phase. The extreme case where CO2 could be seen is at very high injection rates which may not be practically reachable.

6. As a result of the swelling of the oil by CO2, saturation pressure advances like a wave of a constant level which gets wider progressively as it advances until breakthrough. Figure 8-3, Figure 8-11, Figure 8-19 indicated the same Psat propagation but the only difference is the reservoir pressure which shifts down. At 2500 psia the saturation pressure exceeds the reservoir pressure.
7. The oil properties especially viscosity is strongly affected by two factors working in opposite directions. The dissolved CO2 reduces while the injection pressure increases the oil viscosity. The increase in viscosity has negative role on sweep efficiency by increasing mobility ratio.
8. In a 1-D model where no mobile water is present, the effect of pressure on viscosity is greater than the effect of the CO2 content but does not affect the overall recovery, whereas in a 3-D model the increase in oil viscosity in the presence of mobile water results in an unfavorable mobility ratio.
9. High CO2 concentrations do not represent a breakthrough, as seen in the result of the 1-D model. At 1 HCPV injected CO2 concentration in the produced oil was about 70% yet the system remained a single phase of course with a high saturation pressure (Figure 8-7, Figure 8-15, Figure 8-23).
10. A new correlation for predicting CO2 minimum miscibility pressure is developed based on the properties of the oil, CO2 density, and reservoir temperature.
11. Recovery at pressures less than MMP on the long run is very much similar to those at or above slim-tube determined MMP, the reason is that slim-tube experiment ignores many important factors.
12. Commercial compositional simulators treat supercritical state according to the EOS which calculates volumes subsequently densities, and then other properties are derived from correlation regardless of the definition of the phase (vapor, liquid or supercritical fluid). A supercritical fluid (CO2 or any fluid) has properties different from those of both liquid and gas, although it may

behave like a liquid or a vapor it has extremely different characteristics, just to mention the solvency of supercritical CO2 is higher than liquid CO2 even when they have similar densities. Viscosity of the supercritical CO2 is 100 times less than a liquid CO2 which would result in a faster transportation.

13. Relative permeability of CO2 is normally measured as gas-liquid rel-perms at ambient temperature, as discussed in Chapter 1, however the actual state of CO2 is a supercritical fluid which means higher density and higher viscosity, for that reason, the input SCAL data for simulating CO2 injection should be those measured at high pressure high temperature, HPHT.

10.2 Future work

1. More laboratory research is required to better understanding of near wellbore and phase behavior effects during gas injection process taking into account CO2 interaction with formation water and reservoir rocks
2. More laboratory work is required to measure CO2 relative permeabilities at HPHT i.e., at supercritical conditions
3. HSE must be an essential part of any future research on CO2 injection regardless of the purpose of the process
4. Comprehensive risk analysis for the different potential risks including leakage in the surface facilities or subsurface/downhole failure must be undertaken

REFERENCES

[1] AGOCO Sarir C-North In-House Simulation Study, 2006

[2] Alston, R.B., Kokolis, G.P., James, C.F.: "CO2 Minimum Miscibility Pressure: A Correlation for Impure CO2 Streams and Live Oil Systems," SPEJ (Apr. 1985) 268-274, SPE reference 11959-PA

[3] Benham, A.L., Dowden, W.E., and Kunzman W.J.: "Miscible Fluid Displacement - Prediction of Miscibility" Published in Petroleum Transactions, AIME, Volume 219, 1960, pages 229-237. SPE reference 1484-G

[4] Calvin, C. Mattax and Robert, L. Dalton.: Reservoir Simulation, SPE Monograph volume 13, 1990

[5] Campbell, B.T. and Orr Jr., F.M.: "Flow Visualization for CO2/Crude-Oil Displacements," SPEJ (Oct. 1985) 665-78 SPE reference 11958-PA

[6] Chalbaud C., Robin M., Bekri S. and Egermann P.: "Wettability Impact on CO2 Storage in Aquifers: Visualisation and Quantification Using Micromodel Tests, Pore Networkmodel And Reservoir Simulations," paper SCA2007-9 presented at the International Symposium of the Society of Core Analysts held in Calgary, Canada, 10-12 September, 2007

[7] Christensen, J.R., and Stenby E.H., and Skauge A..:" Review of WAG Field Experience" SPE Reservoir Evaluation & Engineering, April 2001 (97-106)

[8] Christiansen, R.L. and Kim, H.: "Apparatus and Method for Determining the Minimum Miscibility Pressure of a Gas in a Liquid", U.S. Patent No. 4,627,273 (1986)

[9] Christiansen, Richard L., Haines, Hiemi Kim: "Rapid Measurement of Minimum Miscibility Pressure With the Rising-Bubble Apparatus", SPJ (November 1987) 523-527, SPE reference 13114-PA

[10] Dawn Deel , Kanwal Mahajan, Christopher R. Mahoney, Howard G. McIlvried, Rameshwar D. Srivastava, "Risk Assessment and Management for Long-Term Storage of CO2 in Geologic Formations" - United States Department of Energy R&D, systemics, cybernetics and informatics, volume 5 – 79-84

[11] Deffrenne, P., Marle, C., Pacsirszki, J., Jeantet, M.: "The Determination of Pressures of Miscibility," paper SPE 116 presented at the SPE Annual meeting 8-11 October 1961, Dallas, Texas

[12] Don W. Green and G.Paul Willhite.: "Enhanced Oil Recovery" SPE Textbook series vol. 6 (1998)

[13] Eakin, B.E. and Mitch, F.J.: "Measurement and Correlation of Miscibility Pressures of Reservoir Oils," paper SPE 18065 presented at the SPE Annual Technical Conference and Exhibition, 2-5 October 1988, Houston, Texas

[14] Egermann P., Bazin B., Vizika O., "An Experimental Investigation of Reaction-Transport Phenomena During CO2 Injection," paper SPE 93674, presented at the 14th SPE Middle East Oil and Gas Show and Conference held in Bahrain Kingdom Mar, 12 - 15, 2005

[15] Egermann, P., Bekri, S., and Vizika, O. "An Integrated Approach to Assess the Petrophysical Properties of Rocks Altered by Rock/Fluid Interactions (CO2 Injection)" paper was prepared for presentation at the International Symposium of the Society of Core Analysts held in Toronto, 21-25 August 2005

[16] Elsharkawy, A.M., Poettmann, F.H., Christiansen, R.L.: "Measuring Minimum Miscibility Pressure: Slim-Tube or Rising-Bubble Method?," paper SPE 24114 presented at the SPE/DOE Enhanced Oil Recovery Symposium, 22-24 April 1992, Tulsa, Oklahoma

[17] Farzad I. and Amani M.: "Evaluating Reservoir Production Strategies in Miscible and Immiscible Gas-Injection Projects," paper SPE 108014 presented at the Latin American & Caribbean Petroleum Engineering Conference, 15-18 April 2007, Buenos Aires, Argentina

[18] Firoozabadi, A. and Aziz, K.: "Analysis and Correlation of Nitrogen and Lean-Gas Miscibility Pressure," SPEJ (Nov. 1986) 575-582, SPE reference 13669-PA

[19] Fredi ,I. and Stalkup JR.: "Miscible displacement," SPE Monograph volume 8, 1984

[20] Glasø, O.: "Generalized Minimum Miscibility Pressure Correlation," SPEJ (Dec. 1985) 927-934, SPE reference 12893-PA

[21] Guo X., Du Z., Sun L., Fu Y., Huang W., Zhang C.: "Optimization of Tertiary Water-Alternate-CO2 Flood in Jilin Oil Field of China: Laboratory and Simulation Studies," paper SPE 99616, presented at the SPE/DOE Symposium on Improved Oil Recovery, Tulsa, Oklahoma, USA, 22-26 April 2006

[22] Holm, L.W. and Josendal, V.A.: "Mechanisms of Oil Displacement By Carbon Dioxide," JPT (Dec. 1974) 1427-1438, SPE reference 4736-A

[23] Holm, L.W., Josendal, V.A.: "Effect of Oil Composition on Miscible-Type Displacement by Carbon Dioxide," SPEJ (Feb. 1982) 87-98, SPE reference 8814-PA

[24] Iman Farzad: "Evaluating Reservoir Production Strategies in Miscible and Immiscible Gas-Injection Projects", Master thesis, Texas A&M University, (2004)

[25] Jackson, D.D., Andrews, G.L., and Claridge, E.L.: "Optimum WAG Ratio vs. Rock Wettability in CO2 Flooding," paper SPE 14303 presented at the 1985 Annual Technical Conference and Exhibition, Las Vegas, Nevada, 22–25 September.

[26] John D. Rogers, Reid B. Grigg, "A Literature Analysis of the WAG Injectivity Abnormalities in the CO2 Process," SPEJ (October 2001) 375-386

[27] John Gale and John Davison, "Transmission of CO2—safety and economic considerations" Energy 29 (2004) 1319-1328

[28] Johns, R.T., and Orr, Jr., F.M.: "Miscible Gas Displacement of Multicomponent Oils," SPEJ (Mar. 1996) 39-50, SPE reference 30798-PA

[29] Johnson, James P., Pollin, James S.: "Measurement and Correlation of CO2 Miscibility Pressures," paper SPE 9790 presented at the SPE/DOE Enhanced Oil Recovery Symposium, 5-8 April 1981, Tulsa, Oklahoma

[30] Jonathan Bellarby, " Well Completion Design" First edition 2009, Elsevier publications

[31] Khataniar S., Kamath V.A., Patil S.L., Chandra S., Inaganti M.S., "CO2 and Miscible Gas Injection for Enhanced Recovery of Schrader Bluff Heavy Oil," paper SPE 54085, paper presented at the 1999 SPE International Thermal Operations and Heavy Oil Symposium held in Bakersfield, California, 17–19 March 1999.

[32] Kuo, S.S.: "Prediction of Miscibility for the Enriched-Gas Drive Process," paper SPE 14152 presented at the SPE Annual Technical Conference and Exhibition, 22-26 September 1985, Las Vegas, Nevada

[33] Luks, K.D., Turek, E.A., Baker, L.E.: "Calculation of Minimum Miscibility Pressure," SPEJ (Nov. 1987) 501-506, SPE reference 14929-PA

[34] Masoner, L.O. and Wackowski, R.K.: "Rangely Weber Sand Unit CO2 Project Update," SPERE (August 1995) 203; Trans., AIME, 299.

[35] Metcalfe, R.S., Fussell, D.D., Shelton, J.L., "A Multicell Equilibrium Separation Model for the Study of Multiple Contact Miscibility in Rich-Gas Drives," SPEJ (Jun. 1973) 147-155, SPE reference 3995-PA

[36] Metcalfe, R.S., Yarborough Lyman, “The Effect of Phase Equilibria on the CO2 Displacement Mechanism,” SPEJ (August 1979) 242-252, SPE reference 7061-PA

[37] Monroe, W.W., Silva, M.K., Larson, L.L., Orr Jr., F.M.: “Composition Paths in Four-Component Systems: Effect of Dissolved Methane on 1-D CO2 Flood Performance,” SPEJ (Aug. 1990) 423-432, SPE reference 16712-PA

[38] Nghiem and Li, “Effect of Phase Behavior on CO2 Displacement Efficiency at Low Temperatures: Model Studies With an Equation of State,” SPEJ (July 1986) 414-422, SPE reference 13116-PA

[39] Nouar, A. and Flock, D.L.: “Prediction of the Minimum Miscibility Pressure of a Vaporizing-gas Drive,” SPEJ (Feb. 1988) 182-198, SPE reference 15075-PA

[40] Orr Jr., F.M. and Silva, M.K.: “Effect of Oil Composition on Minimum Miscibility Pressure-Part 2: Correlation,” SPEJ (Nov. 1987) 479-491, SPE reference 14150-PA

[41] Peng, D.-Y. and Robinson, D.B.: "A New Two-Constant Equation of State," Ind. Eng. Chem. Fundam. (1976) 15, 59.

[42] Raimondi, Pietro, Torcaso, Michael A., “Distribution of the Oil Phase Obtained Upon Imbibition of Water,” SPEJ, (March 1964) 49-55, SPE reference 570-PA

[43] Ram B. Gupta and Jae-Jin Shim, “Supercritical Carbon Dioxide” CRC Press 2007

[44] Ramesh N. Patel: “Stereoselective Biocatalysis”, 2000

[45] Roper Jr., M.K., Cheng, C.T., Varnon, J.E., Pope, G.A., Sepehrnoori Kamy: “Interpretation of a CO2 WAG Injectivity Test in the San Andres Formation Using a Compositional Simulator,” paper SPE 24136 presented at the SPUDOE Eighth Symposium on Enhanced Oil Recovery held in Tulsa, Oklahoma, April 22-24, 1992.

[46] Ross, Graham D., Todd, Adrain C., Tweedie, John A., Will, Andrew G.S., “The Dissolution Effects of CO2-Brine Systems on the Permeability of U.K. and North Sea Calcareous Sandstones,” paper SPE 10685, presented at the SPE/DOE Enhanced Oil Recovery Symposium held in Tulsa, Oklahoma, 4-7 April 1982

[47] Sebastian, H.M., Wenger, R.S., Renner, T.A.: “Correlation of Minimum Miscibility Pressure for Impure CO2 Streams,” JPT (Nov. 1985) 2076-2082, SPE reference 12648-PA

[48] Shelton, J.L., Schneider, F.N.: “The Effects of Water Injection on Miscible Flooding Methods Using Hydrocarbons and Carbon Dioxide,” SPEJ (June 1975) 218-226, SPE reference 4580

[49] Soave, G.: "Equilibrium Constants From a Modified Redlich Kwong Equation of State," Chem. Eng. Sci. (1972) 27, 1197-1203.

[50] Stalkup Jr., F.I.: “Status of Miscible Displacement,” JPT (April 1983) 815-26

[51] Stalkup, F.I., “Displacement of oil by Solvent at High Water Saturation,” SPEJ (December 1970) 337-348, SPE reference 2419-PA

[52] Surguchev, L.M., Rogaland Research; Korbol, Ragnhild, Haugen, Sigurd, Krakstad, O.S.,“ Screening of WAG Injection Strategies for Heterogeneous Reservoirs”, Paper SPE 25027, presented at the European Petroleum Conference , 16-18 November 1992, Cannes, France

[53] Tanner, C.S. et al.: “Production Performance of the Wasson Denver Unit CO2 Flood,” paper SPE 24156 presented at the 1992 SPE/DOE Enhanced Oil Recovery Symposium, Tulsa, Oklahoma, 22–24 April.

[54] Tarek Ahmed: “Hydrocarbon Phase Behavior”, Contributions in petroleum geology & engineering volume 7, 1989

[55] Thomas, F.B., Zhou, X.L., Bennion, D.B., Bennion, D.W.,”A Comparative Study of RBA, P-x Multicontact and Slim Tube Results” The journal of Canadian Technology, February 1994, Volume 33, No. 2

[56] Tiffin, D.L and Yellig,W.F.: “Effects of Mobile Water on Multiple-Contact Miscible Gas Displacements,” SPEJ (June 1983) 447-55. SPE reference 10687-PA

[57] Todd M. R., Todd D., Chase C., William M., McCarter E. D., “CO2 Flood Performance Evaluation for the Cornell Unit, Wasson San Andres Field,” JPT (October 1982) 2271-2282, SPE 10292-PA

[58] Wang, Y. and Orr, F.M., Jr.: “Calculation of Minimum Miscibility Pressure,” paper SPE 39683 presented at the SPE/DOE Improved Oil Recovery Symposium, 19-22 April 1998, Tulsa, Oklahoma

[59] Whitson, Curtis H.: “Characterizing Hydrocarbon Plus Fractions,” SPEJ (Aug. 1983) 683-694, SPE reference 12233-PA

[60] Xiaowei Wang, Arden Strycker, “Evaluation of CO2 Injection with Three Hydrocarbon Phases,” paper SPE 64723

[61] Yarborough, Lyman, Smith, L.R., “Solvent and Driving Gas Compositions for Miscible Slug Displacement,” SPEJ (Sep. 1970) 298-310, SPE reference 2543

[62] Yellig W.F. and Metcalfe R.S.: “Determination and Prediction of CO2 Minimum Miscibility Pressures,” JPT, (Jan. 1980) 160-68. SPE reference 7477.

[63] Zick, A.A., “A Combined Condensing/Vaporizing Mechanism in the Displacement of Oil by Enriched Gases,” paper SPE 15493, presented at the SPE Annual Technical Conference and Exhibition, New Orleans, Louisiana, 5-8 October 1986

NOMENCLATURE

1,2,3-D	One, two or three dimensional model
a	For EOS is a temperature dependent parameter
AAE	Absolute average error
API	Gravity
b	For EOS is a co-volume
CBL	Cement Bond Log
CGD	Condensing gas drive
CO2	Carbon dioxide
DENO	Oil density, lb/cu-ft
EOS	Equation of state
ESD	Emergency Shutdown
F	Weighted composition parameter
FCMP	First contact miscibility pressure
FZI	Flow zone indicator
GOR	Gas oil ratio
H2CO3	Carbonic acid
HCO3	Bicarbonate
HCPV	Hydrocarbon pore volume
HSE	Health, Safety Environment
I	Characterization factor
ID	Inner diameter
IFT	Interfacial tension
K	Waiting factor
kr, p	Relative permeability of phase p
Kw	Watson characterization factor
LPG	Liquefied petroleum gas
M	Molecular weight or mobility ratio
m	Mass
MCM	Multi-contact miscibility
mCO2	Mass of CO2
MMP	Minimum miscibility pressure
MPC1	Mole percent of methane plus nitrogen
Nc	Capillary number
OD	Outer diameter
OOIP	Oil original in place
P	Pressure
Pb	Bubble point pressure
ppm	Part per million
Psat	Saturation pressure, psi
P-T	Pressure-Temperature diagram
PV	Pore volume
P-X	Pressure composition diagram
RBA	Rising bubble apparatus
S_h	hydrocarbon saturation
So	Oil saturation
Sor	Residual oil saturation
SSSV	Subsurface Safety Valve
Sw	Water saturation
Sw avg	Water saturation
Swc	Connate water saturation
Swi	Initial water saturation
T	Temperature
V	Volume
VGD	Vaporizing gas drive
ViCO2	Volume of CO2 at reservoir conditions
VOIL	Oil viscosity, cp
w	Weight fraction
WAG	Water alternating gas
x	Mole percent
Xi	Oil component mole fraction of component i
XMFi	Oil component mole fraction of component i
Yi	Gas component mole fraction of component i
YMFi	Gas component mole fraction of component i
Z	Deviation factor
Zi	Total mole fraction of component i
ZMFi	Total mole fraction of component i
λ p	Phase mobility
μ p	Viscosity of phase p
α	Constant
ρ	Density
γ	Specific gravity
β	Constant
ø	Porosity

Subscript

c	Critical
inj	Injection
RES	Reservoir
LO	Live oil
r	reduced property
vol	Volatile
int	Intermediate
i	component carbon number
ob	Oil bank
s	Sovent
w	Water
init	Initial
avg	Average

APPENDIX A: PVT Characterization

It is essential to characterize reservoir fluids using PVT studies to evaluate their behavior at different ranges of pressure and temperature. For the subject fluid sample, routine laboratory tests are available (Compositional fluid analysis, Constant Composition Expansion Experiment, CCE, Differential Liberation Experiment, DLE, Separator test, SP) analyzed by Core Laboratories UK LTD. March 1984, as well as special laboratory tests, Slim-tube test using separator gas at 3300 psig and pure CO2 at 2500 and 3300 psi and a Swelling test using synthetic gas made by Core Laboratories UK LTD. May 1984.

The intension was to evaluate the fluid sample using a reliable EOS model that can match observed PVT measurements of the mentioned experiments, and predict system behavior at other operating conditions.

The EOS model incorporated three routine tests (CCE, DLE and SP) and one special test (Slim-tube test), the swelling test was not included due to the type of the injection gas (synthetic natural gas).

The EOS model was built with Eclipse PVTi.

A. 1. EOS Model Setup

The fluid was sampled from 8628 ft and 225 ˚F and 3300 psig, observed saturation pressure, Psat, was 715 psig and density at Psat was 0.7486 g/cc. The fluid composition is tabulated below:

Component	Mole Percent	Weight Percent	Density @ 60 °F, g/c.c	API	Mole Weight
CO_2	01.12	0.27			
N_2	01.05	0.16			
C1	10.82	0.96			
C2	04.34	0.72			
C3	08.22	2.01			
iC4	02.22	0.72			
nC4	06.41	2.07			
iC5	02.86	1.14			
nC5	03.54	1.42			
C6	04.45	2.12			
C7+	54.97	88.41	0.8644	32.0	290
	100.00	100.00			

The three parameters Peng-Robinson Equation of State, PR-EOS, was selected, initially the fluid composition was feed to PVTi, the model predicted higher Psat (832.58 psig), but good density at Psat (0.743 g/cc).

A.1.1 Matching Psat and Density @ Psat

Splitting: To match the saturation pressure, the plus fraction (C7+) was split into four pseudo-components namely FRC1, FRC2, FRC3 and FRC4, the splitting method was that proposed by Whitson, the properties of the pseudo-components are as summarized:

Components	ZI (percent)	Weight Fraction (percent)	Mole Weight	Spec. Gravity
FRC1	7.4361	4.4532	107.94	0.74531
FRC2	14.9740	14.0780	169.44	0.79224
FRC3	17.5200	28.1940	290.05	0.85205
FRC4	15.0400	41.7220	500.00	0.91725

Grouping: To reduce the number of components, a total of eleven components was setup as follows: CO2 was left as a pure component because we are going to inject CO2 later, nitrogen was grouped with methane, iso-butane with n-butane, iso-pentane with n-pentane, while preserving ethane, propane and hexane as pure components plus the four pseudo-components.

After splitting C7+ fraction and grouping as mentioned above, the calculated Psat was closer but still below the observed Psat, Binary Interaction Coefficients, BIC, between methane and the pseudo-components were used to match the observed Psat, the following table summaries BIC's:

	C1
FR1	0.01
FR2	0.02
FR3	0.03
FR4	0.08

The matched Psat was exactly 715 psig. BIC's were key parameters for matching Psat but have no influence on density calculations, therefore volume-shift of the heaviest pseudo-component FRC4 was adjusted to match the density at Psat. The V-shifts: FRC4 =0.205

The calculated density at Psat was 0.75 g/cc

A. 2. CCE Experiment

CCE is designed to approximate the two-phase volumetric behavior below bubble point, e.g. flow in the well-bore.

After matching Psat and density at Psat, the CCE experiment was defined, and the measured data was entered.

The following tables summarize the results and the Absolute Average Error (AAE) for the undersaturated oil compressibility, relative volume and Y-function for the CCE experiment:

A.2.1 Relative volume and Y-function

The reported Y-function was plotted versus pressure, the plot shows that Y-function forms a straight line, in fact a straight line with a very small curvature, no

erratic behavior of the data was observed near the bubble point pressure, therefore reported relative volume is considered to be reliable, thus no correction (smoothing) was necessary to the measured relative volume.

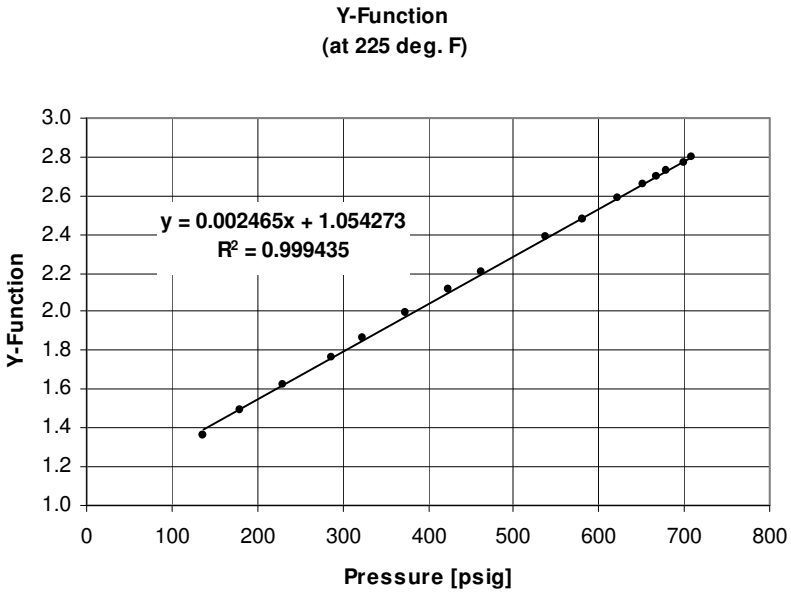

Y-function (relative volume validation)

A. 3. DLE Experiment

DLE is designed to approximate the depletion process in an oil reservoir.

Data from DLE test was feed to PVTi, these are oil related properties, GOR, relative oil volume, oil density and oil viscosity. Reported gas properties (deviation factor, Gas formation volume factor, Incremental gas gravity and Vapor viscosity) were not matching parameters.

A. 4. SP Experiment

Separator test data is used mainly to provide basis for converting differential-liberation data from residual-oil to stock-tank oil basis.

The sample was flashed through a laboratory three separate two-stage separator tests at 150, 100 and 50 psig, the optimum separator pressure as indicated by evaluating oil FVF was 100 psig (field separator conditions are 106 psig and 136 deg F), therefore corresponding data was feed to the program.

A. 5. Tuning EOS

A final step in building the EOS model is tuning the model such that it overcomes the effect of grouping, and matches reported laboratory data and then the model can be considered reliable for predicting the phase behavior at different operating conditions.

The first step –recommended- is to regress on all ΩA and ΩB for all components except CO2 in our case, second step is to regress on viscosity separately, regression on critical properties of light and intermediate components can be dangerous.

The following plots show the quality of the match, the table summaries AAE for CCE and DLE observations, the highest AAE is in the predicted gas properties and the reason -as mentioned earlier- is that they were not matching parameters, however, the deviation is acceptable:

Experiment	**CCE**	**DLE**							
Observation	Rel.vol.	OilFVF	GOR	Liquid density	Liquid visc.	Gas FVF	Vapor Z-factor	Gas Density	Vapor visc.
AAE %	**1.59**	**1.55**	**1.58**	**0.22**	**3.20**	**2.49**	**0.61**	**8.45**	**5.68**

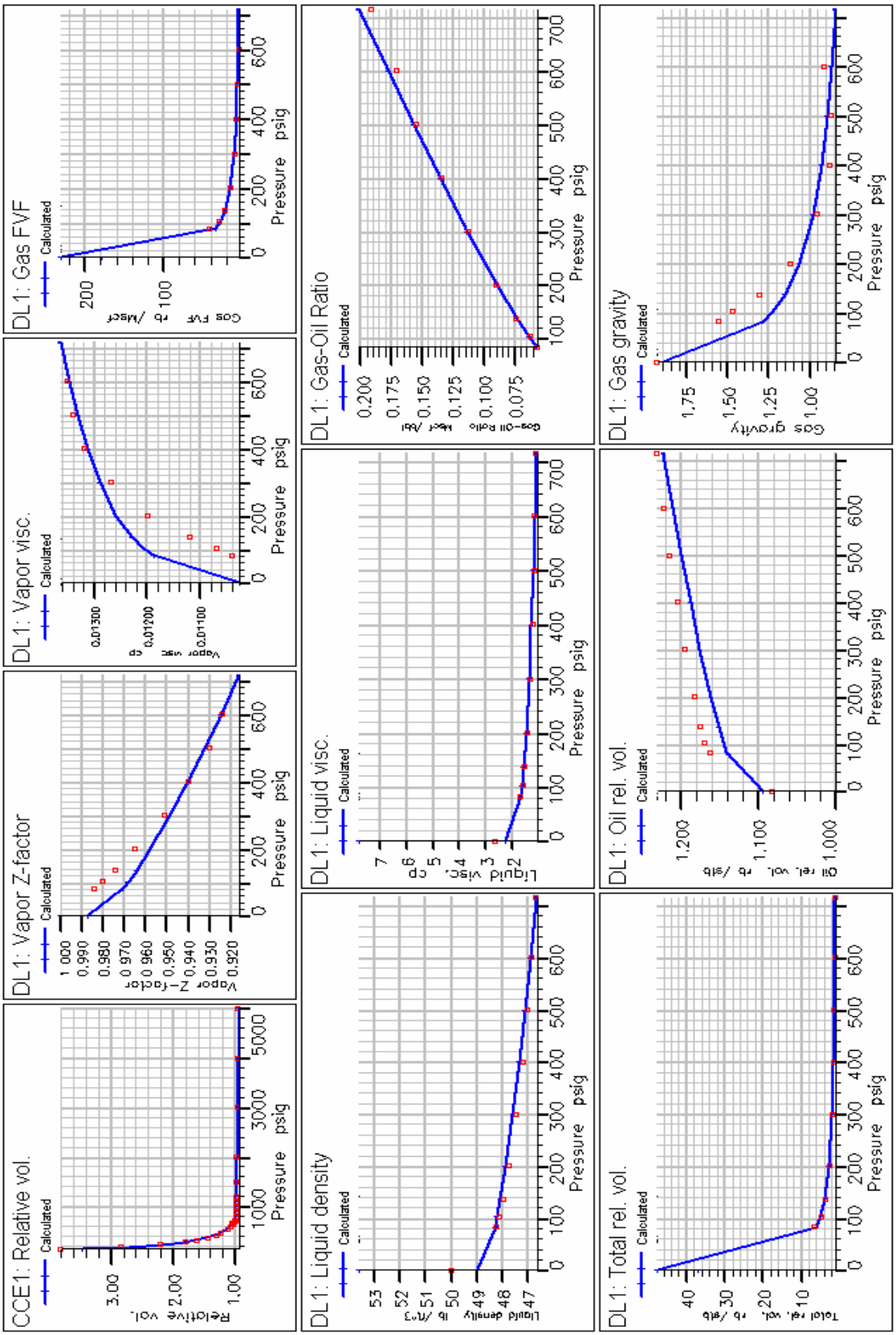
CCE1: Relative vol.
Calculated
Relative vol.
Pressure psig
DL1: Vapor Z-factor
Calculated
Vapor Z-factor
Pressure psig
DL1: Vapor visc.
Calculated
Vapor visc. cp
Pressure psig
DL1: Gas FVF
Calculated
Gas FVF rb /Mscf
Pressure psig
DL1: Liquid density
Calculated
Liquid density lb /ft^3
Pressure psig
DL1: Liquid visc.
Calculated
Liquid visc. cp
Pressure psig
DL1: Gas-Oil Ratio
Calculated
Gas-oil Ratio Mscf /bbl
Pressure psig
DL1: Oil rel. vol.
Calculated
Oil rel. vol. rb /stb
Pressure psig
DL1: Gas gravity
Calculated
Gas gravity
Pressure psig
DL1: Total rel. vol.
Calculated
Total rel. vol. rb /stb
Pressure psig

APPENDIX B: Relative Permeability

Two-phase water-oil and gas-oil relative permeabilities derived from Corey's model

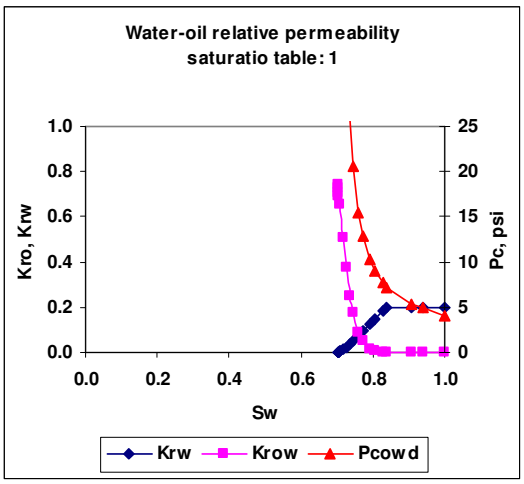

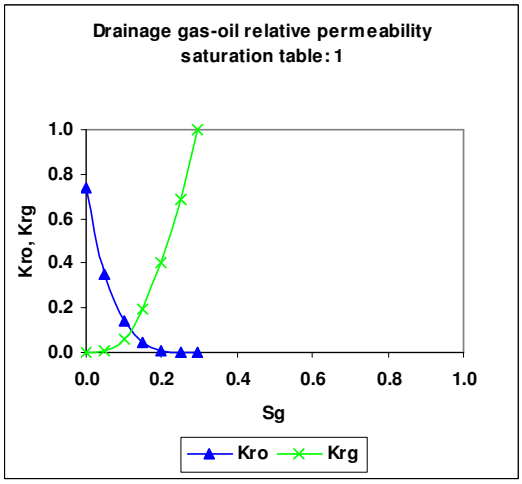

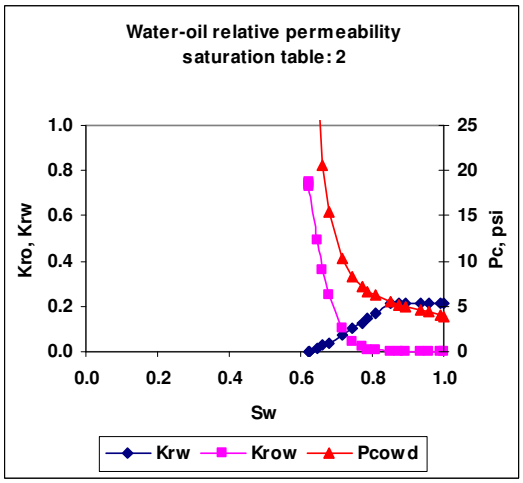

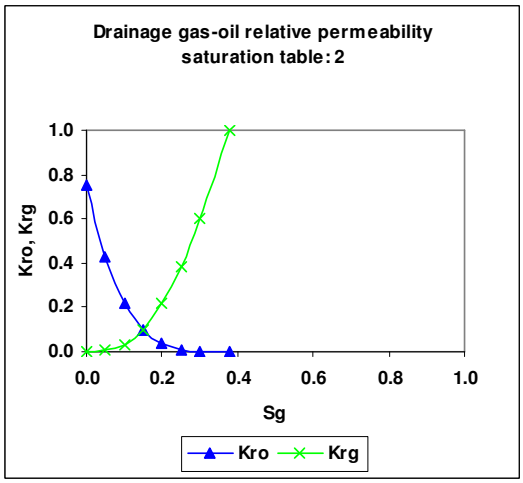

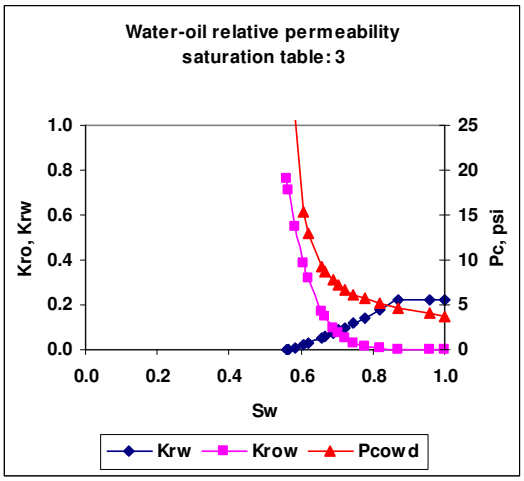
Water-oil relative permeability
saturation table: 3
Kro, Krw
Pc, psi
Sw
Krw
Krow
Pcowd

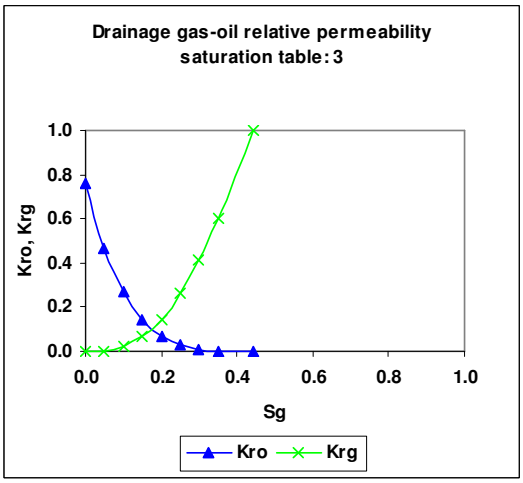
Drainage gas-oil relative permeability
saturation table: 3
Kro, Krg
Sg
Kro
Krg

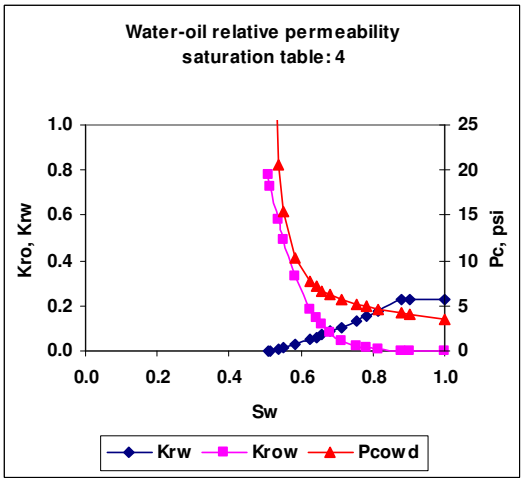
Water-oil relative permeability
saturation table: 4
Kro, Krw
Pc, psi
Sw
Krw
Krow
Pcowd

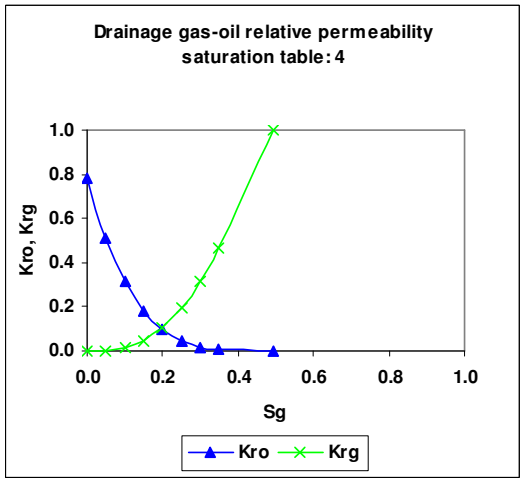
Drainage gas-oil relative permeability
saturation table: 4
Kro, Krg
Sg
Kro
Krg

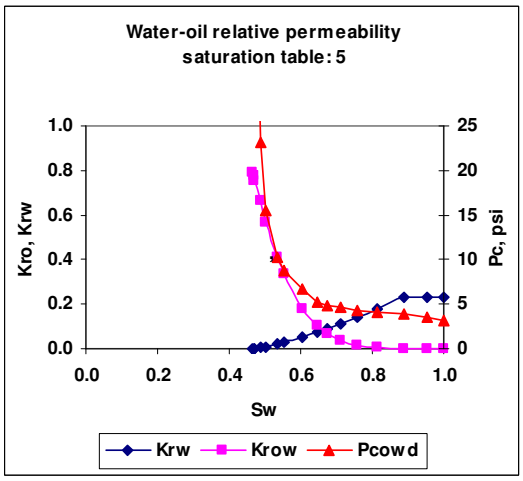
Water-oil relative permeability
saturation table: 5
Kro, Krw
Pc, psi
Sw
Krw
Krow
Pcowd

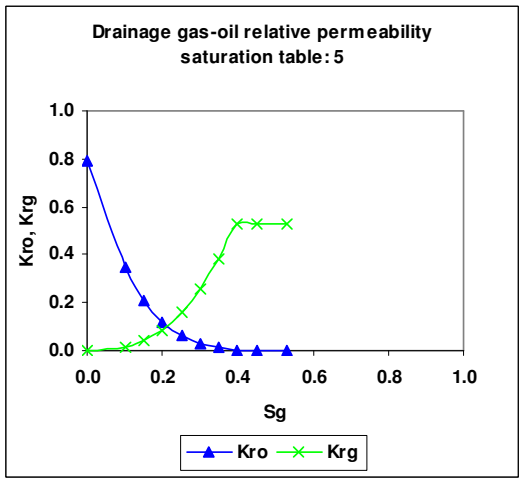
Drainage gas-oil relative permeability
saturation table: 5
Kro, Krg
Sg
Kro
Krg

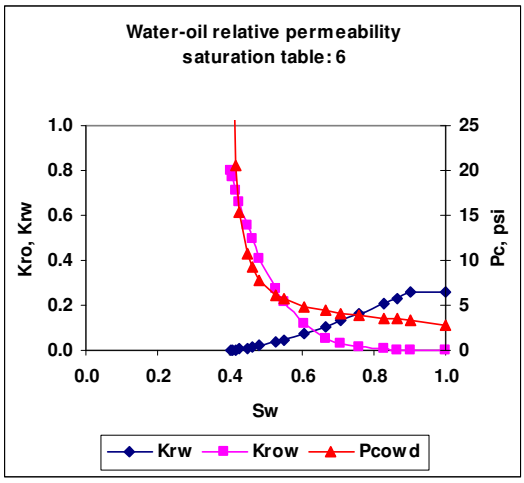
Water-oil relative permeability
saturation table: 6
Kro, Krw
Pc, psi
Sw
Krw
Krow
Pcowd

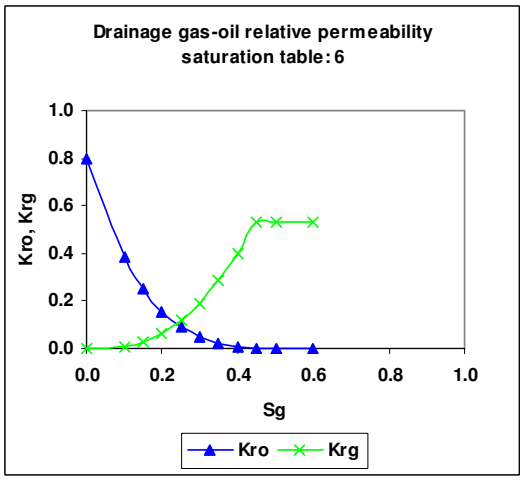
Drainage gas-oil relative permeability
saturation table: 6
Kro, Krg
Sg
Kro
Krg

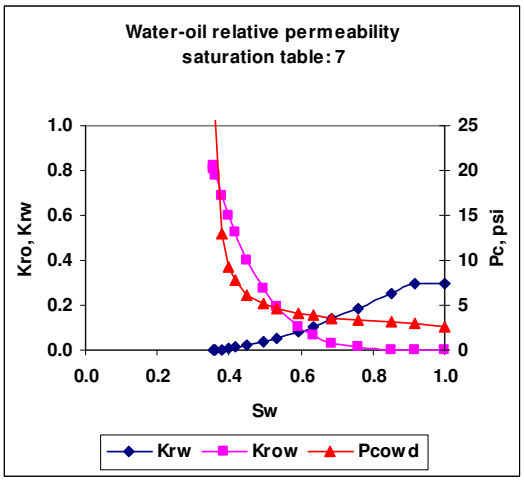
Water-oil relative permeability
saturation table: 7
Kro, Krw
Pc, psi
Sw
Krw
Krow
Pcowd

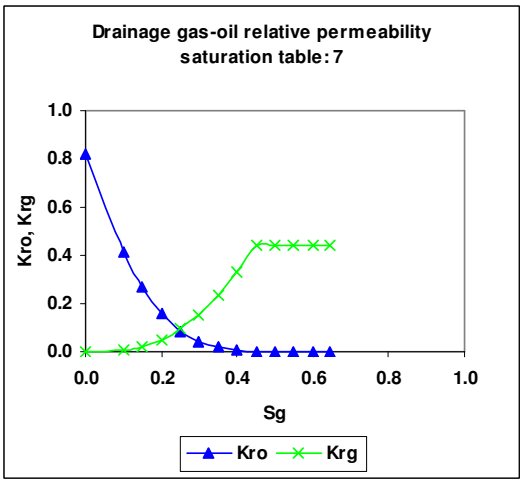
Drainage gas-oil relative permeability
saturation table: 7
Kro, Krg
Sg
Kro
Krg

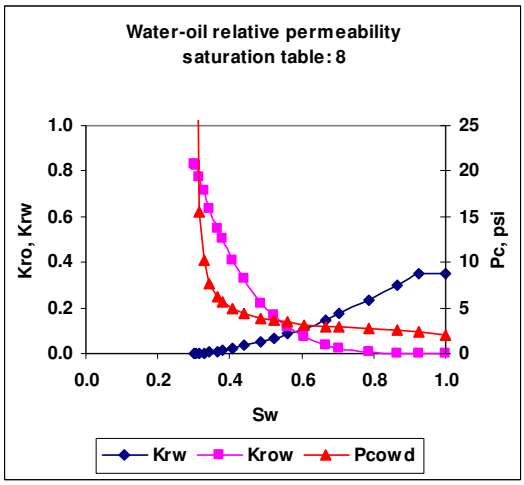
Water-oil relative permeability
saturation table: 8
Kro, Krw
Pc, psi
Sw
Krw
Krow
Pcowd

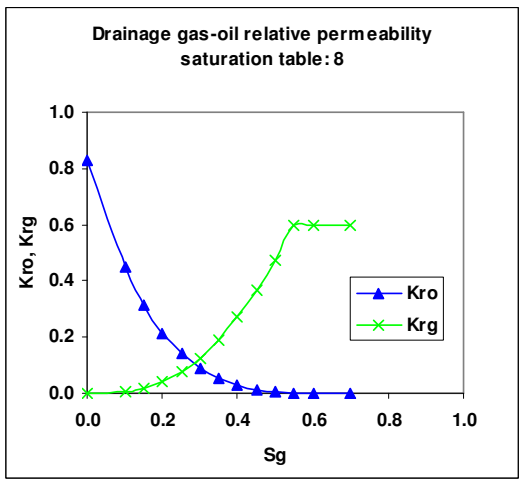
Drainage gas-oil relative permeability
saturation table: 8
Kro, Krg
Sg
Kro
Krg

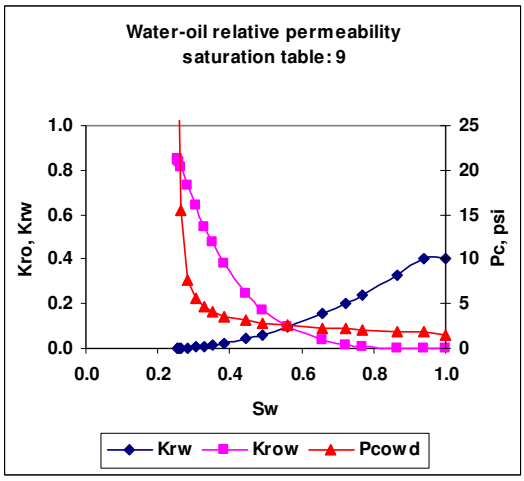
Water-oil relative permeability
saturation table: 9
Kro, Krw
Pc, psi
Sw
Krw
Krow
Pcowd

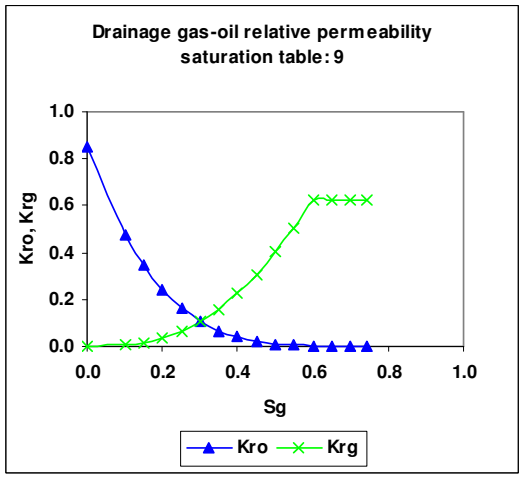
Drainage gas-oil relative permeability
saturation table: 9
Kro, Krg
Sg
Kro
Krg

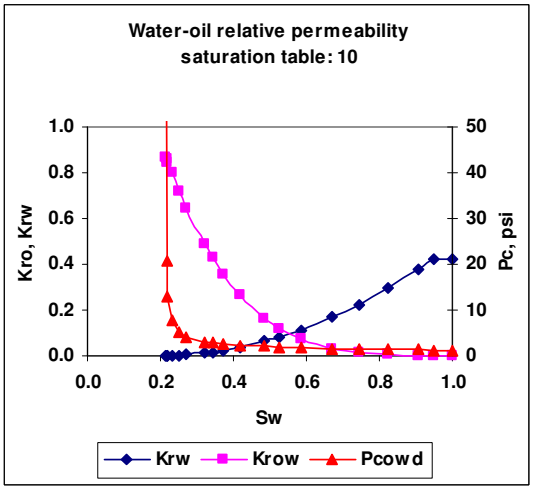
Water-oil relative permeability
saturation table: 10
Kro, Krw
Pc, psi
Sw
Krw
Krow
Pcowd

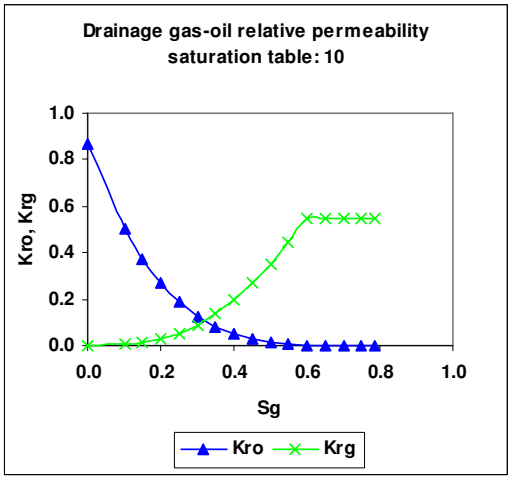
Drainage gas-oil relative permeability
saturation table: 10
Kro, Krg
Sg
Kro
Krg

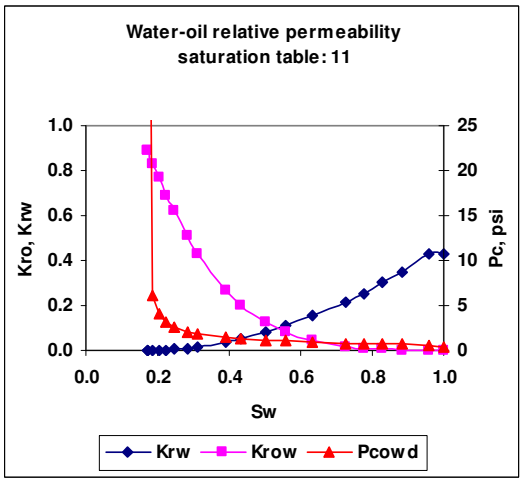
Water-oil relative permeability
saturation table: 11
Kro, Krw
Pc, psi
Sw
Krw
Krow
Pcowd

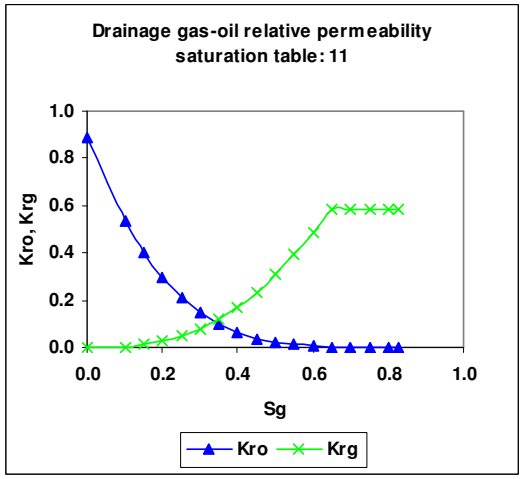
Drainage gas-oil relative permeability
saturation table: 11
Kro, Krg
Sg
Kro
Krg

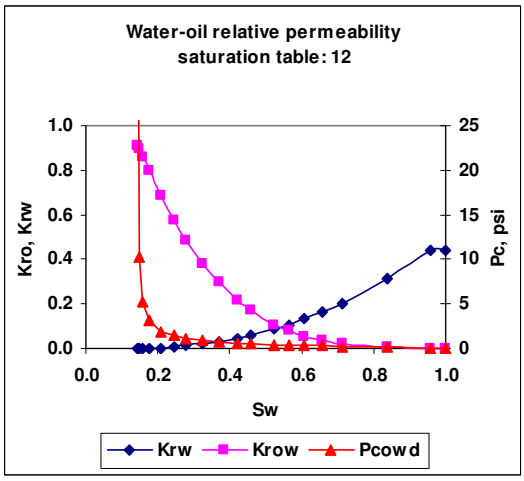
Water-oil relative permeability
saturation table: 12
Kro, Krw
Pc, psi
Sw
Krw
Krow
Pcowd

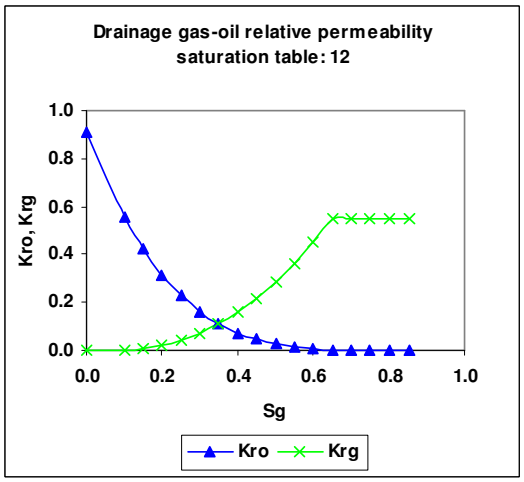
Drainage gas-oil relative permeability
saturation table: 12
Kro, Krg
Sg
Kro
Krg

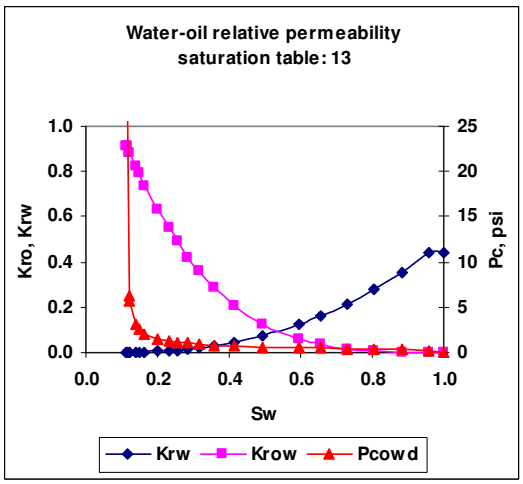
Water-oil relative permeability
saturation table: 13
Kro, Krw
Pc, psi
Sw
Krw
Krow
Pcowd

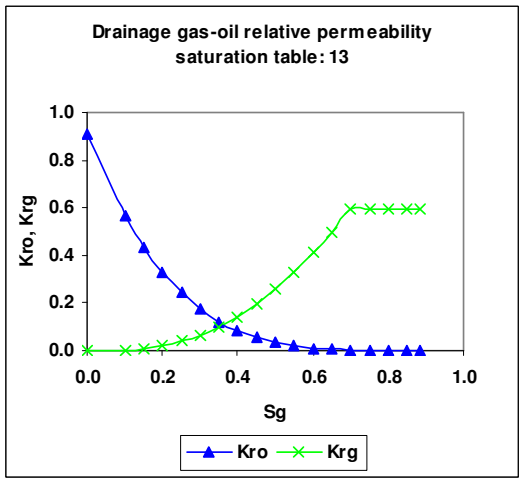
Drainage gas-oil relative permeability
saturation table: 13
Kro, Krg
Sg
Kro
Krg

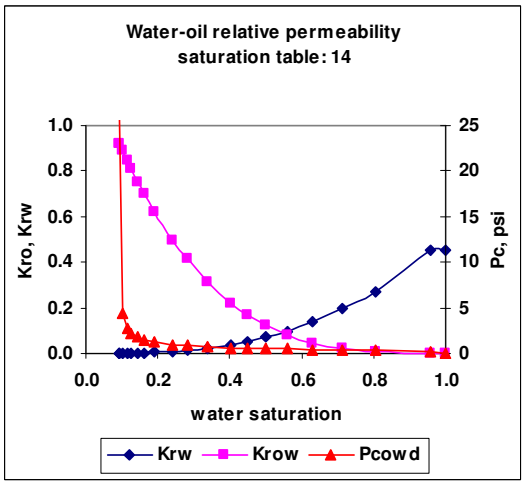
Water-oil relative permeability
saturation table: 14
Kro, Krw
Pc, psi
water saturation
Krw
Krow
Pcowd

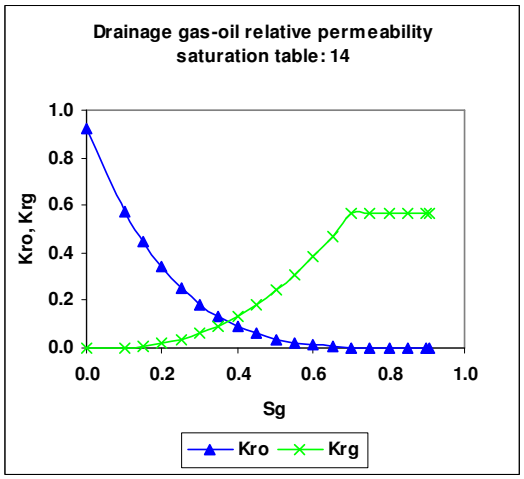
Drainage gas-oil relative permeability
saturation table: 14
Kro, Krg
Sg
Kro
Krg